



Summary Report 277-S-01

For Project

Weld Design, Testing, and Assessment Procedures for High Strength Pipelines

Prepared for the

Design, Materials, and Construction Technical Committee of
Pipeline Research Council International, Inc.
Project MATH-1 Catalog No. L5XXXX
and
U.S. Department of Transportation
Pipeline and Hazardous Materials Safety Administration
Office of Pipeline Safety
DOT Project BAA DTHP56-07-0001

Prepared by

Yong-Yi Wang, Honggang (Michael) Zhou, and Ming Liu
Center for Reliable Energy Systems

Bill Tyson and Jim Gianetto
CANMET Materials Technology Laboratory

Timothy Weeks, Mark Richards and J. David McColskey
National Institute of Standards and Technology

Marie Quintana and V. B. Rajan
Lincoln Electric Company

December 20, 2011

This research was funded in part under the Department of Transportation, Pipeline and Hazardous Materials Safety Administration's Pipeline Safety Research and Development Program. The views and conclusions contained in this document are those of the authors and should not be interpreted as representing the official policies, either expressed or implied, of the Pipeline and Hazardous Materials Safety Administration, or the U.S. Government.

Contribution of an agency of the U.S. government, not subject to copyright



Catalog No. L5XXXX

Summary Report 277-S-01

For Project

Weld Design, Testing, and Assessment Procedures for High Strength Pipelines

Prepared for the

Design, Materials, and Construction Technical Committee of
Pipeline Research Council International, Inc.

Project MATH-1 Catalog No. L5XXXX

and

U.S. Department of Transportation

Pipeline and Hazardous Materials Safety Administration

Office of Pipeline Safety

DOT Project BAA DTHP56-07-0001

Prepared by

Yong-Yi Wang, Honggang (Michael) Zhou, and Ming Liu

Center for Reliable Energy Systems

Bill Tyson and Jim Gianetto

CANMET Materials Technology Laboratory

Timothy Weeks, Mark Richards and J. David McColskey

National Institute of Standards and Technology

Marie Quintana and V. B. Rajan

Lincoln Electric Company

December 20, 2011

Version	Date of Last Revision	Date of Uploading	Comments
Draft	September 2011		
FINAL	January 23, 2012		

This report is furnished to Pipeline Research Council International, Inc. (PRCI) under the terms of PRCI contract [277-PR-348-074512], between PRCI and the MATH-1 contractors:

- Electricore (prime contractor),
- Center for Reliable Energy Systems, CANMET, NIST, and The Lincoln Electric Company (sub-contractors).

The contents of this report are published as received from the MATH-1 contractor and subcontractors. The opinions, findings, and conclusions expressed in the report are those of the authors and not necessarily those of PRCI, its member companies, or their representatives. Publication and dissemination of this report by PRCI should not be considered an endorsement by PRCI of the MATH-1 contractor and subcontractors, or the accuracy or validity of any opinions, findings, or conclusions expressed herein.

In publishing this report, PRCI and the MATH-1 contractors make no warranty or representation, expressed or implied, with respect to the accuracy, completeness, usefulness, or fitness for purpose of the information contained herein, or that the use of any information, method, process, or apparatus disclosed in this report may not infringe on privately owned rights. PRCI and the MATH-1 contractors assume no liability with respect to the use of, or for damages resulting from the use of, any information, method, process, or apparatus disclosed in this report. By accepting the report and utilizing it, you agree to waive any and all claims you may have, resulting from your voluntary use of the report, against PRCI and the MATH-1 contractors.

Pipeline Research Council International Catalog No. L5XXXX

PRCI Reports are Published by Technical Toolboxes, Inc.

3801 Kirby Drive, Suite 520
Houston, Texas 77098
Tel: 713-630-0505
Fax: 713-630-0560
Email: info@ttoolboxes.com

PROJECT PARTICIPANTS

PROJECT TEAM MEMBER	COMPANY AFFILIATION	PROJECT TEAM MEMBER	COMPANY AFFILIATION
Arti Bhatia	Alliance	Jim Costain	GE
Jennifer Klementis	Alliance	Gilmar Batista	Petrobras
Roger Haycraft	Boardwalk	Marcy Saturno de Menezes	Petrobras
David Horsley	BP	Dave Aguiar	PG&E
Mark Hudson	BP	Ken Lorang	PRCI
Ron Shockley	Chevron	Maslat Al-Waranbi	Saudi Aramco
Sam Mishael	Chevron	Paul Lee	SoCalGas
David Wilson	ConocoPhillips	Alan Lambeth	Spectra
Satish Kulkarni	El Paso	Robert Turner	Stupp
Art Meyer	Enbridge	Gilles Richard	TAMSA
Bill Forbes	Enbridge	Noe Mota Solis	TAMSA
Scott Ironside	Enbridge	Philippe Darcis	TAMSA
Sean Keane	Enbridge	Dave Taylor	TransCanada
Laurie Collins	Evraz	Joe Zhou	TransCanada
David de Miranda	Gassco	Jason Skow	TransGas
Adriaan den Herder	Gasunie	Ernesto Cisneros	Tuberia Laguna
Jeff Stetson	GE	Vivek Kashyap	Welpsun
		Chris Brown	Williams

CORE RESEARCH TEAM	
RESEARCHER	COMPANY AFFILIATION
Yaoshan Chen	Center for Reliable Energy Systems
Yong-Yi Wang	Center for Reliable Energy Systems
Ming Liu	Center for Reliable Energy Systems
Dave Fink	Lincoln Electric Company
Marie Quintana	Lincoln Electric Company
Vaidyanath Rajan	Lincoln Electric Company
Joe Daniel	Lincoln Electric Company
Radhika Panday	Lincoln Electric Company
James Gianetto	CANMET Materials Technology Laboratory
John Bowker	CANMET Materials Technology Laboratory
Bill Tyson	CANMET Materials Technology Laboratory
Guowu Shen	CANMET Materials Technology Laboratory
Dong Park	CANMET Materials Technology Laboratory
Timothy Weeks	National Institute of Standards and Technology
Mark Richards	National Institute of Standards and Technology
Dave McColskey	National Institute of Standards and Technology
Enrico Lucon	National Institute of Standards and Technology
John Hammond	Consultant Metallurgist & Welding Engineer

This Page Intentionally Left Blank

FINAL REPORT STRUCTURE

Focus Area 1 - Update of Weld Design, Testing, and Assessment Procedures for High Strength Pipelines		
Report #	Description	Lead Authors
277-T-01	Background of Linepipe Specifications	CRES/CANMET
277-T-02	Background of All-Weld Metal Tensile Test Protocol	CANMET/Lincoln
277-T-03	Development of Procedure for Low-Constraint Toughness Testing Using a Single-Specimen Technique	CANMET/CRES
277-T-04	Summary of Publications: Single-Edge Notched Tension SE(T) Tests	CANMET
277-T-05	Small Scale Tensile, Charpy V-Notch, and Fracture Toughness Tests	CANMET/NIST
277-T-06	Small Scale Low Constraint Fracture Toughness Test Results	CANMET/NIST
277-T-07	Small Scale Low Constraint Fracture Toughness Test Discussion and Analysis	CANMET/NIST
277-T-08	Summary of Mechanical Properties	CANMET
277-T-09	Curved Wide Plate Tests	NIST/CRES
277-T-10	Weld Strength Mismatch Requirements	CRES/CANMET
277-T-11	Curved Wide Plate Test Results and Transferability of Test Specimens	CRES/CANMET
277-S-01	Summary Report 277 Weld Design, Testing, and Assessment Procedures for High Strength Pipelines	CRES

Focus Area 2 - Development of Optimized Welding Solutions for X100 Linepipe Steel		
Report #	Description	Lead Authors
278-T-01	State of The Art Review	Lincoln
278-T-02	Material Selection, Welding and Weld Monitoring	Lincoln/CANMET
278-T-03	Microstructure and Hardness Characterization of Girth Welds	CANMET/Lincoln
278-T-04	Microstructure and Properties of Simulated Weld Metals	CANMET/Lincoln
278-T-05	Microstructure and Properties of Simulated Heat Affected Zones	CANMET/Lincoln
278-T-06	Essential Welding Variables	Lincoln/CANMET
278-T-07	Thermal Model for Welding Simulations	CRES/CANMET
278-T-08	Microstructure Model for Welding Simulations	CRES/CANMET
278-T-09	Application to Other Processes	Lincoln/CANMET
278-S-01	Summary Report 278 Development of Optimized Welding Solutions for X100 Line Pipe Steel	Lincoln

EXECUTIVE SUMMARY

Long-distance high-strength pipelines are increasingly being constructed for the efficient transportation of energy products. While the high-strength linepipe steels and high productivity welding processes are being applied, the procedures employed for linepipe property specification, welding procedure qualification, and weld integrity assessment remain largely unchanged, particularly from the viewpoint of actual pipeline construction. A significant body of knowledge exists in limited circles of researchers and a minority of large energy companies. However, the broad industry does not benefit from this knowledge until the relevant codes and standards are updated. The use of existing codes without proper consideration of the unique features of the modern high-strength linepipes can lead to higher costs, or, in some cases, reduced safety margins.

The overall objective of this project is to develop understanding of the unique features of modern high-strength girth welds and to incorporate this understanding into actionable tools for the pipeline industry. The work products of this project include:

1. Recommended format for linepipe specifications,
2. All-weld-metal tensile test protocol,
3. Low-constraint SE(T) toughness test protocol,
4. Curved-wide-plate (CWP) test protocol,
5. Material property considerations for weld integrity, and
6. Application and validation of strain-based design technology.

A systematic format of linepipe specifications for traditional stress-based design and new strain-based design is recommended. A few key suggested improvements to the current practice are (1) definition of yield strength, (2) allowable strength range for a given grade of pipe, and (3) quality control in yield strength measurement.

A practical all-weld-metal tensile test protocol is developed and used by a number of labs. Such a protocol enables consistent measurement and evaluation of weld tensile properties. It was found that the definition of yield strength of high strength weld metals should be revised to improve consistency and predictability.

A low-constraint SE(T) toughness test protocol developed at CANMET was applied there and at NIST. The SE(T) test is useful for strain-based design because it simulates service conditions better than conventional toughness tests. Consistent and repeatable results were generated by both labs.

A comprehensive CWP test protocol was developed. This protocol was applied at NIST on a large number of test specimens. Many of the elements in the protocol are world-first innovations, including fatigue pre-cracking, resistance curve generation, uniform data presentation format, and post-test imaging and metallurgical examination. Such a protocol is expected to facilitate the in-depth understanding of material properties by minimizing the influence of inconsistent test procedures.

Key material property considerations are presented for modern high-strength girth welds. Practical treatment of weld strength mismatch is suggested to ensure weld quality without putting undue burden on weld procedure qualification or material specification.

In addition to the assessment of material properties, data quality check is necessary to ensure that the reported data are representative of material properties. It is necessary to make available - to the users of the data - test procedures, raw test data, and post-test data processing routines for certain difficult tests, such as large-scale tests aimed at strain-based design.

Processes and considerations for the strain-based design of new pipelines and maintenance of existing pipelines are outlined. The tensile strain capacity models developed by CRES for DOT and PRCI are evaluated in the context of the current X100 girth welds. The test data show that there can be large differences in measured TSC even within a given test, particularly when the averaged TSC is high, primarily owing to the low rate of work hardening of modern high-strength steels and the consequent differences in strain at a given stress for the same nominal material. CRES TSC models developed for DOT and PRCI show similar consistency in predicting the TSC of X100 CWPs as in predicting the TSC of X60 to X70 full-scale pipes. Overall, predicted TSCs agree well with measured TSCs, although with scatter owing to the reason advanced above. The models offer TSC predictions on the basis of initiation control and ductile instability limit state. Designs on the basis of initiation control are preferred for reasons of safety, practicality, and multiplicity of options for estimating initiation toughness.

A large number of large-scale tests have shown that experimentally measured tensile strain capacities can vary widely even for nominally identical conditions. Such variations are a natural outcome of variation in material properties and the fact that strains are very sensitive to such variations. Such variations should be acknowledged and taken into account in practical designs. In cases where extremely high reliability is needed, a robust tensile strain design can be the one that guarantees no failure at the girth welds.

Gaps in current practice and options for future research directions are discussed. Issues having critical practical implications include (1) low fracture toughness due to pop-in, (2) premature fracture of low-toughness test specimens such as SE(T), and (3) toughness test data scatter particularly for HAZ properties. There are no clear industry guidelines on the treatment of those issues. Further work on those issues can provide significant benefits to the industry.

TABLE OF CONTENTS

EXECUTIVE SUMMARY	vii
TABLE OF CONTENTS	ix
LIST OF FIGURES	xi
LIST OF TABLES	xii
1 INTRODUCTION	1
1.1 BACKGROUND	1
1.2 STATE OF THE ART AT THE START OF THIS PROJECT	1
1.3 INCENTIVES	2
1.4 OBJECTIVES OF THE WORK	3
1.5 SCOPE OF THE WORK	3
2 LINEPIPE SPECIFICATIONS	3
2.1 INCENTIVES AND OBJECTIVES	3
2.2 KEY ISSUES IN LINEPIPE SPECIFICATIONS	4
2.3 RECOMMENDED FORMAT FOR LINEPIPE SPECIFICATIONS	9
2.4 TEST PROCEDURES TO OBTAIN RELEVANT AND CONSISTENT PROPERTIES	11
2.5 SUMMARY RECOMMENDATIONS	12
3 ALL-WELD-METAL TENSILE TEST PROTOCOL	13
3.1 INTRODUCTION	13
3.2 TEST DEVELOPMENT	13
3.3 SUMMARY	14
3.4 TENSILE TEST PROTOCOL	14
4 LOW-CONSTRAINT SE(T) TEST PROTOCOL	23
4.1 INTRODUCTION	23
4.2 SE(T) TEST PROTOCOL – RECOMMENDED PRACTICE	24
5 CURVED-WIDE-PLATE TEST PROCEDURES AND DATA ANALYSIS	30
5.1 HISTORY OF CWP TEST	30
5.2 APPLICATION OF CWP TESTS	31
5.3 KEY CONSIDERATIONS FOR CWP TESTS	31
5.4 GENERIC CONSIDERATIONS FOR SPECIMEN DESIGN AND DIMENSIONS	31
5.5 CURRENT CWP TEST MATRIX	32
5.6 INSTRUMENTATION AND DATA ACQUISITION OF THE CURRENT TESTS	34
5.7 SPECIMEN FABRICATION AND PREPARATION	35
5.8 PREPARATION OF TEST MACHINES	40
5.9 PROCESSING OF RAW DATA	43
5.10 POST-TEST METALLOGRAPHIC EXAMINATION	43
5.11 UNIFORM REPORT FORMAT	44
5.12 GENERATION OF RESISTANCE CURVES	45
5.13 DATA QUALITY CHECK	45
5.14 SUMMARY REMARKS	46
6 EFFECTS OF BASIC MATERIAL PROPERTIES ON WELD INTEGRITY	46
6.1 SCOPE OF THIS SECTION	46
6.2 EFFECTS OF YIELD STRENGTH MISMATCH	46
6.3 EFFECTS OF WELD HIGH-LOW MISALIGNMENT	49
6.4 PREVENTION OF GROSS STRAIN CONCENTRATION AT WELDS	50

6.5	TOUGHNESS CONSIDERATIONS	50
7	STRAIN-BASED DESIGN OF PIPELINES	52
7.1	STRAIN-BASED DESIGN IN PIPELINE CONSTRUCTION AND MAINTENANCE	52
7.2	PHYSICAL PROCESS OF TENSILE STRAIN FAILURES	55
7.3	STATUS OF TENSILE STRAIN MODELS	57
7.4	CRES TSC MODELS FOR DOT AND PRCI	58
7.5	ASSESSMENT OF CWP DATA FOR STRAIN-BASED DESIGN	65
7.6	OBSERVATION OF TSC MODELS AND CWP BEHAVIOR	72
7.7	OVERALL DIRECTIONS IN THE APPLICATION OF TENSILE STRAIN MODELS	73
8	SUMMARY AND CONCLUDING REMARKS	75
8.1	SCOPE OF THE DELIVERABLES	75
8.2	SUMMARY OF MAJOR OUTCOMES	75
8.3	GAPS AND FUTURE WORK	77
9	REFERENCES	79

LIST OF FIGURES

Figure 1:	Stress-strain curves of a “high-strain” pipe and the associated yield strength measured according to current codes [36].....	5
Figure 2:	Schematic all-weld-metal tensile specimen location, round bar	13
Figure 3:	Schematic diagrams of alternative tensile specimens for narrow gap welds	14
Figure 4:	Tensile specimen location in narrow-gap weld cross-section. The top of the photographs are on the outside diameter.....	15
Figure 5:	Schematic diagram of AWM strip tensile blank (Broken lines indicate approximate location of AWM strip tensile in the blank.).....	17
Figure 6:	AWM strip tensile blank, (a) elevation view and (b) plan view showing weld cap on OD	17
Figure 7:	Preparation of AWM strip tensile blank.....	18
Figure 8:	Photographs of blanks etched with 3-5 % Nital (a) reveals cap pass(es), (b) reveals hot/root pass, (c) reveals through-thickness profile	19
Figure 9:	Measurement of weld width for determination of specimen width.....	20
Figure 10:	AWM strip tensile specimen dimensional requirements.....	21
Figure 11:	AWM strip tensile specimen prior to test, (a) bottom (ID) surface visible with hot/root pass, (b) end view	21
Figure 12:	AWM strip tensile test.....	22
Figure 13:	SE(T) sample	25
Figure 14:	Schematic of curved wide plate test gauge instrumentation layout along with labels for the strain gage and LVDT channels (units in mm)	35
Figure 15:	Schematic shows a cross-section view of the girth weld indicating an exaggerated misalignment between pipe sections.....	37
Figure 16:	Schematic showing a cross-section view of the girth weld indicating the placement of the starter notch and subsequent fatigue pre-crack in a specimen designated for HAZ testing.	38
Figure 17:	Schematic of contoured outer span loading supports and straight roller inner span loading arrangement used in four-point-bending fatigue pre-crack of CWPs [58].	39
Figure 18:	Photograph of the test frame, limited in view to the specimen loading configuration.	41
Figure 19:	Gauge section centroid positions for CWP specimens with two pipe geometries;	42
Figure 20:	An illustration of the sectioning plan for each specimen is shown.	44
Figure 21:	Comparison of AWM stress-strain curves (round bar biased to OD and ID and strip specimens) with longitudinal stress-strain curves of the X100 pipe (strap tensile specimens in dashed curves).....	49
Figure 22:	CTOD toughness of the X100 weld at -20°C	52
Figure 23:	Flaw profile evolution relative to remote tensile strain.....	55
Figure 24:	Flaw growth vs. strain history from full-scale pipe tests	56
Figure 25:	Crack opening profile vs. CTOD-strain history from full-scale pipe tests [89].....	56

Figure 26: Crack growth vs. strain history from full-scale pipe tests [90]	57
Figure 27: Typical $CTOD_F$ and definition of initiation-control based limit state.....	58
Figure 28: Definition of ductile-instability based limit state	59
Figure 29: Illustration of deriving $CTOD_A$ from SENT resistance curve.....	65
Figure 30: Comparison of measured TSC with TSC predicted from initiation toughness converted from upper shelf Charpy impact energy.	69
Figure 31: Comparison of measured TSC with TSC predicted from initiation toughness converted from upper shelf Charpy impact energy.	69
Figure 32: Comparison of measured TSC with TSC predicted from initiation toughness converted from standard deeply-notched SE(B) specimens.....	70
Figure 33: Comparison of measured TSC with TSC predicted from initiation toughness taken from SE(T) resistance curves.....	70
Figure 34: Comparison of measured TSC with TSC predicted from instability limit state from SE(T) resistance curves.	71

LIST OF TABLES

Table 1: Reported strength values using current codes [36]	5
Table 2: Recommended test requirements for stress- and strain-based designs	12
Table 3: Coefficients r_j in Eqn. (4-1) for $H/W=10$	27
Table 4: Coefficients t_j in Eqn. (4-6) for $H/W=10$ and $0.1 \leq a_i/W \leq 0.7$	27
Table 5: Coefficients ϕ_j in Eqn. (4-8) for $H/W=10$ and $0.1 \leq a_i/W \leq 0.7$	28
Table 6: Coefficients ψ_j in Eqns. (4-10) and (4-11) for $H/W=10$ and $0.1 \leq a_i/W \leq 0.7$	28
Table 7: CWP test matrix	33
Table 8: CWP notch geometry test matrix for 0.6 mm fatigue pre-crack growth	38
Table 9: Recommended data plots	45
Table 10: Input parameters for the CRES TSC equations	60
Table 11: Constants of TSC equations for GMAW	63
Table 12: Constants of TSC equations for FCAW/SMAW	63
Table 13: Applicable range of TSC equations	64
Table 14: Summary of test conditions and results of 22 CWP specimens used in TSC analysis.....	66
Table 15: Summary of small-scale toughness data and calculated apparent toughness	67

1 INTRODUCTION

1.1 BACKGROUND

Up to the late 1960s, linepipes up to American Petroleum Institute (API) Grade X60 were manufactured from hot-rolled and normalized plates [1]. The introduction of thermo-mechanically (TM) processed plates in the late 1960s enabled the production of higher strength linepipes [2]. More recently, thermo-mechanically controlled processing (TMCP) incorporating accelerated cooling with low interrupt temperatures along with micro-alloying has allowed the production of linepipe steels of grades up to X120 [3,4]. The strength increase was primarily derived from the rolling and cooling processes. The modern linepipe steels could have microstructures ranging from very fine ferrite (sometimes acicular ferrite) with bainite to fully bainite or bainite/martensite. They usually exhibit excellent impact toughness and good resistance to cold cracking in the heat affected zone (HAZ) owing to their low carbon and alloying elements [5,6].

In comparison to the hot-rolled and normalized plates of the 1960's, the new high-strength TMCP steels typically have lower strain hardening and lower ductility [7]. Due to the heavy rolling and high thickness reduction, the material can have a high degree of anisotropy, i.e., different properties in the rolling and transverse directions [7]. In addition, the low-carbon low-alloy chemical composition leads to low hardenability when the steels are transformed from austenite to lower temperature constituents [8], and the fine grain structure achieved by TMCP processing is destroyed in the HAZ. Consequently, the thermal cycles of a welding process can cause regions of the HAZ to soften, i.e., the HAZ having lower strength than the base metal. The potential strain concentration in the softened HAZ and the possible existence of fusion boundary defects and low HAZ toughness can negatively impact the structural integrity of the welds [9,10].

Accompanying the development and application of high-strength linepipe steels is the development of high productivity mechanized welding processes, such as variants of multi-wire gas metal arc welding (GMAW) processes and hybrid laser-GMAW processes. These new processes are increasingly being applied to supplement or replace traditional single-torch and single-wire welding processes [11]. Single-torch tandem, dual torch and more recently, dual tandem GMAW have been evaluated for the production of pipe field girth welds [12]. The characteristics of the weld pool and the cooling rates of the weld and HAZ of these high productivity processes are quite different from those of the traditional single-torch and single-wire GMAW and manual shielded metal arc welding (SMAW) processes [13]. The mechanical properties of the weld metal and HAZ generated with the new welding processes are different from those of the traditional processes even with the same base pipe materials. Understanding the differences in the welding processes and the resulting weld properties is critical to the safe application of these high productivity processes.

1.2 STATE OF THE ART AT THE START OF THIS PROJECT

The application of modern high-strength linepipes in conjunction with more demanding pipeline designs, in particular strain-based design, has necessitated the critical re-evaluation of girth weld tensile and toughness properties to ensure adequate weld strength and weld defect tolerance.

Work at CANMET has clearly shown that girth weld metal strength variations exist not only within a given weld but from weld to weld [14,15,16,17]. Methods to measure toughness under low-constraint conditions have been explored at TWI [18], SINTEF [19], and CANMET [20,21].

The Pipeline Research Council International (PRCI) and the US Department of Transportation (DOT) Pipeline and Hazardous Materials Safety Administration (PHMSA) funded a number of research projects aimed at understanding the weld integrity of high-strength pipelines. Much of this understanding can be incorporated into weld integrity assessment procedures which encompass many aspects of material properties, welding processes, and non-destructive testing (NDT). For traditional stress-based designs in which the control of the hoop stress is the primary concern, these recent efforts involved (1) accounting for reduced strain hardening capacity (high Y/T ratio) of high-strength linepipes, (2) incorporation of weld strength mismatch into weld integrity assessment, and (3) more accurate plastic collapse criteria. A significant part of these efforts has culminated in the revision of API Standard 1104 Appendix A [22,23]. For strain-based designs, which refer to pipeline designs with expected applied longitudinal strains greater than 0.5 % (i.e., plastic deformation), understanding the unique features of high-strength linepipe steels requires much more effort. Preliminary deterministic design procedures have been published in Annex C of CSA Z662 [24] which is the result of multi-year PRCI efforts [25,26,27,28]. Preliminary reliability-based methods have also been developed to account for the natural variations of material properties and loads on pipelines [29].

The integrity of welds is critically dependent on the mechanical properties of the weld metal and HAZ. Attempts have been made to understand the welding thermal history and its effects on weld metal and HAZ properties [14,15,30,31]. It is also important to ensure that the correct region of the weld is being assessed, which requires careful metallography, see, for example, reference [32].

1.3 INCENTIVES

As stated above, modern high-strength linepipe steels present many new challenges in weld design, material specification, and construction. The characteristics of these steels and their welds can also have safety implications. For instance, low strain hardening reduces the “implicit” safety factor for the same design factor, if the failure mode is strength controlled, such as rupture from blunt corrosion defects. HAZ softening, when combined with possible weld strength undermatching, can lead to strain concentration in the weld and HAZ regions [9]. Material anisotropy can affect the buckling resistance [10], which is a critical design and safety issue for pipelines in the arctic regions, seismically active areas, and deep water offshore.

While the new high-strength linepipe steels and high productivity welding processes are being put into service, the procedures employed for linepipe property specification, welding procedure qualification, and weld integrity assessment remain largely unchanged, particularly from the viewpoint of actual pipeline construction. A significant body of research exists on the new high-strength linepipe steels and new welding processes. However, much of the work remains in limited circles of researchers and a minority of large energy companies. Because construction projects are principally governed by codes and standards, broad impact of the research work cannot be realized until relevant codes and standards are updated. For instance, weld strength overmatching (implicitly) assumed in existing codes and standards, which had older and lower

strength steels in mind when they were adopted, cannot be guaranteed in high strength pipelines. The response of the modern high strength linepipes to welding thermal cycles is quite different from that of older and lower strength linepipes. The characteristics of new welds can affect both new constructions in which new girth welds are made and pipeline maintenance in which in-service welding may be needed for system modification and maintenance. The use of existing codes without proper consideration of the unique features of the modern high strength linepipes can lead to higher costs, or in some cases, reduced safety margins. In summary, extending the past practice to new high strength pipelines can potentially reduce safety margins inherent in the past design codes and specifications and can cause serious environmental damage if the risks are not properly mitigated.

1.4 OBJECTIVES OF THE WORK

The overall project objectives are:

- provide guidelines on linepipe steel properties that are essential to specific designs,
- provide guidelines and recommended practices for measuring the strength and toughness of weld metal and HAZ regions that are essential to girth weld integrity,
- establish technical basis towards codifying test procedures that are consistent with the requirements of the linepipe and weld property specifications,
- evaluate weld integrity assessment procedures that can predict weld performance from small-scale material property data.

1.5 SCOPE OF THE WORK

This project is designed to fill the most critical gaps identified at the 2006 Advanced Welding and Joining Technical Workshop and to bring the necessary technology together for the practical use of high-strength pipelines [33]. The main deliverables are:

- format for the specifications of high-strength linepipe properties, particularly tensile properties,
- all-weld-metal tensile test protocol,
- low-constraint fracture toughness test protocol,
- medium-scale test (curved-wide-plate) test protocol, and
- update of weld integrity assessment procedures.

2 LINEPIPE SPECIFICATIONS

2.1 INCENTIVES AND OBJECTIVES

Linepipe tensile properties are a basic governing parameter to all aspects of a pipeline's service life. Here *tensile properties* refer to a comprehensive set of property measures. The most commonly referenced strength parameter, the specified minimum yield strength or SMYS, is only one of the measures. Examples of other measures include ultimate tensile strength, total elongation, yield to tensile (or Y/T) ratio, uniform elongation, and transverse (hoop) vs. longitudinal properties. The significance of these measures may vary, depending on specific design and service conditions.

Some of the planned pipelines to be constructed in remote areas are expected to experience higher longitudinal strains than the vast majority of existing pipelines. The environmental conditions leading to such high strains for onshore pipelines include, but are not limited to, frost heave and thaw settlement in the northern arctic regions, seismic activities, slope instabilities, and mine subsidence. Due to the long distance to be covered by those pipelines, there are economic incentives to use high-strength linepipes and high design factor, e.g., 0.80 vs. the more traditional 0.72 for Class 1 designs. For offshore pipelines, high longitudinal strains can exist in the event of lateral and upheaval buckling for pipelines transporting hot fluids, spanning, or pipe lay by reeling.

To ensure pipeline safety and integrity, it is necessary to examine linepipe specifications and new design concepts under the new material and loading conditions. The overall objective of the activity described in this section is the development of a requisite format for linepipe specifications for new design concepts and new pipeline environments, particularly for the strain-based design. The focus is on the tensile properties of linepipes and their influence on the pipeline performance. The alloy design of steels, plate and coil rolling practice, and pipe manufacturing process have profound effects on the resulting mechanical properties of the linepipes. The control of these manufacturing parameters to achieve the desired properties is not a part of this report.

2.2 KEY ISSUES IN LINEPIPE SPECIFICATIONS

2.2.1 Measurement of Yield Strength

2.2.1.1 Nature of the Yield Strength Definition

The yield strength is a fundamental parameter that affects all phases of a pipeline's life, including design, construction, and maintenance. The yield strength is typically reported as the strength at 0.5 % total strain or the strength at the 0.2 % offset strain [34,35]. In response to the requirements for strain-based design, a number of pipe manufacturers have developed manufacturing processes aimed at improving the stress-strain response of the linepipes, including having so-called round-house stress-strain curves (without obvious yield point and Luder's extension), high strain hardening, and resistance to strain ageing during pipe coating [36,37,38]. A representative stress-strain curve is shown in Figure 1 [36]. When the yield strength is measured at either 0.5 % total strain or 0.2 % offset strain, the reported yield strength, as given in Figure 1 and Table 1, can be much lower than the "physical" yield strength, which may be understood as the "knee" of the stress-strain curve. A low yield strength directly leads to a low Y/T ratio. The strength values reported by in Table 1 for a high-strength steel cannot be viewed as representative of the material's true yield strength. Under-representation of the yield strength is attributable to the nonlinearity in the "elastic" part¹ of the stress-strain curve prior to reaching the 0.5 % total strain and its effect on reported yield strength when using the current definition of yield strength. For this type of high-strength material with nonlinear "elastic" behavior, using

¹ The source of nonlinearity prior to the "knee" of the stress-strain curve is not well understood. It's not known if the nonlinearity is fully reversible when the stress level is reduced to zero. Micro-scale plasticity may explain the nonlinearity if the nonlinearity is not fully reversible.

the 0.2 % offset strain for the measurement of yield strength produces similar under-representation of the material’s yield strength.

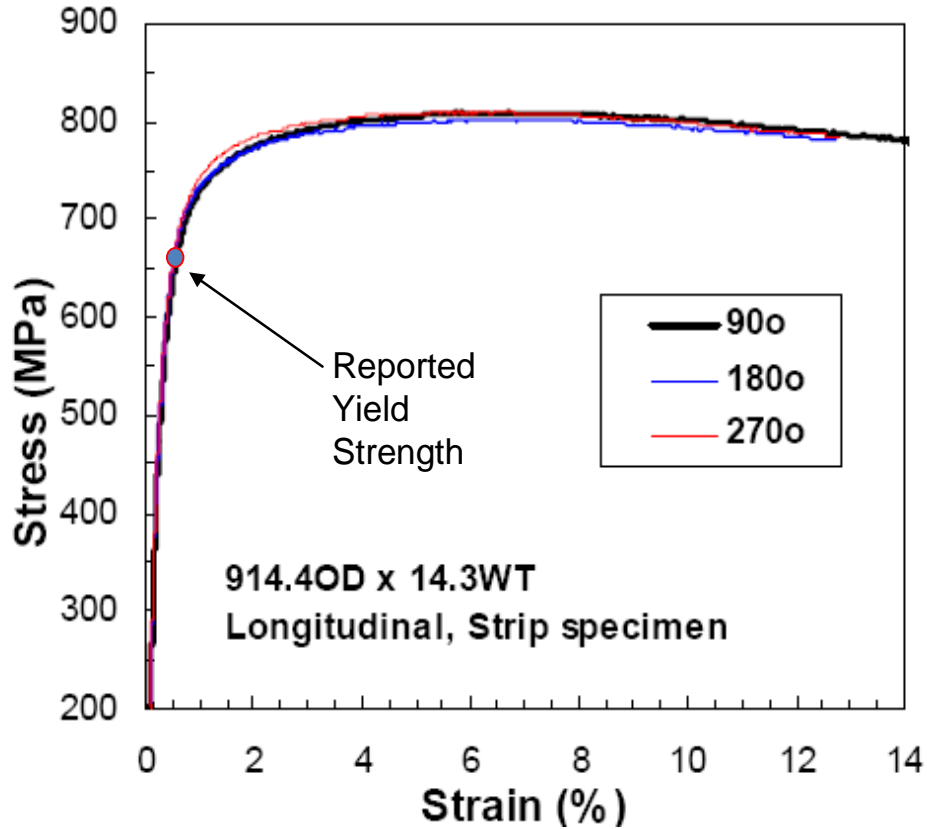


Figure 1: Stress-strain curves of a “high-strain” pipe and the associated yield strength measured according to current codes [36]

Table 1: Reported strength values using current codes [36]

Pipe No.	Direction	Base metal tensile properties *1					Trans weld
		YS (MPa)	TS (MPa)	Y/T (%)	uEl (%)	σ_r *2 $\sigma_{1.5}/\sigma_{0.5}$	TS (MPa)
A	Trans.	713	824	87	-	-	819
	Longi.	668	835	80	7.3	1.17	-
B	Trans.	713	836	85	-	-	825
	Longi.	659	811	81	6.9	1.18	-

*1 Trans: round bar specimen, Longi.: Rectangular strip specimen

*2 Stress ratio, defined by the ratio of stress at $\epsilon=1.5\%$ to that at $\epsilon=0.5\%$ ($\sigma_{1.5}/\sigma_{0.5}$)

2.2.1.2 Implications of the Yield Strength Definition

Having proper representation of the yield strength of the linepipe is critical for a wide variety of pipeline design and maintenance considerations.

One of the fundamental problems in having a yield strength measured on the elastic part of the stress-strain curve is that the reported values can have large variations from one test to another, even when the overall stress-strain responses are almost identical. The large variations of the reported yield strength introduce uncertainties about the strength of linepipes. Such uncertainties can be a major headache for virtually every stakeholder, including pipe mills, pipeline owner companies, pipeline designers, and pipeline construction contractors.

Strain hardening has been recognized as one of the critical parameters in strain-based design [39]. The strain hardening capacity of linepipe materials is often expressed in terms of the Y/T ratio. The under-representation of the yield strength leads to overly optimistic representation of the strain hardening capacity characterized by the Y/T ratio.

One of the most critical considerations in strain-based design is the weld strength mismatch level. It is now generally accepted that weld strength overmatching is preferred for strain-based design. One of the most common definitions of weld strength mismatch is based on the yield strengths of base metal and weld metal. If the yield strength of the pipe material is under-represented but not that of the weld metal, the weld mismatch level can in turn mis-represent the true strength difference between the pipe material and the weld metal. The under-representation of the yield strength can give an impression that the weld metal overmatches the pipe material by a very large margin if the strength mismatch is measured by the yield strength. The full stress-strain curves would suggest that the overall degree of overmatching is much lower.

Consumable manufacturers rely on the mismatch requirements for their product development and delivery. When the yield strength of the pipe material is artificially under represented, pipe mills may choose to increase the overall strength level to meet the yield strength requirement. The increased strength level of the pipe would lead to an increased strength requirement of the weld metal. At very high strength level, the weld metal ductility and toughness may have to be sacrificed to meet the strength requirement.

2.2.2 Upper Bound of Linepipe Strength

2.2.2.1 Upper-Bound Strength Limits in Current Standards

In API 5L and ISO 3182 [34,35], the permissible upper-bound strength is significantly higher than the specified minimum strength for PSL 2 pipes [34,35]. There are no upper bound limits for PSL 1 pipes. For instance, for pipe grades X70 and lower, the upper-bound ultimate tensile strength (UTS) is 758 MPa (110 ksi) for PSL 2 pipes. For grades X80 to X100, the upper-bound yield strength is about 150 MPa higher than the SMYS. For grade X120, the upper-bound yield strength is about 220 MPa higher than the SMYS. For grades X80 and X90, the upper-bound UTS is about 200 MPa and 220 MP higher than the specified minimum UTS, respectively. For X100 and X120, the upper-bound UTS is 230 MPa higher than the specified minimum UTS.

2.2.2.2 Implications for High Upper-Bound Strength

One of the major concerns about the upper limits of yield strength and UTS is its potential impact on the actual weld metal strength mismatch level. Weld strength overmatching relative to the pipe body strength is generally considered preferable in design and construction to prevent

strain localization in the weld region. The wide range of tensile properties permitted for a given grade of linepipe makes it difficult to select proper consumables and welding processes to achieve a certain level of desired mismatch. For instance, the specified minimum yield strength of X80 pipes is 555 MPa and the upper-bound limit of the yield strength is 705 MPa.

assume that the yield strength of the weld is at 630 MPa, i.e., the average of the SMYS and the upper-bound yield strength. This 630 MPa yield strength produces 13.5 % overmatching if the pipe yield strength is at the SMYS or 10.6 % under matching if the pipe yield strength is at the upper-bound value of 705 MPa. To achieve consistent overmatching, the lower bound of the weld strength would have to be higher than the upper-bound pipe strength. For X80 pipes this implies that the yield strength of the weld has to be greater than 705 MPa and the UTS greater than 825 MPa (120 ksi). The control of the welding processes will have to be very precise to have the weld metal at this strength level while maintaining adequate toughness and ductility. Such requirements are achievable with well-controlled mechanized GMAW processes. However achieving the same strength and toughness level for FCAW and SMAW processes can be a challenge. For pipes of grades greater than X80, achieving consistent weld strength overmatching can become even more challenging for most of the welding processes on the market.

From the viewpoint of pipe performance, there is no good reason to have the upper limit of UTS for pipe grades X70 and lower at 758 MPa (110 ksi). Such a limit does offer the flexibility of marketing pipes of the same strength level in multiple grades. For instance, pipes meeting X70 strength requirements may be sold as X60 or even lower grades. It should be noted that welding procedure qualifications are often performed by pipe grade. If a procedure qualified on X52 is applied to pipes with an actual strength level of X70, there could be a high possibility of weld strength undermatching. The undermatching condition is generally not a concern from the viewpoint of traditional pipeline design, which is based on limiting the hoop stress to a certain percentage of the SMYS. However, threats to girth weld integrity are often associated with ground movement hazards. Having undermatching girth welds can cause strain concentrations in the girth welds, thus potentially increasing the likelihood of girth weld failures.

2.2.3 Y/T Ratio

2.2.3.1 Maximum Y/T Ratio Limits in Current Standards

In API 5L and ISO 3182, the maximum permissible Y/T ratio for X80 pipes is 0.93 [34, 35]. The maximum Y/T limits are incrementally increased to 0.95, 0.97, and 0.99 for X90, X100, and X120.

2.2.3.2 Implications of High Y/T Ratio

The pipeline industry has very limited experience with linepipes having Y/T ratio greater than approximately 0.93. The allowance of higher Y/T ratio brings many unknowns. Even in the domain of traditional stress-based design, certain implicit assumptions about material's strain hardening capacity are made in various stages of operation and maintenance. For instance, corrosion assessment tools were calibrated and validated with materials not having extremely high Y/T ratios. The applicability of those tools in the context of very high Y/T ratios is unknown and should be critically evaluated. Pipelines designed by traditional stress-based

principles may still experience certain displacement controlled loading after the pipelines are put in service, such as in the event of ground settlements. The extremely high Y/T is expected to have a negative impact on the tolerance to this type of loading.

2.2.4 Representation of Strain Hardening

The Y/T ratio is often used as an approximation of a material's strain hardening capacity. This simplified representation is meaningful only when the reported yield strength of the material is reasonably close to the physical yield strength. If the reported yield strength is significantly lower than the physical yield strength of the material due to a nonlinearity in the "elastic" part of its stress-strain curve as described in Section 2.2.1, the use of Y/T ratio to represent strain hardening is potentially non-conservative.

Instead of using the Y/T ratio as an approximation of a material's strain hardening capacity, its entire stress-strain curves may be fitted into a mathematical relation, such as the CSA Z662 format or Ramberg-Osgood format. The strain hardening exponents of these mathematical formats provide more complete representation of the strain hardening capacity than the Y/T ratio. It should be recognized that the stress-strain curves of the modern "high-strain" pipes typically do not fit into one single CSA Z662 or Ramberg-Osgood stress-strain relation. In the low strain range (e.g., when the engineering strain is less than ~3 %), the plastic part of the stress-strain curve typically have much high strain hardening rate than the curve at higher strain range (e.g., engineering strain is greater ~3 %). Consequently, these two parts of the curves cannot be accurately represented by a CSA Z662 or Ramberg-Osgood stress-strain relation with a single strain hardening exponent.

2.2.5 Anisotropy

2.2.5.1 Nature of Anisotropy

Modern high-strength linepipe steels can have highly anisotropic mechanical properties due to the textures created in the plate/coil rolling processes and the deformation induced by the pipe forming and expansion processes. The degree of anisotropy can vary, depending on the steel rolling practice and pipe forming processes. The anisotropy can manifest itself as differences between the properties in the longitudinal and hoop directions in (1) yield strength, (2) UTS, and/or (3) shape of the stress-strain curves. In most cases, the difference in UTS is less than that in yield strength. The shape of the stress-strain curves can be quite different in the two directions. Strain ageing may increase the differences between the longitudinal and hoop properties and thus further exacerbating the anisotropy.

2.2.5.2 Implications of Anisotropy

Anisotropy can have strong impact on the strength and strain capacity of pipelines [40]. One immediate impact is on the girth weld procedure qualification. One of the required tests in the weld procedure qualification is the cross-weld tensile test. The UTS from test specimens is required to be equal to or higher than the specified ultimate tensile strength of the pipe. For large diameter welded pipes, the pipe strength is qualified on the basis of hoop tensile properties. Current linepipe standards, API 5L and ISO 3183, do not require testing of longitudinal tensile

specimens. Some have argued that the minimum tensile property requirement in the cross-weld tensile tests should be lower, as the longitudinal strength of the pipes could be lower than the hoop strength. Pipes with longitudinal UTS lower than the specified minimum UTS (hoop direction) could meet the API 5L and ISO 3183 requirements, as no longitudinal property is required. Published test data have shown that the tensile strength in the longitudinal direction can be either lower or higher than that in the hoop direction, depending on the type of pipes (UOE vs. spiral) and the plate/coil manufacturing practice. Without a complete picture of the anisotropy, it is difficult to form a consensus on the requirements of the weld procedure qualification.

2.3 RECOMMENDED FORMAT FOR LINEPIPE SPECIFICATIONS

2.3.1 Recommendations for Yield Strength Definition

Two possible options may be considered for revising the definition of the yield strength so that the physical yield strength of the materials can be accurately captured.

The first option is to set the strain value at which the yield strength is defined as a variable that is tied to the pipe grade. For instance, the strain value may be set at 0.5 % for X70 and 1.0 % for X100. A linear scaling factor may be applied to grades in between. For instance, the strain at which the yield is defined for X80 would be $0.5 + 1/3 \times 0.5 = 0.67$ % and 0.83 % for X90. The downside of this approach is that the actual strength of a pipe of the same grade can vary greatly. If the actual yield strength of an X80 pipe is close to 689 MPa (100 ksi), it requires further thought to determine if the material should be treated as X80 or X100 in terms of selecting the strain value at which the yield strength is defined.

The second option is to define the yield strength by specifying a predefined slope on the stress-strain curve. The “turning point” from the elastic to the plastic part of the curve is the yield point. This definition is theoretically the most rigorous. However, it can be difficult to apply within the framework of current practice. Most of the commercial test labs and perhaps pipe mills are not equipped to producing full stress-strain curves. However, the technology is available to automate the data acquisition and post-test data processing, so the yield strength can be uniquely determined from the stress-strain curves.

The implementation of the two proposed options is predicated on the assumption that high-quality raw data are reliably and consistently generated. Procedures for data quality check are described in Section 2.4.

2.3.2 Recommendation for Upper Bound Strength Limit

For pipe grades X70 and lower, the upper-bound limits should be revised. At a minimum, the upper-bound limits should be correlated to the SMYS, similar to the limits of higher grades, such as X80 and X90.

The possibility of lowering the upper-bound limits should be explored, particularly for higher grades, i.e., X70 and above. Lowering the upper-bound limits would reduce the likelihood of girth weld strength undermatching. Experience has shown that a yield strength range of 120

MPa (17.4 ksi) between the SMYS and upper limit is possible. For UTS, a range of 150 MPa (21.8 ksi) is possible. The feasibility of those limits may depend on the production characteristics of pipe mills. At a minimum, pipe specifications should take into account the possible strength level of girth welds. There should be a plan to assess the impact of the strength distributions of the linepipes and the girth welds.

2.3.3 Recommendation for the Representation of Strain Hardening

The strain hardening capacity may be represented by one of three options, depending on the shape of the stress-strain curves.

- *Option 1, Y/T ratio.* This representation is simple. However it is meaningful only when the reported yield strength is reasonably close to the physical yield strength.
- *Option 2, strain hardening exponent of a mathematical stress-strain relation.* The most commonly used forms are the CSA Z662 stress-strain relations and Ramberg-Osgood power-law hardening relations. The goodness of fit for the entire stress-strain curve should be checked.
- *Option 3, two-piece power-law stress-strain relations.* This option may be necessary for the stress-strain curves of the modern “high-strain” pipes. There could be two separate power-law fits to the low and high strain ranges, respectively.

2.3.4 Recommendations for Tensile Tests

This section covers the key considerations for tensile tests: test specimen geometry, specimen dimensions, and instrumentation. The current practice of using flattened traps has served the industry well. The practice may be continued for lower grade pipes, i.e., X70 and lower. For higher grade pipes, this practice can lead to underrepresentation of the yield strength of the pipe with the current yield strength definition at 0.5 % total strain or 0.2 % offset strain. It is in the interest of all stakeholders, including pipe mills and pipeline owner companies to move away from testing flattened straps for high grade pipes.

2.3.4.1 Test for Hoop Properties

The following recommendations are for high-strength linepipes (X80 and higher) and those linepipes for strain-based design:

- Round-bar specimens without flattening should be tested for hoop properties.
- Within the reduced gauge section of the specimen where the test data are taken, the length-to-diameter ratio should be no less than four.
- The mounting points of the extensometer should be sufficiently far away from the shoulder (the transition zone from the reduced gauge section to the end tab) to assure uniform deformation within the gauge section.
- The diameter of the reduced gauge section should be as large as possible while meeting the requirement of length to diameter ratio.

2.3.4.2 Test for Longitudinal Properties

Testing for longitudinal properties is mandatory for strain-based design. Such testing is optional for traditional stress-based design.

- Full thickness strap or round-bar specimens should be tested for longitudinal properties.
- The specimen should be of “dogbone” shape with a reduced gauge section in the middle of the specimen.
- No parallel-sided strip specimens, similar to those in the main body of API 1104 20th Edition, should be used.
- Within the reduced gauge section where the test data are taken, the length over the diameter/thickness ratio should be no less than four.
- The mounting points of the extensometer should be sufficiently far away from the shoulder to assure uniform deformation within the gage section.
- The diameter of the reduced gage section should be as large as possible for the round-bar specimens.
- Different total elongation values may be specified for the round-bar or full-thickness specimens.

2.3.5 Recommendation for Round-House Behavior

The following definition is proposed for the portion of the stress-strain curve, with the strain less than 50 % of the uniform strain: “A stress-strain curve is deemed to have round-house shape if any region in which the stress decreases is limited to a stress drop no greater than 0.5 % of UTS and a strain range no greater than 0.2 %.” The stated requirements allow for stress plateaus or even dip in stress values, provided that this occurs within a small strain increment of 0.2 %.

2.4 TEST PROCEDURES TO OBTAIN RELEVANT AND CONSISTENT PROPERTIES

2.4.1 Test Temperature

The test temperature can affect both tensile and toughness properties. Ideally, mechanical tests should be done at temperatures corresponding to the postulated failure events. Alternatively, the effects of temperature should be considered and corrections applied.

2.4.2 Test Specimen Geometry and Dimensions

For the same material, the reported mechanical property data are affected by the test specimen geometry (e.g., round bar vs. rectangular strip) and dimensions. To the extent possible, full thickness properties are preferred to partial thickness properties. For tensile tests aimed at yield strength measurement, it is necessary to ensure that the gauge section within the mounting points of the extensometer experience uniform straining.

2.4.3 Data Check for Elastic Slope

The initial part of the stress-strain curve should be checked against theoretical elastic modulus. The initial slope of the stress-strain curve at the stress level up to one third of the UTS should be computed and compared with the elastic modulus. If the initial slope differs by more than 10 %

from the theoretical value, possible sources of the discrepancy should be examined. After the possible sources of systematic errors are eliminated, the test data may be updated by applying a compliance correction.

2.4.4 Data Check for Uniform Elongation

When the stress-strain curves are flat around the point of UTS, a curve fit around the point should be conducted to “smooth” out the local data oscillations. The point of UTS should be determined by obtaining the maximum stress level of the fitted curve. The corresponding uniform elongation can be obtained accordingly from the same procedure.

2.5 SUMMARY RECOMMENDATIONS

A summary of current and proposed tensile property requirements is given in Table 2. The generic issues are relevant to both stress- and strain-based designs. Reducing the upper-bound limits of strength distribution can yield benefits for both design conditions. For strain-based design, the additional requirements are associated with longitudinal properties and the characterization of full stress-strain curves.

Table 2: Recommended test requirements for stress- and strain-based designs

Property Parameters	Orientation	Features	Current Requirement	Stress-based design in addition to the generic issues	Strain-based design in addition to the generic issues	Generic Issues to Be Considered
Yield Strength and UTS	Hoop	Test Form	Flattened strap	Round bar and/or ring expansion	Round bar and/or ring expansion	Definition of yield strength, test specimen form and dimensions, test temperature, effects of strain ageing, effects of cyclic plastic strain
		Minimum	Yes	Yes	Yes	
		Maximum	No for PSL 1, Yes for PSL 2	Yes	Yes, lower than the current code limits	
	Longitudinal	Test Form	Not required	Optional, Full-thickness strap or round bar	Full-thickness strap or round bar	
		Minimum	Not required	Optional	Yes	
		Maximum	Not required	Optional	Yes	
Y/T Ratio	Hoop	Maximum	No for PSL 1, Yes for PSL 2	Yes	Yes	
	Longitudinal	Test Form	Not required	Optional	Yes	
Total Elongation	Hoop	Minimum	Yes	Yes	Yes	
	Longitudinal	Minimum	Not required	Optional	Yes	
Uniform Strain or Elongation	Hoop	Minimum	Not required	Optional	Optional	
	Longitudinal	Minimum	Not required	Optional	Yes	
Shape of Stress-Strain Curve	Hoop		Not required	Optional	Optional	
	Longitudinal		Not required	Optional	Yes	

3 ALL-WELD-METAL TENSILE TEST PROTOCOL

3.1 INTRODUCTION

Narrow-gap welds, in general, present unique challenges in the measurement of all-weld-metal tensile properties because the geometry of the weld makes it difficult to extract all-weld-metal test specimens of reasonable size. Test specimen extraction from narrow-gap pipe welds can be even more challenging due to pipe curvature. For multiple-pass arc welds in particular, industry practice is to use the largest standard [41] test specimen possible without running the risk of incorporating HAZ or base material in the reduced section of what is intended to be an all-weld-metal test. One such example is the specification for SMAW electrodes [42], where the size of the round bar specimen changes with the volume of the weld joint employed. This practice ensures that the measurement of tensile properties is representative of the weld metal as a whole and not merely an incremental snapshot of a small region within the weld metal. Figure 2(a) illustrates how the reduced section of the round bar tensile specimen in a conventional groove weld samples a relatively large fraction of the weld metal. In the narrow groove weld the largest round bar tensile specimen that can be used samples a small fraction of the total weld area (Figure 2 (b)). Depending on the specific placement of the small round specimen with respect to the weld pass sequence, the result measured is more likely to be determined by a single weld pass or reheat zone and is less likely to represent the performance of the weld as a whole.

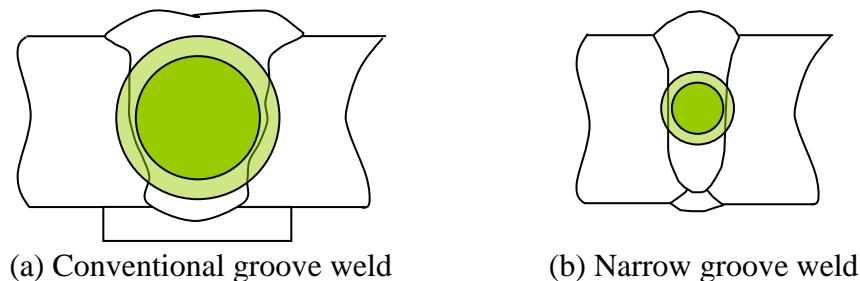


**Figure 2: Schematic all-weld-metal tensile specimen location, round bar
(Dark green area represents tensile specimen reduced section)**

This situation is of particular concern for strain-based design (SBD) pipeline applications, where narrow groove weld joints are commonly used for automatic GMAW of girth welds, and reliable tensile properties measurements are essential in determining the strain capacity of the weld.

3.2 TEST DEVELOPMENT

CANMET-MTL has developed alternatives to the conventional round bar test specimen for narrow gap welds in large diameter line pipe [14,15,43,44,45]. Initial work with multiple round bar specimens, Figure 3(a), demonstrated a wide variation in tensile properties due to local conditions within the weld metal. Averaging the outside diameter (OD) and inside diameter (ID) results proved to be a better representation of the weld metal, as a whole, than the individual measurement of local conditions. Ultimately, this led to the strip specimen illustrated in Figure 3(b). The strip specimen has been used successfully to document the tensile properties of girth weld metal in both X80 and X100 applications.

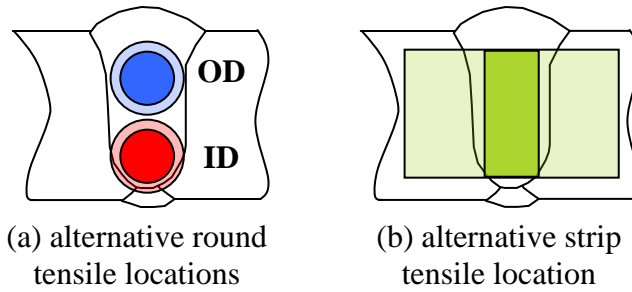


Figure 3: Schematic diagrams of alternative tensile specimens for narrow gap welds

3.3 SUMMARY

A standard testing protocol was developed for this program to ensure the consistency of tensile property measurements among the laboratories involved. While CANMET-MTL conducted most of the tensile tests, the mechanical testing laboratory at The Lincoln Electric Company also adapted the methods for narrow-gap welds. These included the tensile property measurements for narrow-gap plate welds and the Round 3 pipe welds. The testing protocol presented here, represents the work of both laboratories. Additional detail on the application of the strip specimen to this program is reported by Gianetto *et al* [46]. The testing protocol presented here is specific to the pipe diameters and pipe wall thicknesses employed in this program.

3.4 TENSILE TEST PROTOCOL

3.4.1 Scope

This recommended practice describes a method to measure the all-weld-metal tensile properties in narrow-gap welds. While the methodology can be used for narrow-gap welds in plate, this practice addresses the specific case of narrow-gap girth welds in large diameter linepipe. It differs from other weld metal testing methods in that the specimen configuration has been modified to sample as much of the weld fusion zone as possible. In this way, results will be representative of the weld metal as a whole and not dominated by the local conditions in a single weld bead or reheat region.

3.4.2 Purpose and Intended Use

The tensile test protocol described herein is intended for assessment of narrow-gap pipeline girth welds with emphasis on strain-based design pipeline applications where weld strength overmatching in relation to actual pipe properties is a design requirement. In the narrow groove geometry, the all-weld-metal strip test specimen and corresponding test procedures provide better quantification of weld metal strength than is possible with the traditional round bar tensile test specimen. By use of the all-weld-metal strip test, it is possible to significantly increase the cross-sectional area of the specimen in the weld and sample a greater percentage of the fill passes, as shown in Figure 4. Also, to support SBD applications it is intended that the full stress-strain curve be determined for each tensile test.

The instructions provided for test specimen preparation are specific to narrow-gap welds made in two sizes of pipe:

- 19 mm (0.750 in) nominal wall thickness, 914 mm (36 in) diameter and
- 14.3 mm (0.563 in) nominal wall thickness, 1067 mm (42 in) diameter.

The general approach may be applied to other girth welds produced in pipe of different diameters or wall thicknesses by modifying the length, width, and thickness dimensions. However, application to nominal pipe diameter below 762 mm (30 in) is not considered feasible because the pipe curvature will limit specimen length and/or thickness to the point that there will be little, if any, advantage over a conventional round bar test specimen.

Testing of the specimens is to be conducted in accordance with ASTM E8/E8M. Additional information relevant to the AWM strip test specimen configuration is provided when applicable.

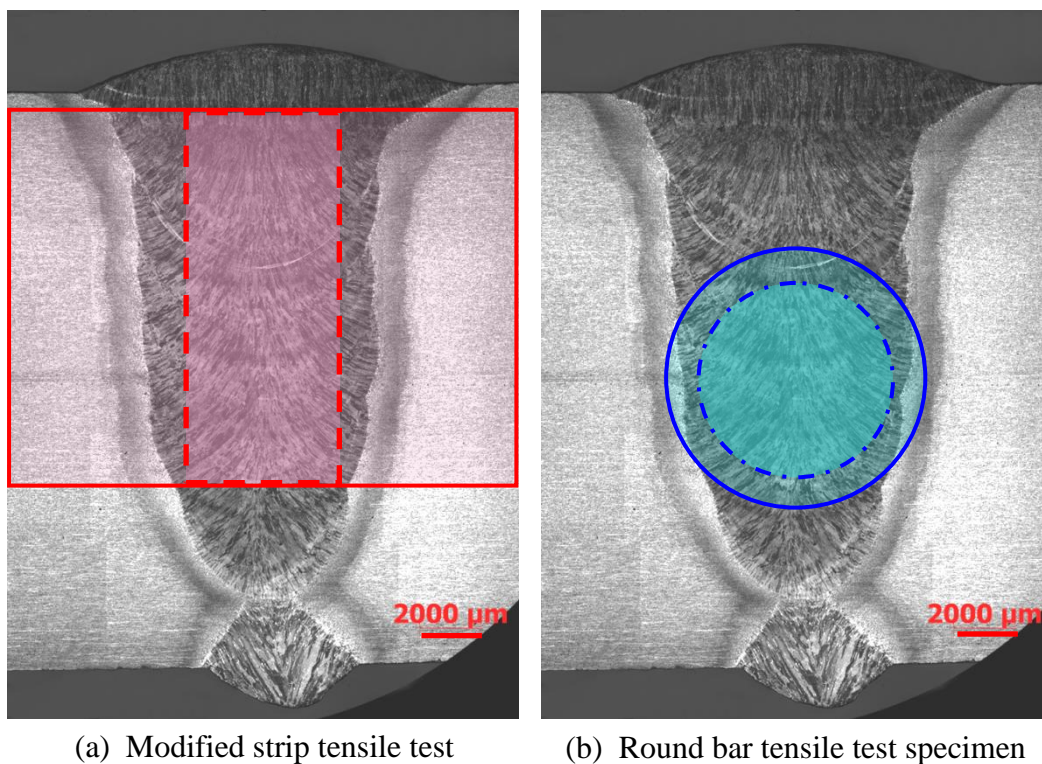


**Figure 4: Tensile specimen location in narrow-gap weld cross-section. The top of the photographs are on the outside diameter.
(Darker shaded area in the middle of each test specimen indicates the reduced section of the gauge length.)**

3.4.3 Referenced Documents

- ASTM E8/E8M-09, Standard Test Methods for Tension Testing of Metallic Materials, ASTM International, West Conshohocken PA US
- AWS B4.0: 2007, Standard Methods for Mechanical Testing of Welds, 7th Edition, American Welding Society, Miami FL, US

3.4.4 Terminology

ASTM E8/E8M standard terminology applies.

3.4.5 Test Specimen

The all-weld-metal strip tensile specimen is a rectangular tension test specimen, modified from ASTM E8/E8M. The requirements and recommendations of ASTM E8/E8M apply, except as modified herein.

As illustrated in Figure 4(a), the AWM strip tensile specimen is shifted toward the weld cap, or OD, to ensure that a majority of weld fill passes are sampled. The height and width of the reduced section of each modified strip tensile specimen are governed by the actual width of the weld fusion zone in each case. This is influenced by the pipe diameter, pipe wall thickness, weld joint details, any high/low misalignment at the root, etc. Therefore, the layout of the specimen in the weld and correct positioning of the gauge section at the middle of the specimen is essential to ensure that the test measure all-weld-metal tensile properties.

3.4.5.1 Test Specimen Blank(s) Preparation

One blank, 82 mm (3.25 in) minimum along the circumference by 70 mm (2.75 in) minimum transverse to the weld, is needed for each AWM strip tensile specimen. The 70 mm (2.75 in) dimension must be roughly centered on the weld.

It is recommended that saw cutting, or other mechanical mean, be used to remove the blank(s) from the pipe girth weld. If flame cutting is used to rough cut the blank(s), a distance of at least 203 mm (8 in) must be maintained from the girth weld centerline to ensure that the weld region is not overheated. If further flame cutting is used to cross the girth weld (*e.g.* to produce smaller rings or curved sections of pipe weld), add at least 25.4 mm (1 in) to the rough blank length since the grip ends of the AWM strip tensile specimens are relatively short and any overheating of the gage section must be avoided.

1. Locate and mark the nominal position(s) where rectangular blank(s) are to be cut from the girth weld. This is generally indicated by clock position for pipe welds. However, any means of uniquely identifying the location of each test block with regard to circumference on the pipe is acceptable. This information must be reported with the test result.
2. Cut the blank(s) from the pipe girth weld, as indicated in Figure 5. Initial cuts can be made normal to the pipe wall so that further machining will produce rectangular blank(s) that are tangent to the pipe outer and inner walls at mid-length. The excess pipe material on either side of the weld should be cut parallel to the weld longitudinal axis to obtain blank(s) that are centered on the weld.

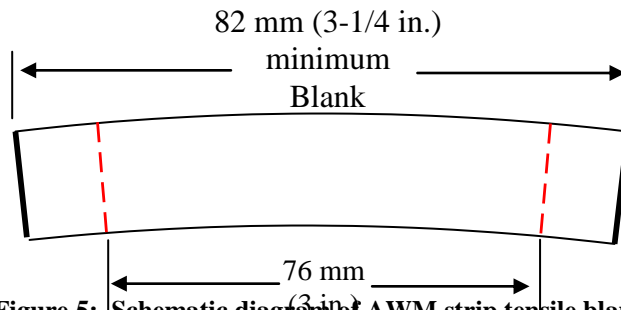


Figure 5: Schematic diagram of AWM strip tensile blank
 (Broken lines indicate approximate location of AWM strip tensile in the blank.)

- Machine and grind both ends parallel, Figure 6(a). Etch the ground ends to locate the weld centerline. Then, machine the two curved sides, Figure 6(b), parallel to the weld centerline and square with the ends.

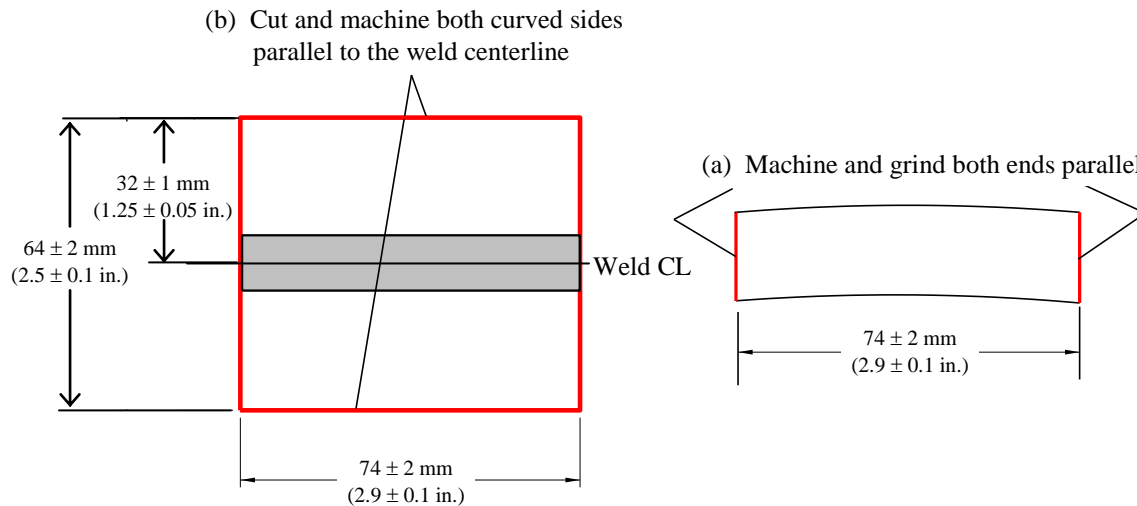


Figure 6: AWM strip tensile blank, (a) elevation view and (b) plan view showing weld cap on OD

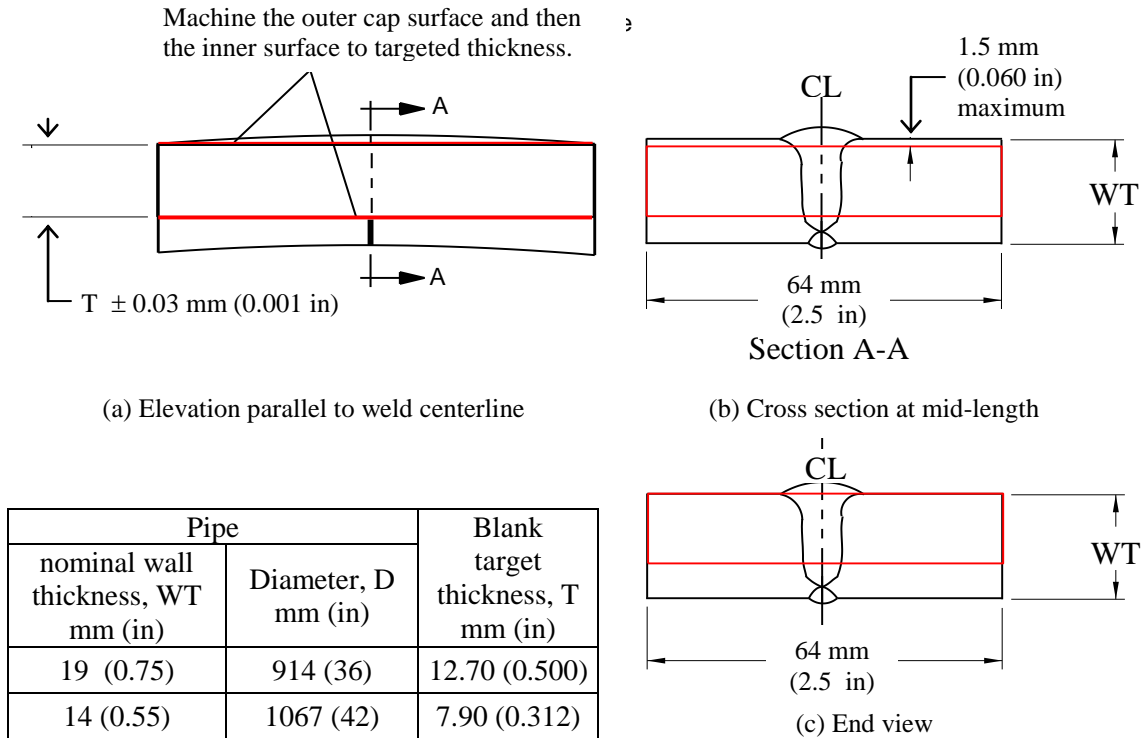


Figure 7: Preparation of AWM strip tensile blank

- Machine the outer (OD) surface flat by removing no more than 1.5 mm (0.060 in) at the mid-length, Figure 7. Machine the inner (ID) surface flat to achieve target thickness, T, as indicated.
- Etch top and bottom surfaces to make weld fusion zone clearly visible on four surfaces, Figure 8. Note that the ends should have been etched at 3.4.5.1.. Re-etch ends, as needed, to ensure that the weld fusion zone is visible on four sides as illustrated in Figure 8. Relocate and re-scribe weld centerline on both ends as needed for visibility.
- Scribe weld centerline on bottom (ID) surface in line with the scribe lines on both ends. At mid-length on the bottom (ID) surface, check to ensure that the scribe line is actually centered in the weld. Measure the weld width at this location and subtract 0.5 mm (0.020 in) to determine finished width of the AWM strip tensile specimen reduced section, w in Figure 9, to the nearest 0.1 mm (0.005 in). This reduction is needed to ensure that only weld metal is in the gauge section.

3.4.5.2 Test Specimen Preparation

- Prepare a single all-weld-metal tensile test specimen from each blank. Figure 8 illustrates three views of etched blanks. Note the rough edges still remaining on the outer (OD) surface, Figure 8(a), to one side of the weld (towards top of photograph). This condition is caused by variation in pipe alignment (*e.g.* high/low condition) that can exist around the circumference of a pipe girth weld. If these regions are sufficiently narrow that the

grip area of the finished specimen will be adequate to conduct the tensile test, proceed with test specimen preparation. Otherwise, reduce the target thickness and repeat 3.4.5.1.4 for the outer (OD) surface. Figure 8(b) illustrates the bottom (ID) surface revealing the hot/root pass. It is this surface that is used to determine the final width of the finished AWM strip tensile specimen at the reduced section. The end view in Figure 8(c) is used to establish weld centerline, as described previously.

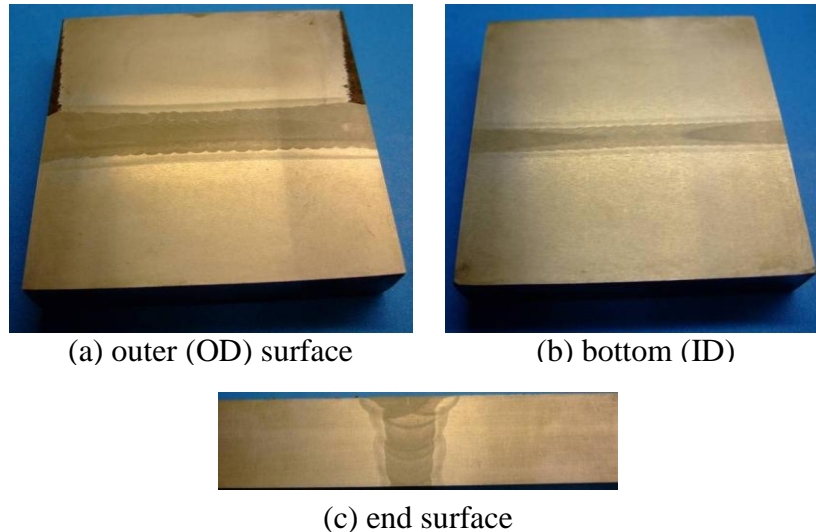


Figure 8: Photographs of blanks etched with 3-5 % Nital
(a) reveals cap pass(es), (b) reveals hot/root pass, (c) reveals through-thickness profile

- 2. Reduced Section Width** - Determine the test specimen width from the width of the weld fusion zone on the bottom (ID) surface, as illustrated in Figure 9. At the mid-length, measure the weld width. Subtract 0.5 mm (0.020 in) to determine the finished width w of the AWM strip tensile specimen reduced section. This reduction is needed to ensure that only weld-metal is in the gauge section.

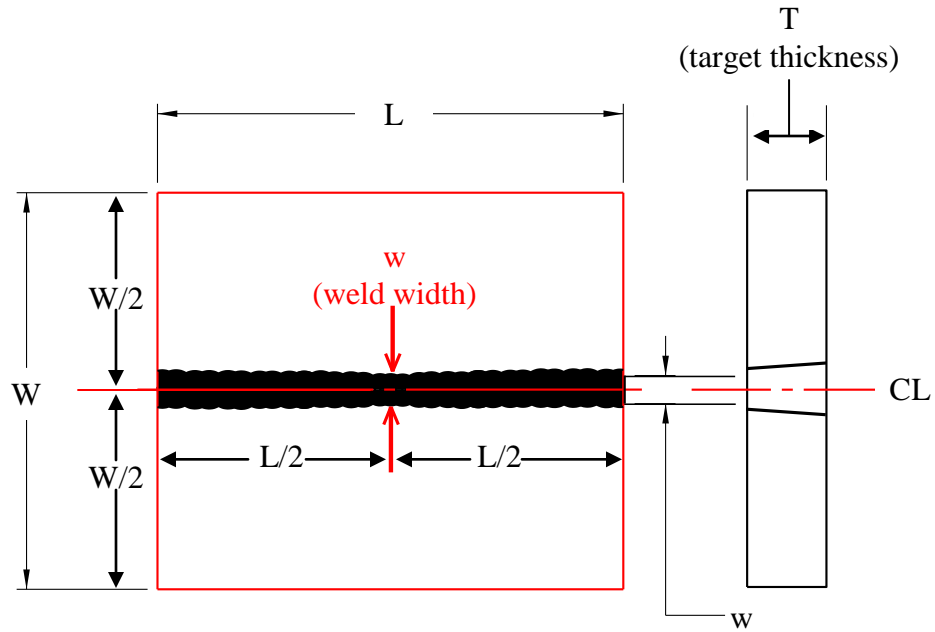
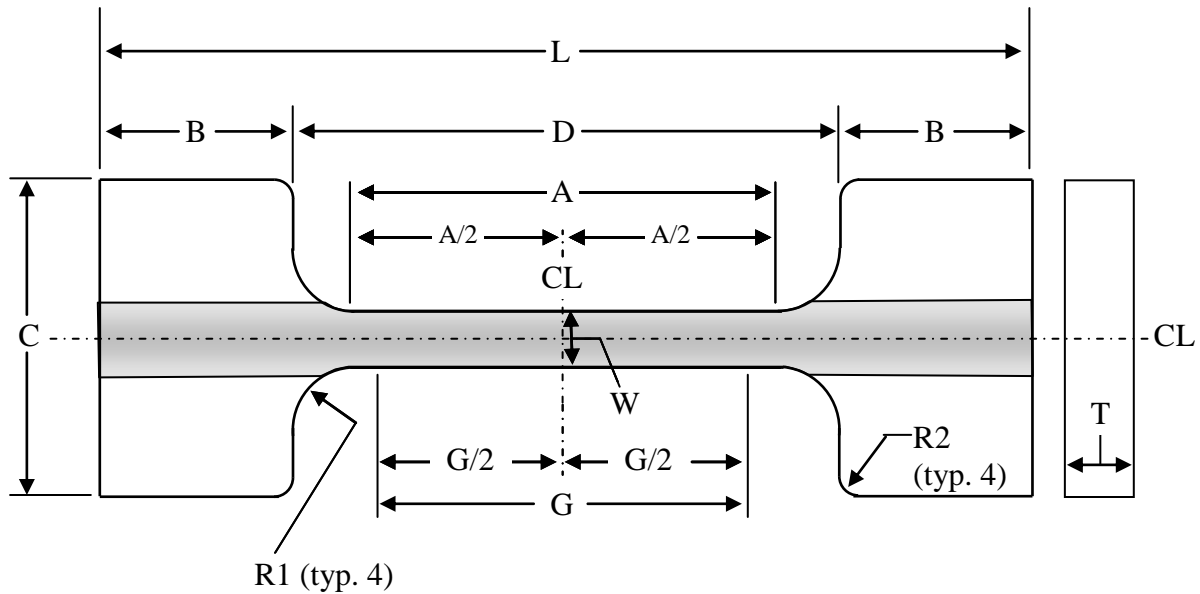


Figure 9: Measurement of weld width for determination of specimen width

3. **Final Specimen Preparation** - With the scribed centerlines for reference, CL in Figure 9, machine the AWM strip tensile specimen from the prepared blank to the dimensional requirements of Figure 10. Figure 11 illustrates a typical AWM strip tensile specimen in finished condition prior to test.



	Dimension (in.)	Tolerance (in.)
G - gage length	1.000	± 0.003
W - width of reduced section	See 3.5.5.1.6	± 0.001
T - specimen thickness	See Fig. 3.5-4	See Fig. 3.5-4
R1 - radius of fillet	0.20	minimum
L - overall length	2.9 (see Fig. 3.5-3)	± 0.1 (see Fig. 3.5-3)
A - length of reduced section	1.25	minimum
B - length of grip section	0.6	approximate
C - width of grip section	1.0	minimum
D - distance between grip ends	1.70	± 0.05

Figure 10: AWM strip tensile specimen dimensional requirements



Figure 11: AWM strip tensile specimen prior to test, (a) bottom (ID) surface visible with hot/root pass, (b) end view

3.4.6 Testing

The AWM strip tensile specimen must be tested with either hydraulic or mechanical wedge grips by clamping the wide machined surfaces as illustrated in Figure 12. Careful alignment of the specimen is necessary. It is important that the specimen is held tightly and does not slip or bend during test. Attachment of the extensometer requires care because of the potential for residual

stresses in weld specimens. The surface used for attachment of the strain gage is important, since an error in initial strain measurement can occur when the gage is placed on the through thickness face.

The test shall be conducted in accordance with ASTM E8/E8M. Because the intent is to document the complete stress-strain behavior for the specimen, the extensometer must remain in place for the entire test, and the loading rate must not be increased after yield.

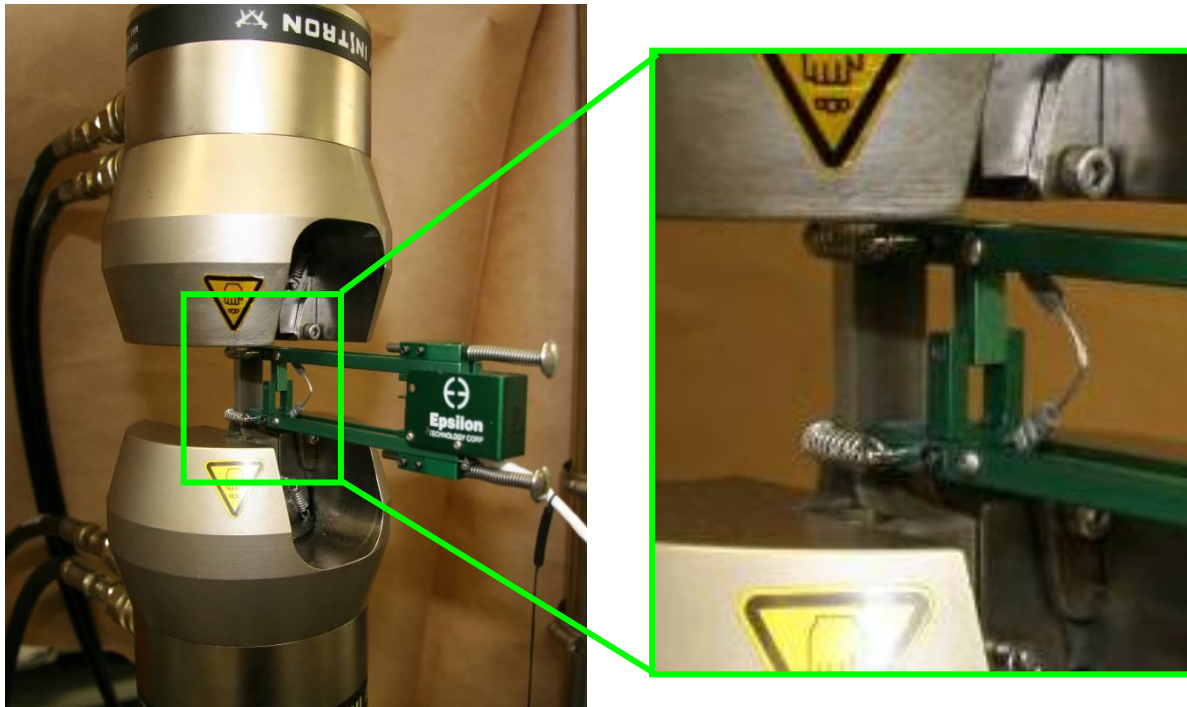


Figure 12: AWM strip tensile test

3.4.7 Post Test Analysis and Reporting

The tensile property data obtained from AWM strip tensile specimens can be processed and evaluated in several ways. As a minimum, the following information is to be reported for each test unless otherwise specified:

- Weld identification
- AWM strip tensile identification
- AWM strip tensile dimensions, T and W
- AWM strip tensile location (e.g. clock position, quadrant, etc.)
- Yield strength, 0.2 % offset method
- Yield strength, 0.5 % total strain method
- Flow stress at 1.0 % total strain
- Ultimate tensile strength
- Uniform strain
- Percent total elongation
- Percent reduction of area
- Strain hardening exponent
- Elastic modulus
- Full engineering stress-strain curve

4 LOW-CONSTRAINT SE(T) TEST PROTOCOL

4.1 INTRODUCTION

4.1.1 Background

Currently standardized methods to measure fracture toughness, *e.g.* ASTM E1820 [47], are designed to maximize constraint and, thereby, obtain a lower-bound value of toughness to ensure conservatism. It is well recognized that this conservatism may unnecessarily penalize materials in applications where it is known that the constraint is lower than that imposed in the standard tests. An example may be found in the assessment of girth weld imperfections in pipe, which are subject to tensile stresses in service. The constraint experienced by such flaws is low, and significant benefit could be realized if the enhanced toughness in the low-constraint situation could be used in defect assessment. It is with this benefit in mind that the development of a low-constraint toughness test was undertaken.

At the time of initiation of the work at CANMET, an industry standard was available for low-constraint girth weld characterization [48]. However, it was felt desirable to develop a single-specimen test procedure to maximize the amount of data from each test and decrease the overall testing cost by minimizing the number of specimens needed. This required the development of a method to estimate crack growth. It was decided at an early stage to use a crack mouth opening displacement (*CMOD*) elastic unloading compliance technique for this. In addition, equations were developed for evaluation of *J* and *CTOD* from measurements of load and *CMOD*. Finite element analysis (FEA) showed that constraint matching to typical girth weld flaws in pipes dictated the use of clamped (“fixed grip”) specimens rather than pin loaded specimens, and test simplicity dictated the use of *CMOD* data rather than load-line displacement data. Development of the test is described in the complementary report, “Development of Procedure for Low-Constraint Toughness Testing Using a Single-Specimen Technique” [49].

4.1.2 Status Summary

The procedure developed in this work is outlined below in Section 4.2. Several independent laboratories are participating in a round robin evaluation at the time of writing of this report; the material in Section 4.2 is edited slightly from the round-robin version of the protocol. Although written for homogeneous materials, the procedure has been used by CANMET to characterize the weld metals and heat-affected zones (as well as base metals) produced in this program at ambient and low temperatures. The data are reported in two topical reports of this program.

4.2 SE(T) TEST PROTOCOL – RECOMMENDED PRACTICE

4.2.1 Scope

This recommended practice describes a method to measure the J -integral fracture toughness and the extent of crack growth in a SE(T) specimen. The specimen geometry and loading mode are designed to produce a level of crack-tip constraint in the test that is similar to the constraint experienced in service for a surface circumferential flaw in a pipe under tension or bending load. The test is intended to be used for structural steels.

4.2.2 Referenced Documents

ASTM Standards: ASTM E1820 Standard Test Method for Measurement of Fracture Toughness.

4.2.3 Terminology

a	crack size
a_o	original crack size at the starting of test
A_{pl}	plastic area under the load versus crack mouth opening displacement ($CMOD$)
b	remaining ligament ($=W-a$)
B	specimen thickness
B_e	effective thickness for side grooved specimen ($=B-(B-B_N)^2/B$)
B_N	specimen net thickness
$CMOD$	Crack Mouth Opening Displacement, displacement of crack faces measured at the surface
C_{CMOD}	$CMOD$ compliance, the ratio of $CMOD$ increment to load increment ($=\Delta v/\Delta P$)
$C_{CMOD(i)}$	$CMOD$ compliance at point i
E	modulus of elasticity
G	geometry factor of SE(T) sample
H	specimen span between grips
J	J -integral
J_c	J -integral at onset of unstable brittle crack extension after less than 0.2 mm of crack growth
J_u	J -integral at onset of unstable brittle crack extension after at least 0.2 mm of crack growth
J_m	J -integral at maximum load
K	stress intensity factor
n	strain hardening exponent
P	load
$P_{(i)}$	load at point i
P_Y	limit load in tension evaluated at the effective yield strength= $\sigma_Y B_N b$

v	<i>CMOD</i>
v_{pl}	plastic part of <i>CMOD</i>
W	specimen width
δ	crack tip opening displacement (<i>CTOD</i>)
ν	Poisson's ratio
σ_{YS}	0.2 % offset yield strength
σ_{TS}	ultimate tensile strength
σ_Y	effective yield strength (or flow stress) = $(\sigma_{YS} + \sigma_{TS})/2$
Δa	crack extension
Δv	<i>CMOD</i> increment
ΔP	load increment

4.2.4 Summary

In this test, a fatigue pre-cracked SE(T) specimen is loaded in tension. Crack extension may occur by ductile tearing, or by unstable brittle crack extension. In the latter case, the value of J is recorded as either J_c , or as J_u if the brittle extension is preceded by at least 0.2 mm of ductile growth. The value of J at maximum load is recorded as J_m if there has been no prior brittle crack extension. If crack extension occurs by stable ductile tearing, this recommended procedure enables construction of J -R and δ -R “resistance curves” from measured data.

4.2.5 Apparatus

The test is normally conducted with a universal test frame, and ancillary equipment for cooling the specimen if required. The load capacity is significantly higher than that required for bend tests; for an un-cracked $B \times B$ specimen, the limit load is $\sigma_Y B^2$ in tension but only $\sigma_Y B^2/4$ in bending (with the usual span of $S=4W$). The apparatus required for measurement of load and crack mouth opening displacement is described in ASTM E1820. A clip gauge mounted on integral knife edges has been found satisfactory, but other methods such as double clip gauge arrangements are acceptable provided they give an accurate measure of the *CMOD*.

4.2.6 Specimen

A SE(T) specimen with $W=B$ is used. The specimen is clamped at both ends to impose “fixed grip” loading with a “daylight” between the load points of $H=10W$. This distance between load points has been found to give crack tip constraint similar to that of a circumferential surface crack in a pipe loaded in tension [50]. The sample is schematically shown in Figure 13. The length of the clamped ends must be sufficient to transmit the load without slippage; a value of $4W$ at each end has been found sufficient in practice.

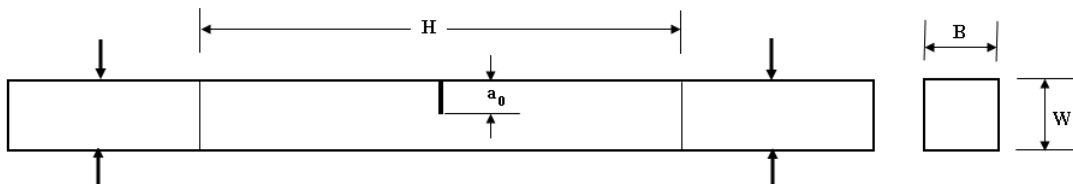


Figure 13: SE(T) sample

The notch should be machined following the procedures described for SE(B) samples in ASTM E1820, Section 7. Specimens are normally precracked in three-point bending fatigue, following the requirements described in ASTM E1820, section 7. Pre-cracking in tension is allowed provided that the load does not exceed $0.6P_Y$.

Side grooves are recommended to promote straight-fronted crack growth during the test. The root of the side groove is located along the specimen centerline. The side groove geometry shall conform to ASTM E1820 requirements: the angle of the groove shall be less than 90° , and the root radius shall be 0.5 ± 0.2 mm. A total reduction of $0.15B$ (three-quarters of that found to work well for bend testing) has been found optimal for tension testing. Pre-cracking is performed prior to side grooving.

4.2.7 Procedure

The gripping method must be such that there is no rotation of the clamped ends. This is most conveniently done with hydraulic grips, with load applied preferably to the faces parallel to the crack front (*i.e.* so that the crack grows in a direction parallel to the clamping force). The test requires continuous measurement of load versus *CMOD* from a single specimen. The area under the load vs. plastic *CMOD* curve is used to evaluate the *J*-integral.

The unloading compliance technique (with the *CMOD* compliance) is recommended for measurement of the crack length. During the test, unload/reload cycles for compliance measurement are repeated at interval *i* with the increment of load-line displacement between the intervals not to exceed $0.01b_0$. The recommended range of unload/reload for crack extension measurement is 25 % of the load immediately prior to unloading. Equations relating compliance to crack length are given in Section 4.2.8 below. Other methods of measuring crack length, such as potential drop, may be used provided it can be demonstrated that the validity requirements of this recommended practice can be met.

The specimen temperature shall be measured during the test to an accuracy of $\pm 3^\circ\text{C}$.

4.2.8 Calculations: equations for *a*, *J*, and *K*

If the unloading compliance method is used to measure crack size a_i , $C_{CMOD(i)}$ is measured at each point *i* as the slope $(\Delta v/\Delta P)_{(i)}$ and used to calculate a_i by the following equation [51]:

$$a_i/W = \sum_{j=0}^9 r_j U_i^j \quad (4-1)$$

where

$$U_i = \frac{1}{\sqrt{B_e C_{CMOD(i)} E + 1}} \quad (4-2)$$

The values of r_j , developed from finite element analysis (FEA) calculations, are listed in Table 3. The modulus to be used in Eqn. (4-2) is *E* rather than $E/(1-\nu^2)$ because the bulk of the specimen is close to plane stress and so the equations for crack length use plane-stress compliance, although the crack tip is subject to nearly plane-strain conditions.

Table 3: Coefficients r_j in Eqn. (4-1) for $H/W=10$

j	0	1	2	3	4	5	6	7	8	9
r_j	2.044	-15.732	73.238	-182.898	175.653	60.930	-113.997	-113.031	8.548	142.840

(Values that can be used to check for correct transcription of Equation (4-1) to spreadsheet: for $U_i=0.4579$ and 0.2704 , $a_i/W=0.2002$ and 0.5009 respectively).

The effect of rotation on the unloading compliance can be significant, especially for deeply cracked samples. Plastic deformation in the ligament changes the geometry, causing the crack mouth to move away from the load line and reducing the $CMOD$ compliance. The following load dependent equation takes the effect of both rotation and necking into consideration. It was developed with FEA for X100 pipe steel with $a/W=0.25$ and 0.5 , and works well in both cases (the correction is very small for the shallow crack, but more significant for the deep crack):

$$(BC_{CMOD(i)}E)_{corrected} = \frac{BC_{CMOD(i)}E}{F} \quad (4-3)$$

where

$$F = 1 - 0.165 \frac{a_0}{W} \left(\frac{P_i}{P_Y} \right)$$

and both crack length a and limit load P_Y are evaluated at the initial values of $a=a_0$ and $b=b_0$. The J evaluation equations below have been developed from FEA assuming plane-strain crack-tip constraint [52]. $J_{(i)}$ is calculated at point i at current values of crack length $a_{(i)}$, $CMOD$ $v_{(i)}$, and load $P_{(i)}$ from:

$$J_{(i)} = \frac{(K_{(i)})^2 (1 - \nu^2)}{E} + J_{pl(i)} \quad (4-4)$$

The value of the stress intensity factor $K_{(i)}$ is given by

$$K_{(i)} = \left[\frac{P_i \sqrt{\pi a_i}}{(BB_N)^{1/2} W} \right] G \left(\frac{a_i}{W} \right) \quad (4-5)$$

where

$$G \left(\frac{a_i}{W} \right) = \sum_{j=1}^{12} t_j \left(\frac{a_i}{W} \right)^{j-1} \quad (4-6)$$

and the parameters t_j ($j=1$ to 12) are listed in Table 4.

Table 4: Coefficients t_j in Eqn. (4-6) for $H/W=10$ and $0.1 \leq a_i/W \leq 0.7$

j	1	2	3	4	5	6	7	8	9	10	11	12
t_j	1.197	-2.133	23.886	-69.051	100.462	-41.397	-36.137	51.215	-6.607	-52.322	18.574	19.465

(Values that can be used to check for correct transcription of Eqn. (4-6) to spreadsheet: for $a_i/W=0.2$ and 0.5 , $G(a_i/W)=1.319$ and 2.191 respectively).

The value of the plastic part of the J integral $J_{pl(i)}$ is given by

$$J_{pl(i)} = \left[J_{pl(i-1)} + \left(\frac{\eta_{CMOD(i-1)}}{b_{(i-1)}} \right) \left(\frac{A_{pl(i)} - A_{pl(i-1)}}{B_N} \right) \right] \left[1 - \frac{\gamma_{LLD(i-1)} (a_{(i)} - a_{(i-1)})}{b_{(i-1)}} \right] \quad (4-7)$$

where $\eta_{CMOD(i-1)}$ and $\gamma_{LLD(i-1)}$ are evaluated from:

$$\eta_{CMOD(i)} = \sum_{j=0}^{10} \phi_j (a_i / W)^j \quad (4-8)$$

and

$$\gamma_{LLD(i)} = \eta_{LLD(i)} - 1 - \left(1 - \frac{a_i}{W} \right) \frac{\eta'_{LLD(i)}}{\eta_{LLD(i)}} \quad (4-9)$$

where

$$\eta_{LLD(i)} = \sum_{j=0}^{10} \psi_j (a_i / W)^j \quad (4-10)$$

and

$$\eta'_{LLD(i)} = \sum_{j=1}^{10} j \psi_j (a_i / W)^{j-1} \quad (4-11)$$

Table 5: Coefficients ϕ_j in Eqn. (4-8) for $H/W=10$ and $0.1 \leq a_i/W \leq 0.7$

j	0	1	2	3	4	5	6	7	8	9	10
ϕ_j	1.000	-1.089	9.519	-48.572	109.225	-73.116	-77.984	38.487	101.401	43.306	-110.770

(Values that can be used to check for correct transcription of Equation. (4-8) to spreadsheet: for $a_i/W=0.2$ and 0.5 , $\eta_{CMOD(i)}=0.9215$ and 0.7601 respectively).

Table 6: Coefficients ψ_j in Eqns. (4-10) and (4-11) for $H/W=10$ and $0.1 \leq a_i/W \leq 0.7$

j	0	1	2	3	4	5	6	7	8	9	10
ψ_j	-0.880	15.190	-35.440	18.644	18.399	-1.273	-12.756	-12.202	-4.447	5.397	14.187

(Values that can be used to check for correct transcription of Eqn. (4-9) to spreadsheet: for $a_i/W=0.2$ and 0.5 , $\gamma_{LLD(i)}= -3.395$ and 0.505 respectively).

The quantity $A_{pl(i)} - A_{pl(i-1)}$ is the increment of plastic area under the load vs. plastic crack mouth opening displacement between points $i-1$ and i . The quantity $J_{pl(i)}$ represents the total crack growth corrected plastic J at point i and is obtained by incrementing the existing $J_{pl(i-1)}$ (from η_{CMOD} and A_{pl}) and then modifying the result to account for the crack growth increment (with γ_{LLD}). Accurate evaluation of $J_{pl(i)}$ from Equation (4-7) requires small crack growth increments; the increase in load-line displacement between unloading points shall not exceed $0.01b_0$. The quantity $A_{pl(i)}$ can be calculated from:

$$A_{pl(i)} = A_{pl(i-1)} + \left[P_{(i)} + P_{(i-1)} \right] (v_{pl(i)} - v_{pl(i-1)}) / 2 \quad (4-12)$$

where $v_{pl(i)}$ is the plastic part of the crack mouth opening displacement and is determined from $v_{(i)} - (P_{(i)} C_{CMOD(i)})$.

Values of $CTOD$ shall be calculated from J by use of [53]:

$$\delta_i = \frac{J_i}{m_i \sigma_Y} \quad (4-13)$$

where

$$m_i = m_{c(i)} \quad \text{for } P \leq P_Y$$

$$m_i = m_{c(i)} - m_{p(i)} \left(\frac{P_i}{P_Y} - 1 \right) \quad \text{for } P > P_Y \quad (4-14)$$

and

$$m_{c(i)} = A_1 \frac{a_i}{W} + A_2 \quad (4-15)$$

Here,

$$A_1 = -0.1293 + 0.1152 \left(\frac{1}{n} \right) - 0.00986 \left(\frac{1}{n} \right)^2 + 0.000263 \left(\frac{1}{n} \right)^3 \quad (4-16)$$

$$A_2 = 3.0867 - 0.297 \left(\frac{1}{n} \right) + 0.0194 \left(\frac{1}{n} \right)^2 - 0.000427 \left(\frac{1}{n} \right)^3 \quad (4-17)$$

and

$$m_{p(i)} = B_1 \frac{a_i}{W} + B_2 \quad (4-18)$$

The coefficients B_1 and B_2 are given by

$$B_1 = 1.0169 - 0.0634 \left(\frac{1}{n} \right) + 0.00567 \left(\frac{1}{n} \right)^2 - 0.000200 \left(\frac{1}{n} \right)^3 \quad (4-19)$$

$$B_2 = 0.6969 - 0.1216 \left(\frac{1}{n} \right) + 0.01487 \left(\frac{1}{n} \right)^2 - 0.000393 \left(\frac{1}{n} \right)^3 \quad (4-20)$$

and n is the strain-hardening exponent determined from the stress-strain curve:

$$\varepsilon = \frac{\sigma}{E} \quad \text{for } \sigma \leq \sigma_{YS}$$

$$\varepsilon = \frac{\sigma_{YS}}{E} \left(\frac{\sigma}{\sigma_{YS}} \right)^{1/n} \quad \text{for } \sigma > \sigma_{YS} \quad (4-21)$$

(Note: practical methods to estimate n from Y/T will be established following ASTM procedures.)

All $J_i a_i$ pairs determined before the specimen reached its maximum load are identified. As required by ASTM E1820, there must be at least eight of these pairs, unless instability occurred before maximum load. If there was instability, a_{oq} shall be determined with the available measurements and the result indicated with an asterisk. Any spurious “apparent negative crack growth” values during the initial loading shall be ignored, so that only values beginning with the minimum crack length shall be used to estimate a_{oq} . The $J_i a_i$ pairs are used to calculate an estimate of initial crack size a_{oq} by the following equation:

$$a = a_{oq} + J/(2\sigma_Y) + BJ^2 + CJ^3 \quad (4-22)$$

The coefficients of this equation are found with a least-squares fitting procedure. The value of a_{oq} is then used to estimate values of crack growth $\Delta a_i = a_i - a_{oq}$.

After completion of the test, the specimen is heat tinted at about 300 °C for 30 min and then broken open. The nine-point technique described in ASTM E1820, Section 8, is used to measure the initial crack size a_{op} and final crack size a_{fp} for comparison with estimated values.

4.2.9 Validation

Validity requirements for agreement between a_{oq} and a_{op} , and between total crack growth $\Delta a_f = a_f - a_{oq}$ where a_f is the estimated value of a_i at the final unloading and $\Delta a_{fp} = a_{fp} - a_{op}$, will be established following completion of the independent laboratory round robin testing. Note that no validity requirement is to be imposed on specimen size because the values of J and $CTOD$ measured in this procedure are not expected to be size-independent material properties; rather, they are values that are relevant for the geometry tested. That is, for surface cracks in pipe for example, the specimen width is expected to be equal to the wall thickness so that the toughness values may be used for assessment of surface flaws in the pipe.

4.2.10 Report

The results of the test shall be reported in the form of a spreadsheet with original data of load and $CMOD$, and calculations of a , J and δ . High-resolution pictures of the fracture surfaces must also be reported. There should be a summary including, as a minimum: material; test temperature; specimen dimensions including side grooving; initial crack length from Equation (4.14); initial and final crack length measured on the fracture surface by use of the nine-point average technique; J_c , J_b , J_m as appropriate; and resistance curves J vs. Δa and δ vs. Δa .

5 CURVED-WIDE-PLATE TEST PROCEDURES AND DATA ANALYSIS

5.1 HISTORY OF CWP TEST

Curved-wide-plate (CWP) testing is one of the most recognized large scale tests for the characterization of pipeline girth welds. The test specimen is a curved piece of pipe with a nominal gauge width of 200 mm to 450 mm and is loaded in longitudinal tension. The girth weld in the middle of the specimen has a machine-notched or fatigue sharpened flaw. The strain across the weld is monitored while the specimen is pulled longitudinally until failure. Many organizations now have CWP testing capabilities, including the University of Ghent, C-FER, Stress Engineering Services, National Institute of Standards and Technology (NIST), Evraz, JFE, Nippon Steel Corporation, and POSCO.

CWP testing has been used as a tool for material and weld procedure qualification [54]. It has also been used for project-specific design validation. A large database of the failure strains of girth welds has been established from CWP tests [55].

Until recently, there have been no universally accepted test standards governing the specimen dimensions, instrumentation, data acquisition and post-test processing. A study has shown that

the specimen width, weld strength mismatch, and specimen length have strong impacts on the reported failure strains [56]. Significant progress has been made in recognizing the importance of the having consistent specimen dimensions and test procedures [56]. Denys, et al., has published a recommended testing procedure of CWP specimens [57].

5.2 APPLICATION OF CWP TESTS

In comparison to small-scale test specimens, CWP specimens allow the testing of significantly more materials (e.g., length of girth weld) under more representative loading conditions, i.e., tension in the longitudinal direction. Given the large width of the specimen, flaws of finite length with varying flaw depth can be introduced, whereas small-scale specimens typically start with a straight-fronted flaw of constant depth.

CWP tests may be used for one of following purposes:

- (1) evaluate the girth weld performance for a given set of material properties,
- (2) evaluate the flaw tolerance level of girth welds,
- (3) determine the strength capacity of pipe sections with girth welds,
- (4) determine the strain capacity of pipe sections with girth welds,
- (5) compare weld performance of welds made by different procedures,
- (6) act as a complementary test for welding procedure qualification, and
- (7) provide test data for the confirmation of weld integrity assessment procedures.

CWP tests are not suited to evaluate the effects of weld high-low misalignment without further analysis, as local rotation would occur around the misalignment. Such rotation is more restricted in full-scale pipes. The effects of internal pressure on the strength and strain capacity cannot be evaluated through CWP tests.

5.3 KEY CONSIDERATIONS FOR CWP TESTS

CWP tests are generally not considered routine tests. Load frames of large capacity are required, along with special specimen preparation, instrumentation, data acquisition, post-test data analysis, and post-test metallography. CWP tests can, however, be used effectively as a test form complementary to small-scale tests and occasionally to full-scale tests.

The cost of CWP tests is relatively high and the turn-around time can be long due to the lengthy period required for specimen preparation.

5.4 GENERIC CONSIDERATIONS FOR SPECIMEN DESIGN AND DIMENSIONS

5.4.1 Width of the Specimen

The width of the specimens is primarily determined by (1) diameter of the pipe, (2) wall thickness of the pipe, (3) pipe/weld strength level, and (3) expected flaw length to be introduced. For small diameter pipes, the width of the specimen may be limited by the thickness of the

loading plates, due to the pipe curvature. The pipe wall thickness, pipe and weld strength, and the load capacity of the test machine may limit the plate width.

In general the flaw length should not exceed one fifth of the plate width. This relation may determine the desired plate width based on the expected flaw length.

5.4.2 Length of the Reduced Section

The length of the reduced section should be at least three times the plate width. To give extra length for load transfer between the reduced section and the specimen shoulder, the nominal length of the reduced section should be about four times the plate width.

5.4.3 Other Dimensions

The width of the shoulder sections should be sufficiently wide to ensure enough load carrying capacity at the weld between the shoulder and the loading plates.

5.5 CURRENT CWP TEST MATRIX

The CWP test matrix includes 34 specimens from three rounds of welds.

Table 7: CWP test matrix

Order of Test	Specimen ID	Flaw Location	Target Final Flaw Size (depth x width, mm x mm)	Clock Position (o'clock)	Test Temperature (°C)
1	BM-RT	BM (base metal)	3 x 50	N/A	Room Temp.
2	CWP-16	WMC (Weld Metal Centerline)	3 x 50	7:30	Room Temp.
3	CWP-03	HAZ (heat affected zone)	3 x 50	7:00	Room Temp.
4	CWP-01	WMC	6 x 30	1:30	Room Temp.
5	CWP-15	HAZ	6 x 30	6:00	Room Temp.
6	BM-LT	BM	3 x 50	N/A	-20
7	CWP-11	WMC	3 x 50	6:45	-20
8	CWP-19	WMC	3 x 50	5:30	-20
9	CWP-10	WMC	6 x 30	4:00	-20
10	CWP-12	HAZ	6 x 30	8:30	-20
11	CWP-02	HAZ	3 x 50	4:30	-20
12	CWP-23	HAZ	3 x 50	7:30	-20
13	CWP-20	WMC	3 x 50	2:15	Room Temp.
14	CWP-21	HAZ	3 x 50	4:00	Room Temp.
15	CWP-22	WMC	3 x 50	5:30	-20
16	CWP-14	WMC	3 x 50	5:15	-40
17	CWP-13	WMC	3 x 50	3:30	-40
18	CWP-18	HAZ	3 x 50	9:00	-40
19	CWP-17	HAZ	3 x 50	4:00	-40
20	CWP-05	HAZ	3 x 50	2:00	-20
21	CWP-07	WMC	2 x 75	8:00	-20
22	CWP-06	WMC	2 x 75	4:15	Room Temp.
23	CWP-08	HAZ	2 x 75	11:00	Room Temp.
24	CWP-09	HAZ	2 x 75	2:00	-20
25	CWP-24	WMC	6 x 30	2:00	Room Temp.
26	CWP-27	HAZ	6 x 30	2:00	-20
27	CWP-25	HAZ	6 x 30	4:30	Room Temp.
28	CWP-26	WMC	6 x 30	7:30	-20
29	CWP-28	WMC	3 x 50	9:30	-40
30	CWP-29	HAZ	3 x 50	11:00	-40
31	CWP-30	WMC	2.5 x 50	11:15	-20
32	CWP-31	HAZ	2.5 x 50	4:00	-20
33	CWP-32	HAZ	2.5 x 50	11:15	-20
34	CWP-33	WMC	2.5 x 50	4:00	-20

5.6 INSTRUMENTATION AND DATA ACQUISITION OF THE CURRENT TESTS

The data acquisition system used was custom designed for this series of tests and consisted of various conditioning sources linked to a common LabVIEW (National Instruments, Austin, TX)² based acquisition and storage system. The signal conditioning sources included the MTS (MTS Systems Inc., Eden Prairie, MN) controller for load, stroke and crack mouth opening displacement (CMOD) gauge conditioning. The linear variable differential transformers (LVDT) were conditioned by Schaevitz (Measurement Specialties, Hampton, VA) conditioners and the strain gages were conditioned and amplified with Vishay (Micro-Measurements, Raleigh, NC) hardware. Thermocouples were input directly to the National Instruments data acquisition hardware.

Instrumentation layout was developed between CRES and NIST. The instrumentation layout schematic is shown in Figure 14, which includes views of the OD and ID surfaces of the specimen and the positions of the various instruments on the specimen. On the schematic in Figure 14 are the location of fifteen strain gage “T” rosette pairs (30 gages total), six LVDTs and their associated end points, thermocouples, photo-elastic coating, and a CMOD gage.

Strain gage rosettes were used in the test program to determine the local strain values at various points on the specimen. LVDTs are used to capture gross section strains and to determine the extent of bending in the specimen as it is loaded. Thermocouples were used only on sub-ambient temperature tests to capture the temperature uniformity along the specimen gauge length. The CMOD gage was used to capture the elastic and plastic crack mouth opening displacement. This value, along with the load data, was analyzed for the determination of compliance and J -integral.

² The brands and modes and manufacturers presented here are provided to describe the equipment that was used to conduct the tests. The authors, project sponsors, and U.S. Government do not endorse one product or manufacturer over another.

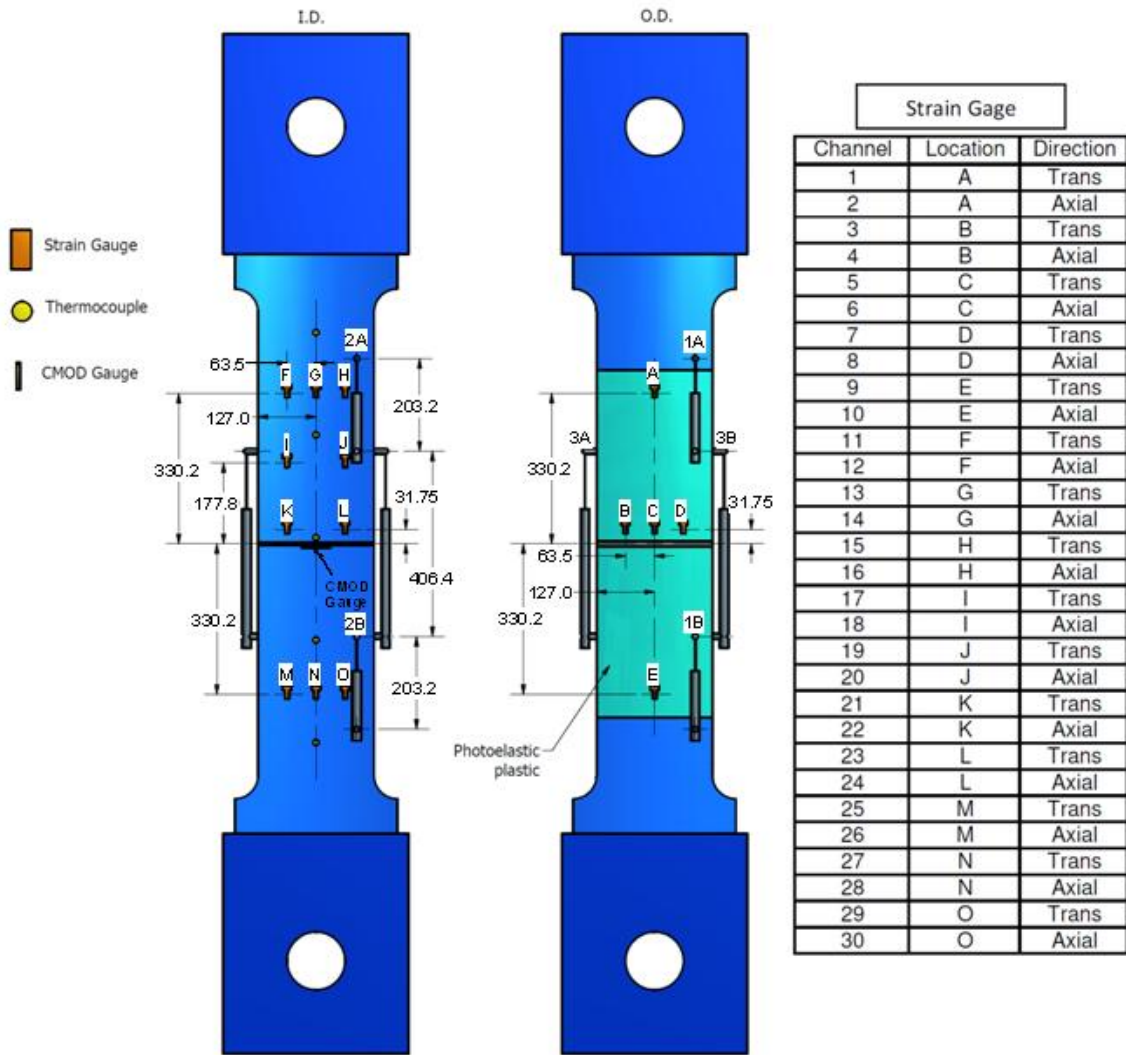


Figure 14: Schematic of curved wide plate test gauge instrumentation layout along with labels for the strain gage and LVDT channels (units in mm)

5.7 SPECIMEN FABRICATION AND PREPARATION

5.7.1 Alignment of the Specimen with respect to the Loading Plates

The centroid of the reduced section should be aligned with the centroid of the loading plates. It is understood that the centroid of the reduced section may shift when the material undergoes plastic deformation.

5.7.2 Notch Placement and Fatigue Pre-cracking

Two different procedures were used to introduce a “starter” notch in the CWP specimen. A custom built slotting saw designed and fabricated for this study was replaced with a sinker electric discharge machining (EDM) technique. The saw cutting method was used to introduce notches in the specimens at the final flaw geometry. The EDM technique was used to introduce

starter notches for specimens where the final flaw size would be achieved through fatigue pre-cracking.

5.7.2.1 Saw-cut Notches

A surface notching method developed to introduce a notch into the ID surface of the pipe used an electric motor driven slotting saw blade. The blades had a thickness of 0.5 mm (0.020 inch), a diameter of 70 mm, and 72 teeth. Two different blades were used: one with a square tooth for initial notch machining and another with a 60° included angle tooth for the final 0.5 mm of notch machining.

The weld toe from the ID surface of the CWP specimen was ground down flush with the ID surface of the upper plate; see Figure 15.

5.7.2.2 EDM Notches

A sinker EDM machine was used to introduce notches where the notch-shape was controlled by a profiled copper-tungsten electrode. The copper-tungsten electrodes were cut and profiled from a flat plate with a wire EDM machine. Two electrode thickness values were selected for machining the notch, 0.05 mm thick and 0.41 mm thick. In order to prepare the weld region on the ID surface, the toe of the weld was removed with the EDM with an electrode that matched the contour of the ID surface of the plate. That electrode was approximately 25 mm thick and spanned the surface arc length of the selected notch from Table 8. The weld toe was removed until it was flush with the upper plate of the weld, see Figure 15.

The EDM notching process was completed in two stages. The depth values of each EDM process were referenced to the surface of the lower plate of the weld. First, the 0.41 mm thick electrode was used to cut to the final depth less 0.35 mm, which left a notch kerf of approximately 0.50 mm due to “overburn”. The thin electrode (0.05 mm) was then used to remove an additional 0.35 mm to achieve the final notch depth. The thin electrode was positioned within the center of the initial notch.

Because no accepted CWP test standards exist, ASTM standards for fracture mechanics testing were used as guidelines in selecting the geometries of the various notches. ASTM E1820 requires that the tip of a V-shaped notch has a root radius of less than 0.08 mm (0.003 inch). The thin (0.05 mm) electrode provided a starter notch with an approximate 0.075 mm root radius. The 0.41 mm thick electrode was selected to provide a final notch thickness of 0.50 mm, which matched the thickness of the notch, machined with the slitting saw method. This also allowed the placement of CMOD gauges without the use of knife edges.

5.7.2.3 Notch Location and Geometries

CWP specimens were notched to test the properties in the base metal, weld metal and the heat affected zone. For the two base metal specimens tested, the notch was located at the midpoint between the fillets in the reduced width section on the ID surface. The remaining specimens with girth welds were prepared by polishing and etching the edges of the specimens to reveal the weld structure and location.

In order to evaluate weld metal and HAZ behavior, two notch locations were selected. The ID surfaces of the two mating pipe segments were rarely flush with one another at the weld. In order to determine a flaw depth, a reference datum was identified as the ID pipe surface that was closest to the other pipe sections OD surface and will be herein termed the “lower plate.” The reference datum used for notch depth measurements is illustrated in Figure 15.

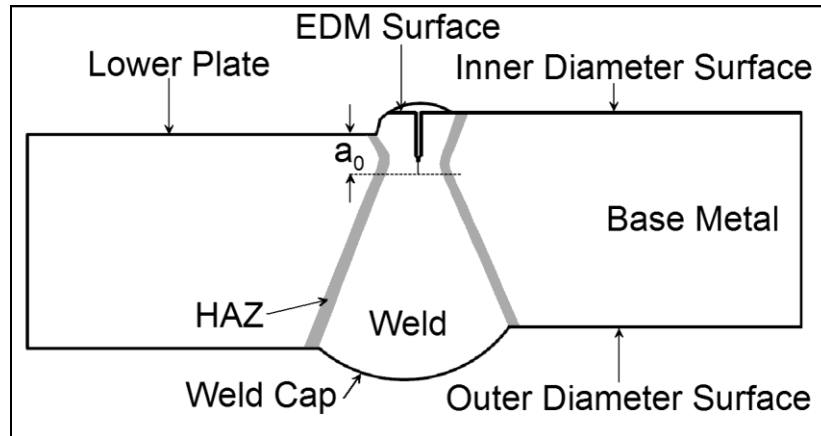


Figure 15: Schematic shows a cross-section view of the girth weld indicating an exaggerated misalignment between pipe sections. The reference datum for notch measurements is the ID surface of the lower plate.

After etching, a caliper was used to measure and guide a scribe on the edges of the specimen at a depth corresponding to the final flaw size along the edges of the lower plate. The scribe line was used to identify the position of the notch along the length of the specimen. For a weld specimen, the notch was located in the centerline of the “V” shape formed by the weld metal, and a scribe line was placed in the through-thickness direction of the plate. For a HAZ specimen, a scribe line was placed in the through-thickness direction of the plate at a position that placed the tip of the final flaw in the middle of the HAZ region of the weld. The through-thickness scribe lines were used during the notching procedure to align the machining fixtures. The reference schematic in Figure 16 illustrates the placement and alignment of the notches.

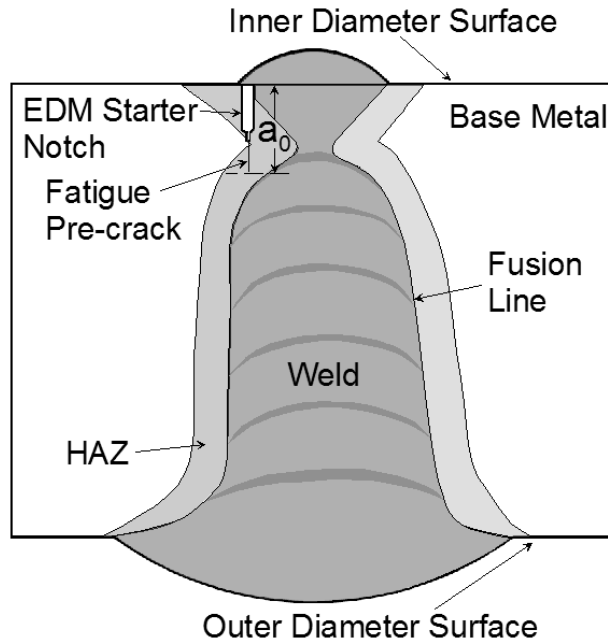


Figure 16: Schematic showing a cross-section view of the girth weld indicating the placement of the starter notch and subsequent fatigue pre-crack in a specimen designated for HAZ testing.

5.7.2.4 Fatigue Pre-Cracking

The CWP test matrix in Table 7 lists the notch geometry, notch location, notch type and notch condition. The saw-cut notches for CWP-03 and CWP-16 as well as the EDM notches for CWP-01 and CWP-15 were tested without fatigue pre-cracking. The remaining CWP specimens were EDM notched to a final dimension smaller than that listed in Table 8. The EDM starter notch was extended to the final notch dimension by fatigue. In accordance with ASTM E740/E740M the fatigue crack extension from the tip of the machined starter notch shall not be less than 5 % of the final crack depth, and must lie entirely within an imaginary 30° wedge whose apex is at the crack tip. From ASTM E1820, the length of the fatigue pre-crack extension from the machined notch shall not be less than 0.6 mm. Selection of a constant fatigue pre-crack extension of 0.6 mm for all crack geometries and use of the two stage EDM starter notch machining process satisfies these requirements. In order to achieve 0.6 mm of fatigue pre-crack length for the final flaw size, the initial starter notch size was scaled down accordingly. Table 8 lists the final flaw geometries and their respective depth and width values to allow for 0.6 mm of fatigue pre-crack growth.

Table 8: CWP notch geometry test matrix for 0.6 mm fatigue pre-crack growth

Notch Identification	Final Flaw Target Depth (mm)	Final Flaw Target Length (mm)	CWP Plate Thickness (mm)	Starter Notch Depth (mm)	Starter Notch Width (mm)
2x75	2.0	75	19	1.4	73.3
2.5x50	2.5	50	14.5	1.9	48.3
3x50	3.0	50	19	2.4	48.3
6x30	6.0	30	19	5.4	28.3

The development of the procedure for fatigue pre-cracking the CWPs in bending has been reported previously [58]. The four-point-bending loading arrangement is shown in Figure 17.

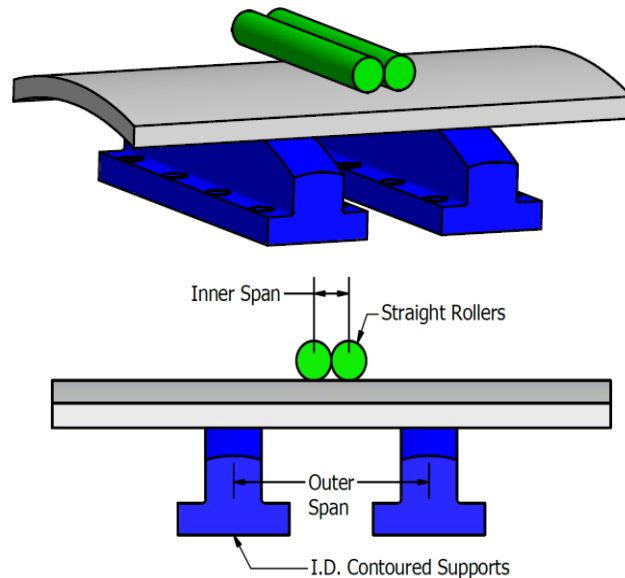


Figure 17: Schematic of contoured outer span loading supports and straight roller inner span loading arrangement used in four-point-bending fatigue pre-crack of CWPs [58].

In order to accurately predict the instantaneous crack length during fatigue pre-cracking the starter notch depth was measured and used in the predictions developed for this program and described in reference [58]. A CMOD gauge was used to determine the instantaneous compliance of the specimen, which was validated as an indication of crack length for all pipe geometries and notch configurations.

5.7.3 Placement of Instruments

After the specimen was fatigue pre-cracked, gage layout lines were scribed onto the specimen according to the instrumentation layout schematic in Figure 14. The surfaces of the ID and OD were sanded in the gage area using commercially available grinders and sanding pads. The surfaces were sanded to remove the surface oxidation layer and provide an oxide- and pit-free surface for mounting strain gages and securing the LVDTs. Careful attention was given to avoid unnecessary material removal and undercutting near instrumentation installation sites.

Once the specimen layout and sanding was complete, the specimens were shipped to Lincoln Electric along with the end plates shown in Figure 14 for welding. The endplates were welded onto the test specimen. The specimens were secured onto a special pallet and were shipped back to NIST to complete the testing. Once the specimens were received from Lincoln Electric, the strain gage locations were re-sanded by hand to provide a clean and oxide-free surface for gage attachment. The strain gages were applied, wired and prepared for specimen installation. The LVDTs were attached to the specimen on two $\frac{1}{4}$ "-20 threaded studs that were welded onto the specimen surface with a capacitive discharge stud welder.

For sub-ambient temperature testing, E-type thermocouples were also welded to the surface of the specimen. Two thermocouple patterns were used throughout the experiment. Both patterns used ten thermocouples, five each on both the OD and ID surfaces of the specimen. The first pattern consisted of a linear pattern of equally spaced thermocouples across the diagonal of the specimen on each ID and OD surface. Due to the location of the notch, the center thermocouple was placed 50 mm above the mid-gauge length on the OD surface and 50 mm below the mid-gauge length on the ID surface. The remaining thermocouples were positioned at 250 mm and 500 mm above and below the mid-gauge length.

Photo-elastic (birefringent) film was used on four specimens tested at room temperature to visually determine the strain field patterns over the full loading spectrum of the specimens. Photo-elastic film was adhered to the OD surface of the specimen and covered 75 % of the whole gauge length. These tests were video-taped and photographed to indicated changes in strain-field with load increments.

5.8 PREPARATION OF TEST MACHINES

The CWP tests were conducted with a MTS Systems Inc., 4.5 MN (1 Mlbf) universal servo-hydraulic test frame located at NIST in Boulder, CO. The frame consists of an upper cross-head that is fixed for testing and a hydraulic actuator at the base. The load cell was attached to the upper cross-head with a clevis grip installed in the load cell. The lower clevis was attached to the actuator. A photograph of the frame is shown in Figure 18. The stroke signal was generated from an externally mounted LVDT that was attached to the actuator. The system was controlled using a digital controller. The MTS controller used was a FlexTest SE with multi-channel input and output capabilities. The controller was also used to condition and amplify the CMOD gauge signal.

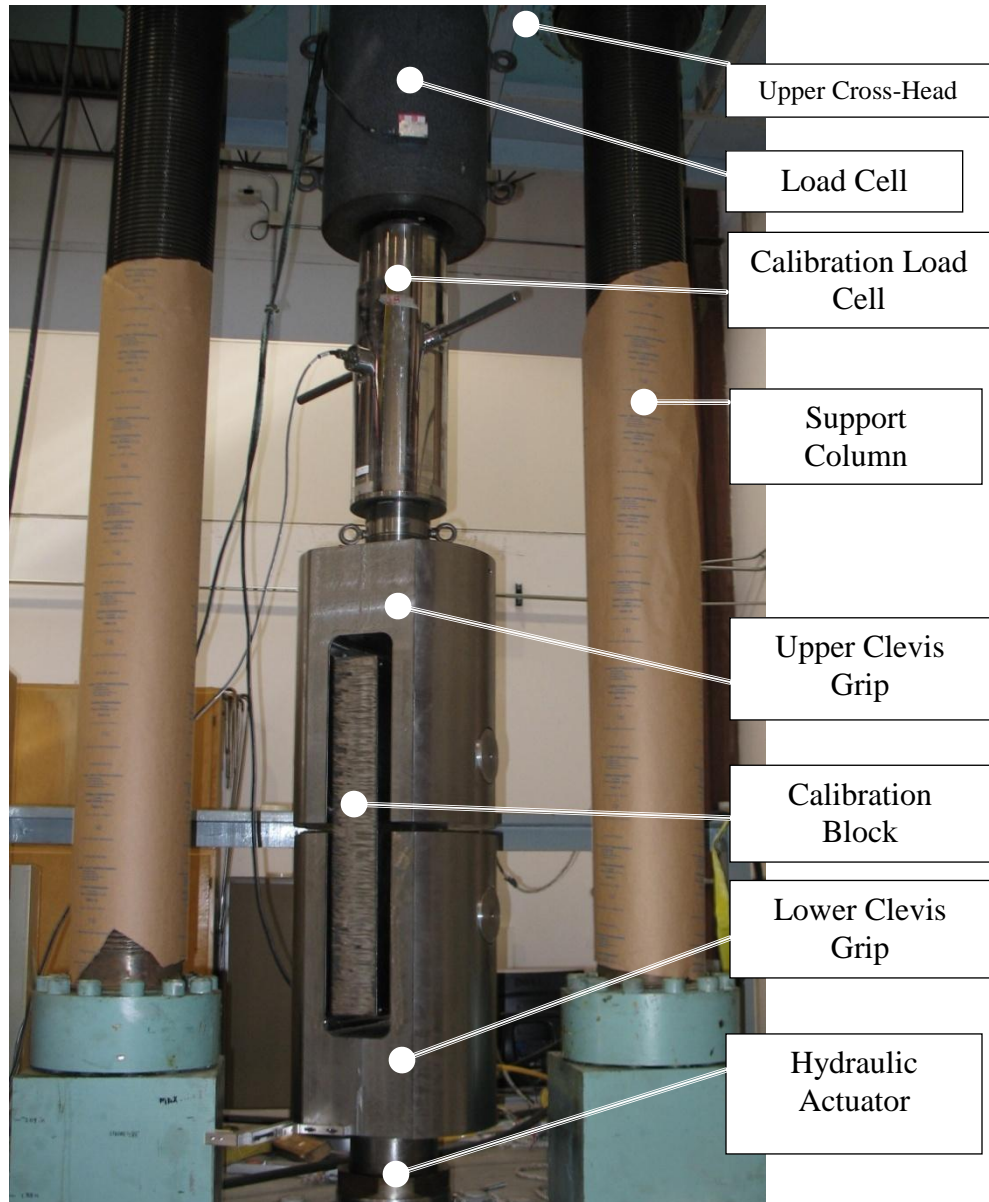


Figure 18: Photograph of the test frame, limited in view to the specimen loading configuration. Annotations include locations of the upper cross-head, testing load cell, calibration load cell (not present during normal testing), frame support columns, clevis grips, the calibration block and the hydraulic actuator.

Clevis grips were manufactured specifically for this test program from 4340 steel. Clevis pins were 5-inch-diameter hardened steel pins. A calibration block was manufactured from HSLA 100 plate steel to carry the full load of the frame capacity. An annotated photo of the calibration set-up is shown in Figure 18.

5.8.1 Calibration

All sensors were calibrated according to ASTM standards and all sensors were used according to manufacturer's specifications and engineering best practices. When practical, all calibrations

were done with an “end-to-end” method where a known mechanical change resulted in digitally acquired data and were verified with reference standards. Strain gage conditioners were calibrated with shunt calibration resistors which is standard practice for strain gage installations.

5.8.2 Alignment

Once the specimen was installed in the test frame, shims were placed between the inner walls of the clevis and the end plates in order to position the specimen in the clevis such that the centroid of the gauge section was in line with the loading axis of the test frame. Schematics showing the centroid position for the two CWP plate geometries are shown in Figure 19. Figure 19(a) shows the centroid location of the gauge section for the 914 mm (36 inch) diameter pipe and Figure 19(b) shows the centroid location of the gauge section of the 1067 mm (42 inch). Once the positioning shims were in place, the specimen was positioned against the shims and the opposite was filled with shims to prevent specimen movement.

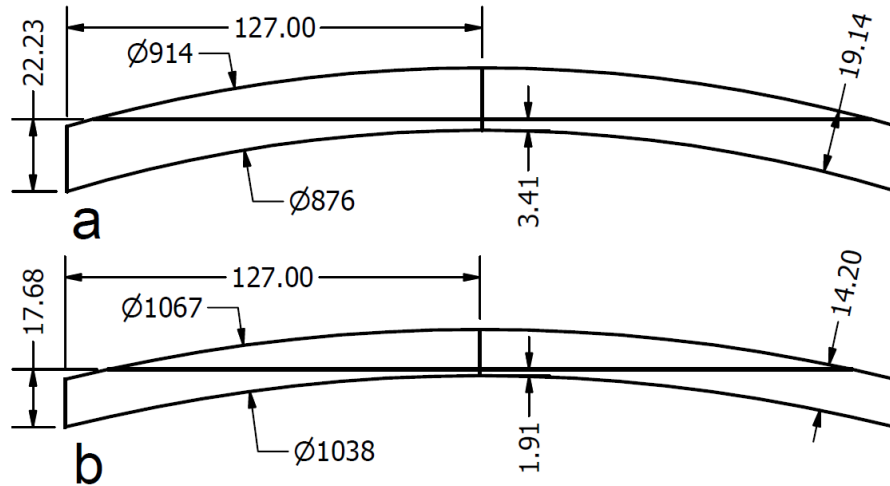


Figure 19: Gauge section centroid positions for CWP specimens with two pipe geometries; (a) the 914 mm (36 inch) diameter and (b) the 1067 mm (42 inch) diameter (units in mm).

5.8.3 Environmental Conditioning

A specially designed environmental chamber was manufactured for this test program to complete sub-ambient temperature testing. The chamber was installed above the actuator using an aluminum frame and has rails to allow access to the specimen for installation and removal while eliminating the need to remove the chamber using rigging and an over-head crane.

Specimens were cooled convectively using the chamber controller supplied with liquid nitrogen. The end tabs and clevis grips were a significant heat sink. To overcome the loss, active conductive cooling blocks were mounted to the specimen inside the chamber as close to the end tabs as possible. The copper cooling blocks were designed to flow liquid nitrogen through them. The flow of nitrogen to the cooling blocks was manually controlled in such a way as to keep the specimen temperature as uniform as possible. The temperature of each specimen over the entire gauge length was controlled to ± 3 °C of the target test temperature.

5.8.4 Software Programming/Unloading Cycles

The MTS system controller was programmed with MTS' Multi-Purpose Testware (MPT). The specimen was pre-loaded to 13 kN (3000 lbf). The specimens were loaded in tension at a stroke controlled rate of 6.00 mm/min. Specimens were loaded in the elastic regime with a minimum of six unloading cycles; load limits were used to trigger the unloading and loading ramps. The upper triggers incremented by 222.4 kN and the lower load triggers were 20 % of the upper trigger (e.g. The first trigger for the 14mm thick specimen was 889.6 kN and the lower-reversal trigger was set at 771.7 kN). Above the yield point the program shifted to stroke limited upper triggers. The specimens were unloaded in stroke control by 889.6 kN using load signal thresholds and then reloaded by 800.7 kN, at which point the stroke limit (2.0 mm) was in effect again. This cycle was repeated until after the maximum load was reached or until the CMOD vs. stroke plot approached a vertical asymptote. The intention was to gather as much data surrounding the on-set of tearing up to the maximum load. The test was ended before complete specimen rupture for all specimens except two. The goal was to end the test after the maximum load at a load equal to 80 % of the maximum load. However not all specimens reached this value gradually. It was more reliable to monitor the CMOD vs. stroke response to determine the end of the test. This method was not empirical and therefore was difficult to repeat precisely between tests.

5.9 PROCESSING OF RAW DATA

Raw data were checked for completeness and validity. Signal drop outs were documented with notations for the time and reason for the dropped signal. Raw data sets were provided to CRES for analysis. Very few data sets needed corrections due to mechanical slippage or loss of signal. The data were saved and compressed for easy storage and transmission between NIST and CRES.

5.10 POST-TEST METALLOGRAPHIC EXAMINATION

Metallographic procedures include photographing the residual flaw after testing. Three-dimensional laser scans were also done on each of the residual flaws. Additionally, each specimen was cut along its centerline to complete two more fractographic analyses. Figure 20 illustrates the sectioning plan. First, one half was cooled using liquid nitrogen and then broken open to expose the inner fracture surface using a three-point bend fixture. Photographs of the projection views of the liberated crack surfaces were taken. The other half was sectioned using an EDM wire to expose increments of the flaw cross-section. These increments or slices were prepared for microscopy by mounting, polishing, and etching the surfaces. Each of these mounts was digitally photographed at different scales using a hi-resolution flatbed scanner and a low-power stereo microscope. Each specimen had two projection views of the fracture surface as well as three transverse cross-sectional views of the flaw profile.

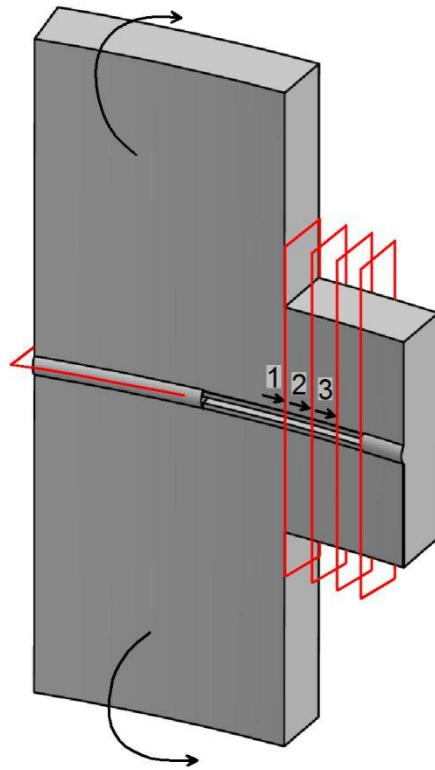


Figure 20: An illustration of the sectioning plan for each specimen is shown. The specimens were sectioned to measure initial and final crack lengths as well as verify the location of the cracks relative to the weld structure.

The projection views of the fracture surfaces were used to determine the crack lengths. The central cross-sectional scans were used to validate the crack length measurements and to provide location and direction data for each test. Crack angle measurements were used to correct for out-of-plane crack growth. The location of the starter notch and fatigue crack tip in the HAZ was validated using the central cross-section.

5.11 UNIFORM REPORT FORMAT

A variety of information is generated in a CWP test. The report should include the following groups of data:

- (1) specimen ID,
- (2) specimen dimensions,
- (3) basic material properties of the specimen,
- (4) instrumentation plan,
- (5) test machine setup,
- (6) test conditions,
- (7) raw data acquired from test,
- (8) data process procedures and/or protocols,
- (9) presentation of processed data,

- (10) post-test metallurgical examination,
- (11) specimen validation check, such as notch location and flaw size, and
- (12) special notes and comments.

The recommended data plots are given in Table 9.

Table 9: Recommended data plots

No.	X-axis	Y-axis 1	Y-axis 2
1	Ram Displacement	Load	CMOD
2	Ram Displacement	Stress Applied	
3	Ram Displacement	Remote Strains above Weld (1A, 2A and AVE)	
4	Ram Displacement	Remote Strains below Weld (1B, 2B and AVE)	
5	Ram Displacement	Strains cross Weld	
6	Average Remote Strain below Weld	Average Remote Strain above Weld	
7	CMOD	Average Strains above and below Weld	
8	CMOD	Average Strains cross Weld	
9	CMOD	Compliance	
10	Average Remote Strain above Weld	Compliance	
11	Average Remote Strain below Weld	Compliance	
12	Flaw Depth	CMOD	
13	Strain	Flaw Depth	
14	Average Remote Strain above Weld	Stress above Weld	
15	Average Remote Strain below Weld	Stress below Weld	
16	Average Remote Strain above Weld	CMOD	
17	Average Remote Strain below Weld	CMOD	
18	Flaw Growth (Δa)	J	
19	CMOD	Stress Applied	

5.12 GENERATION OF RESISTANCE CURVES

The procedures to generate fracture resistance curves are given in a companion report [59]. Examples of *J* resistance curves are also given in the same report.

5.13 DATA QUALITY CHECK

The quality of the CWP test data should be carefully examined before final report of the data. A few points of considerations are:

- (1) Defining zero-points of deformation measurements. It is often necessary to “zero” the deformation measurement, such as LVDT for remote strain measurement and strain gages, at zero applied load.

- (2) The remote nominal stress vs. remote nominal strain relation is similar to a generic tensile stress-strain curve. The elastic part of the stress-strain relation should be examined to determine whether the elastic slope is close to the theoretical value. Proper adjustment may be made using a procedure similar to that suggested in Section 2.4.3.
- (3) When the nominal stress is plotted against nominal remote strain, the curve can be flat around the point of maximum load. The digital data may be fitted to a polynomial relation to assist the determination of the point of maximum load with a procedure similar to that suggested in Section 2.4.4.

5.14 SUMMARY REMARKS

CWP testing is a valuable tool for the evaluation of pipeline girth welds. Key elements in the specimen design, dimension, instrumentation, test machine setup, acquisition of data, post-test data analysis, post-test metallurgical examination, and final reporting are recommended in this section. CWP tests are yet to be viewed as routine tests. Caution must be taken in all steps involving the testing. It is critical to report test data in the context of the specific test setup, and all relevant information listed in this section should be reported.

6 EFFECTS OF BASIC MATERIAL PROPERTIES ON WELD INTEGRITY

6.1 SCOPE OF THIS SECTION

The assessment of weld integrity depends on understanding critical material property parameters and their influence on the performance of the welds. The focus of this section is material parameters that can have significant impact on weld performance but are not well understood by the general pipeline industry. Although a large portion of this section may be viewed as more relevant to strain-based design, most of the issues are also applicable to traditional stress-based design.

6.2 EFFECTS OF YIELD STRENGTH MISMATCH

6.2.1 Status of Code Requirements

Weld metal strength is generally not an explicit requirement in codes and standards that govern pipeline girth welding practice [60,61,62,63]. Contrary to some public domain misconceptions, weld strength overmatching is not a requirement in most pipeline codes and standards. In girth weld procedure qualification, the ultimate tensile strength of the cross-weld tensile specimen is required to meet the specified minimum tensile strength of the pipe. Since the average strength of linepipe in a given pipe order is almost certainly greater than the specified minimum strength and because the linepipe specifications in the current standards have upper-bound strength limits much higher than the specified minimum, there is no assurance of having actual weld strength overmatch when the maximum tensile strength in a cross-weld tensile test is greater than the specified minimum value. The current requirements have served industry well. However, the actual degree of weld strength mismatch is not known as there are no requirements for all-weld-metal tensile tests and large strength ranges are permitted for a given pipe grade by the current standards.

6.2.2 Past Work on Weld Strength Mismatch

The effect of weld strength mismatch was the subject of intensive research in the early 1990s, as symbolised by two symposia dedicated to the subject [64,65]. The following subject areas were investigated:

- impact of weld strength mismatch on the structural integrity of welds,
- influence of weld strength mismatch on standard toughness testing procedures, and
- incorporation of weld strength mismatch into weld integrity assessment procedures.

The effects of weld strength mismatch on fracture toughness testing were examined by a number of organizations. A large international program led by EWI and TWI defined the limits of fracture toughness correlation equations for welds with strength mismatch [66,67,68,69,70]. Procedures to account for the weld strength mismatch in weld integrity assessment have been proposed by GKSS [71] and by a European research consortium [72]. The consensus view on the treatment of weld strength mismatch was developed by a group of leading experts in the mid-1990s [73]. A procedure specifically formulated for pipeline girth welds that incorporates the effects of weld strength mismatch was developed and validated by Wang, et al. [74,75].

Almost all work prior to approximately the year 2000 focused on stress-based applications where the nominal applied stress is less than the yield strength of the materials. Some of the earliest work on the effects of weld strength mismatch on strain-based design was by Horsley and Wang for X100 girth welds [76]. Their work showed that a remote tensile strain capacity of 2.0 % to 2.5 % was achievable, provided certain restrictions are specified on weld metal overmatching and allowable flaw size.

6.2.3 Weld Strength Mismatch in Stress-Based Design

There has been a renewed interest in re-examining the need for actual weld strength overmatching in the pipeline standard committees, such as API 1104, even in the domain of traditional stress-based design. This is a complex issue, and there is no quick and easy fix.

There are at least two ways to achieve actual weld strength overmatching. The first approach is to require that the minimum weld strength be greater than the upper-bound limit of the pipe strength distribution. The second option is to require that the failure stress in cross-weld tensile tests of a weld procedure qualification close to the upper limit of the pipe strength distribution. To implement the first option, all-weld-metal tensile tests have to be done. To implement the second option, the strength of the pipe in the welding procedure qualification has to be close to the upper limit so the weld strength can be tested to the upper limit of the pipe strength distribution. When a failure occurs in the pipe, the test only proves that the weld strength is at least as high as that of the pipe material. If the actual strength of the pipe in the field is greater than the strength of the qualification pipe, there is still a chance of having weld strength undermatching.

The requirement for actual weld strength overmatching can be difficult to satisfy in the current environment and could be counterproductive. For instance the upper limit of UTS of API 5L grades X70 and lower is 758 MPa (110 ksi). To ensure weld strength overmatching, the lower-

bound UTS of the weld metal has to be 758 MPa (110 ksi) or higher. Welds at such strength level can have some undesirable features, such as a high propensity for hydrogen cracking.

To avoid strain concentration in the girth welds, which should be a desirable and necessary goal for all girth welds, the weld strength requirements have to be examined in the context of weld high-low misalignment, weld bevel geometry, and the beneficial effects of weld reinforcement.

A relatively more practical approach towards avoiding strain concentration in the girth welds is perhaps requesting the weld strength to be at or higher than the median value of the pipe strength distribution. Again, such requirements should be considered in the context of weld high-low misalignment, weld bevel geometry, and weld reinforcement.

6.2.4 Weld Strength Mismatch in Strain-Based Design

It is generally recognized that actual weld strength overmatching will be required for strain-based design. If the strength mismatch is examined on its own merit, the higher the overmatching the better for high strain capacity. However, overly high requirements on weld strength can have negative consequences:

1. The selection of welding consumable and welding processes may become restrictive for high-strength pipelines.
2. The weld toughness may be negatively impacted.
3. There could be increased risk of weld metal hydrogen cracking.

One also has to consider the distributions of the pipe and weld strength in specifying weld mismatch requirements. An example of the ranges of stress-strain curves of pipe and girth welds from this project is shown in Figure 21 [77]. Depending on the “pairing” of the stress-strain curves, the yield strength of the weld metal can be as much as 150 MPa higher than that of the base pipe (880 MPa vs. 730 MPa) or slightly below that of the base pipe. The mismatch level as measured by the yield strength could therefore range from 0 % to 20 % overmatching. The ranges shown in Figure 21, from the same pipe and girth weld, are entirely from the natural variation of the pipe properties and differences in the type of all weld metal tensile specimens. Other factors that may contribute to strength variation, but not included in Figure 21, are (1) strain ageing effects, (2) joint-to-joint variation and (3) steel heat-to-heat variations.

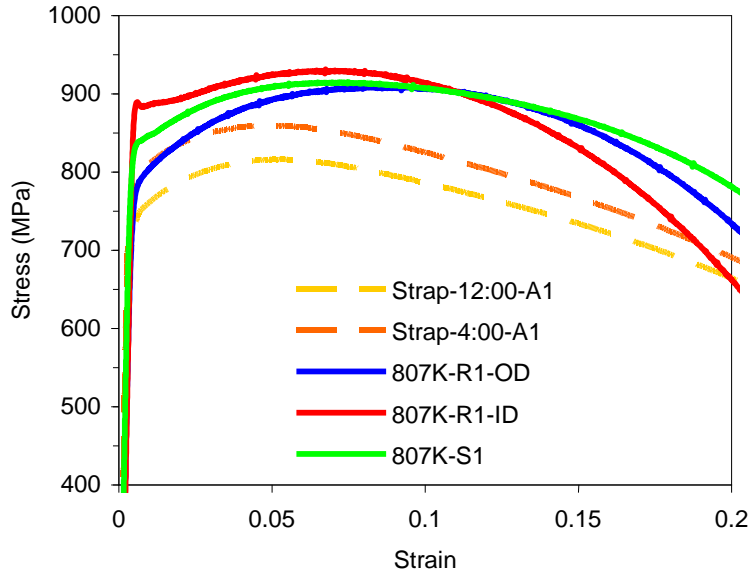


Figure 21: Comparison of AWM stress-strain curves (round bar biased to OD and ID and strip specimens) with longitudinal stress-strain curves of the X100 pipe (strap tensile specimens in dashed curves) [77]

6.3 EFFECTS OF WELD HIGH-LOW MISALIGNMENT

6.3.1 Industry Status

Girth weld failures have been reported in a number of newly constructed pipelines. The failures were typically discovered during pre-service hydrostatic proof tests. In a DOT PHMSA workshop on New Pipeline Construction Practices [78], several contributing factors were identified. These factors include a large degree of high-low misalignment, high stresses at the girth welds, inadequate tie-in and repair procedures, insufficient adherence to qualified welding procedures, improper inspection, and insufficient delay time for inspection. The high degree of high-low misalignment occurred in both mechanized welds with nominally the same wall thickness on either side of the girth welds and transitional joints between thick-walled bends and thin-walled pipes/pups. The high stresses at the girth welds are associated with lifting and lowering-in practice.

Long-term pipeline service experience demonstrates that pipelines can survive a large degree of high-low misalignment at girth welds without negative impact on the safety and integrity of pipelines. Therefore, high-low misalignment in itself does not necessarily lead to unsafe girth welds. High-low misalignment can, however, lead to other events that can ultimately cause girth weld failures. For mechanized girth welds, a high degree of high-low misalignment increases the probability of having weld defects in the root region. These defects would need to be repaired if they exceed the acceptance level. Repair welds cannot be controlled as precisely as mechanized welds. Repair welds can be susceptible to hydrogen assisted cracking (HAC) due to (1) the hydrogen environment from cellulosic-coated electrodes, (2) the increased stress level from restrained weld metal solidification environment, and (3) the high cooling rate. Repairs of deep flaws are problematic as they have much higher risk of HAC, particularly for X70 or higher grades. Tie-in welds are typically made with manual or semi-automatic welding processes. The potential welding issues associated with the repair welds can also exist in tie-in welds.

6.3.2 Understanding the Effects of High-Low Misalignment

The effects of high-low misalignment have been a focus point for strain-based design [79]. The overall view is that the high-low misalignment can have a significant negative impact on the tensile strain capacity of girth welds. Recent examination of more realistic weld profiles shows that the impact of the misalignment is strongly dependent on the weld profile and to a lesser extent to the weld strength mismatch. Welds with smooth profiles and sufficient net section thickness can tolerate a high degree of misalignment when the weld strength is even- or over-matching.

6.4 PREVENTION OF GROSS STRAIN CONCENTRATION AT WELDS

To ensure weld integrity, the possibility of strain concentration at the welds should be minimized. There are a number of contributing factors to possible strain concentration, including weld strength mismatch, high-low misalignment, weld bevel angle, weld profile (such as weld reinforcement), and flaw size. These factors need to be examined collectively to arrive at practical solutions. A number of projects are under way to develop practical and technically sound solutions [80,81].

6.5 TOUGHNESS CONSIDERATIONS

6.5.1 Characteristics of Weld and HAZ Toughness

The mechanical properties of the single- and dual-torch P-GMAW X100 pipe welds are summarized in separate topical reports [82,83,84,85]. The test results showed that good notch toughness values can be achieved in high-strength welds. However, for the materials tested in this program there was a tendency for failures in the HAZ by brittle cleavage in conventional (high-constraint) SE(B) tests, especially at -20 °C and below. Cleavage failures were less frequent in low-constraint tests.

The low-constraint SE(T) toughness (J at 0.5 mm crack growth for 3 mm initial crack size) was higher than the conventionally measured high-constraint SE(B) toughness (J at maximum load) in all cases but one, the average ratio being about 1.7. For the shallow-notched B×B base metal specimens used in this project ($a/W=0.17$ to 0.35), early tests did not show much difference between the toughness at 0.5 mm crack growth of specimens tested in tension and in bending. For more recent tests on shallow-notched girth welds, the J values at 0.5 mm crack growth were noticeably higher in SE(T) than in SE(B) specimens.

For the low-constraint SE(T) specimens tested in this project, the maximum load was attained at a crack extension around 0.5 mm. Some specimens fractured soon after the attainment of the maximum load, preventing the generation of full resistance curves, while much more flaw growth was possible in other specimens. Strain-based design assumes ductile crack propagation. If low-constraint tests reveal a possibility of brittle fracture under design conditions (of temperature and maximum flaw size), this should be addressed separately. The best way to do this remains an open issue.

6.5.2 Significance of Low HAZ Toughness

Measurement of an occasional low HAZ toughness value is often attributable to a local brittle zone (LBZ). The structural significance of LBZs has been the subject of considerable debate. Some argue that LBZs exist in virtually all welds, and that finding a low value of HAZ toughness during testing is only a matter of statistics. There is a small but finite chance that a crack in a test specimen will encounter a small LBZ.

The HAZ toughness of single-torch and dual-torch welds is shown in Figure 22. There are three test results from each weld. On the basis of the average toughness, the single-torch weld has lower toughness than the dual-torch weld. This is contrary to prior observations [86]. More in-depth examination shows that two of the specimens in each weld type have the same toughness (0.27 vs. 0.28 mm and 0.14 mm vs. 0.19 mm). The difference is the third pair, in which the single-torch weld had a CTOD of 0.04 mm while the dual-torch weld had a CTOD of 0.14 mm.

The low CTOD toughness found in modern pipeline girth welds is often associated with pop-in events at test temperatures common for welding procedure qualifications, generally from 0°C to -20°C. The pop-in events are usually associated with some degree of load drop, but in most cases, specimens do not fracture. An important question is whether the lowest pop-in toughness should be used for the prediction of large-scale structural behavior. Using the absolute lowest value of CTOD toughness can lead to unnecessary conservatism and weld repair. Since repair welds tend to have inferior quality than that of mechanized welds, unnecessary repairs lead to overall lower quality of the completed welds.

A more appropriate approach is perhaps taking into account the local nature of the microstructure that leads to the pop-in related low toughness. One might assume the low toughness exists over a small, but finite width of a weld path, say one weld pass height. The structural significance of a weld flaw may be assessed by assuming a flaw larger than the initial size, for example, initial height plus one weld bead height, and with the average toughness as opposed to the lowest pop-in value. The essential argument here is that the flaws may pop through the LBZ but become stable after the pop-through event, provided that the pop-in is small enough and that the dynamic toughness of the surrounding material is high enough. If the low toughness zone is local and the structural stability is maintained with the larger-size flaw, this approach is appropriate and would not lead to overly conservative assessment.

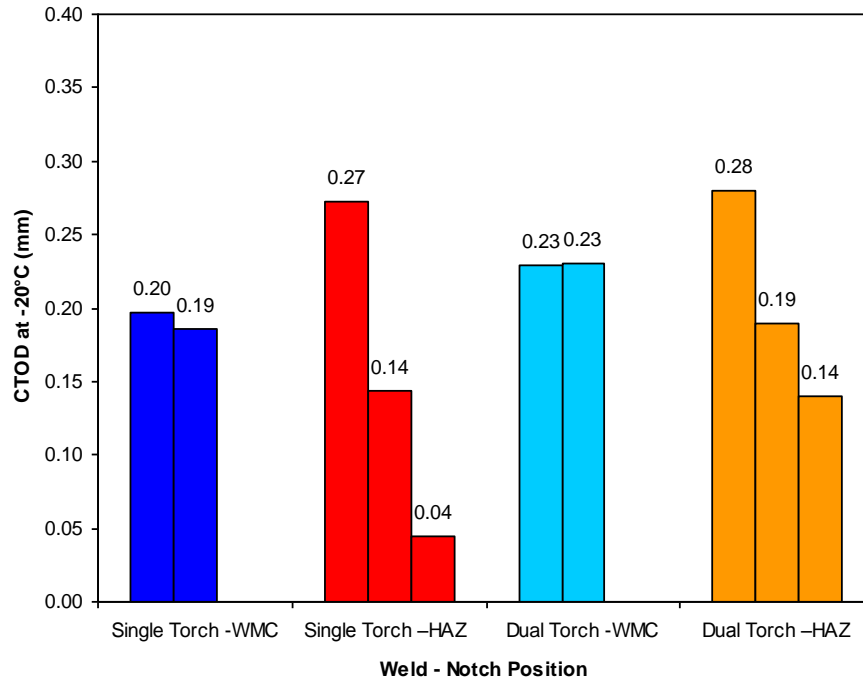


Figure 22: CTOD toughness of the X100 weld at -20°C

7 STRAIN-BASED DESIGN OF PIPELINES

7.1 STRAIN-BASED DESIGN IN PIPELINE CONSTRUCTION AND MAINTENANCE

7.1.1 Stress- vs. Strain-Based Design

Traditional pipeline designs primarily focus on pressure containment through limiting the hoop stress to a certain percentage of the specified minimum yield stress (SMYS). For instance, the concept of class location is based on the ranking of the maximum applied hoop stress as a percentage of SMYS.

Strain-based design (SBD) refers to pipeline design methodologies which have a specific goal of maintaining pipeline service and integrity under large longitudinal plastic strains (>0.5 %). Such large strains may come from frost heave and thaw settlements in arctic regions, seismic activities, landslides, mine subsidence, or other events. For offshore pipelines, large longitudinal strains may be induced by upheaval or lateral buckling or pipeline movements due to underwater landslides. In North America, the need for SBD is primarily driven by northern pipeline projects where these pipelines may traverse regions of discontinuous permafrost. In other parts of the world, SBD is playing an increasingly important role for pipelines going through areas of seismic activity and mine subsidence.

Contrary to some misconception, stress- and strain-based designs are not mutually exclusive. Strain-based design should be viewed as additional design considerations complementary to the traditional stress-based design. A pipeline designed using strain-based design still needs to meet the requirements of traditional stress-based design.

Strain-based design encompasses at least two limit states: tensile rupture and compressive buckling. The tensile rupture is an ultimate limit state which is related to the breach of the pressure boundary. The compressive buckling could be either a service limit state or an ultimate limit state. To analyze the limit states, it is necessary to know the magnitude of strain demand (applied strain) and strain capacity (strain limit).

7.1.2 Strain-Based Design for New Pipeline Construction

A process highlighting the key considerations for strain-based design is outlined by Wang, et al. in a report to US DOT and PRCI [87]. The process starts from high level considerations and directs users to specific steps for detailed technical designs.

1. *Determine the nature of the strain demand.* The strain demand could be a one-time event, such as the strain at a fault crossing in a seismic event. The strain demand can vary and/or accumulate over time, such as in the case of frost heave and thaw settlement. The strain demand in the area of mine subsidence could be a one-time event or a time-dependent accumulative event.
2. *Determine and classify postulated failure events.* In some cases, the most critical event might be in the construction/installation phase, such as an offshore installation by reeling. For most onshore pipelines, the operation phase is the most critical as the tensile strain capacity is reduced by the internal pressure.
3. *Determine a set of target tensile strain capacity levels by introducing appropriate safety factors to the estimated strain demand.*
4. *Collect basic design and material information which affect the tensile strain capacity.* Some of the key parameters are (but are not limited to): (1) pipe wall thickness, (2) pipe tensile properties, (3) weld tensile properties, (4) weld toughness, (5) pipe dimensional tolerance, (6) field control of high-low misalignment, (7) target acceptable flaw size, and (8) inspection method.
5. *Determine if there are time-dependent degradation mechanisms of the material properties, such as strain aging or hydrogen embrittlement.* If present, these mechanisms should be considered. The effects of the material property degradation may be incorporated into the material qualification phases or monitored as a part of the pipeline integrity management program.
6. *Conduct a preliminary assessment of the limit states for all postulated failure events.*
7. *Select an appropriate level of assessment by balancing the need for accuracy and the requirements for material property data, flaw sizing, and construction quality control.*
8. *Develop linepipe specifications and welding procedure requirements based on the input requirements of the assessment procedures.*
9. *Conduct material characterization tests per the requirements of No. 8.*
10. *Evaluate strain capacity against the target values, taking into consideration the material property variations.*
11. *Conduct confirmation tests when needed.*
12. *Develop and implement material property surveillance protocol if time-dependent degradation mechanisms exist and their effects are not fully covered in the material qualification phase.*

13. *Develop and implement strain demand monitoring systems.* When needed, verify the reliability and accuracy of such systems.
14. *Develop and implement continuous evaluation and mitigation plans if the strain demand and material properties evolve over time.*

A successful design often involves multiple iterations involving material specifications, welding procedure qualification, NDT, flaw acceptance criteria, and field implementation protocol. Design procedures capable of correlating those relevant parameters, such as those developed in another DOT/PRCI project by CRES [87], are very useful to effectively work towards a near-optimal design with all constraints duly considered.

7.1.3 Strain-Based Design for Pipeline Maintenance

Under normal operating conditions, pipelines experience greater stress in the hoop direction than in the longitudinal direction. Consequently, traditional pipeline designs focus on the control of the hoop stress, normally limiting its maximum value to a certain percentage of the specified minimum yield strength (SMYS). The detection and assessment of threats for in-service pipelines also assume the hoop stress being the primary driver to potential failures.

Even though most pipelines are designed on the basis of controlling hoop stress, these pipelines may still experience longitudinal loading in service. Such loading may come from ground movements. Even in the absence of large ground movements, longitudinal stresses can exist from pipeline construction, temperature changes of the pipeline and the variations in terrain and support conditions. Therefore, some degree of tolerance to longitudinal stresses and strains is necessary for all pipelines.

For most in-service pipelines, failures driven by longitudinal stresses or strains are relatively rare events, in comparison to failures driven by hoop stresses. However, the consequence of failures due to longitudinal stresses and strains can be just as devastating as other failures. In most cases, those failures are associated with ground settlement or movement. The loading transmitted to pipelines from the ground settlement and movement is typically a combination of displacement and load controlled events. The resulting applied stresses and strains can have a wide spectrum, ranging from small strains to very large strains.

One of the emerging concerns of pipeline operators is that the historical safe operation of pipelines may not be sufficient to justify the continued operation of pipelines, without further assurance of the pipeline integrity. Recent incidents of pipeline failures and subsequent investigations by US federal agencies have led to greater public scrutiny of pipeline safety. It is reasonable to expect that the risk of pipeline failures due to ground settlement and movement hazards is one of the critical issues that will need to be addressed. Unfortunately, most of the integrity verification options, such as hydrostatic testing and inline inspection, are not particularly effective in ensuring the integrity of pipeline girth welds without proper considerations of the weld features and applied stresses and strains imposed on the pipelines.

7.2 PHYSICAL PROCESS OF TENSILE STRAIN FAILURES

The physical process of tensile strain failure starting from a planar girth weld flaw may be described as follows. Under increasing remotely-applied stress or strain, the flaw first blunts from the initial sharp flaw. The blunted flaw would initiate ductile tearing upon further loading. The small ductile tear would then grow in size, and eventually form a growing flaw with a sharp tip. The initial blunted profile remains behind the sharp flaw. The evolution of the flaw profiles is shown in Figure 23.

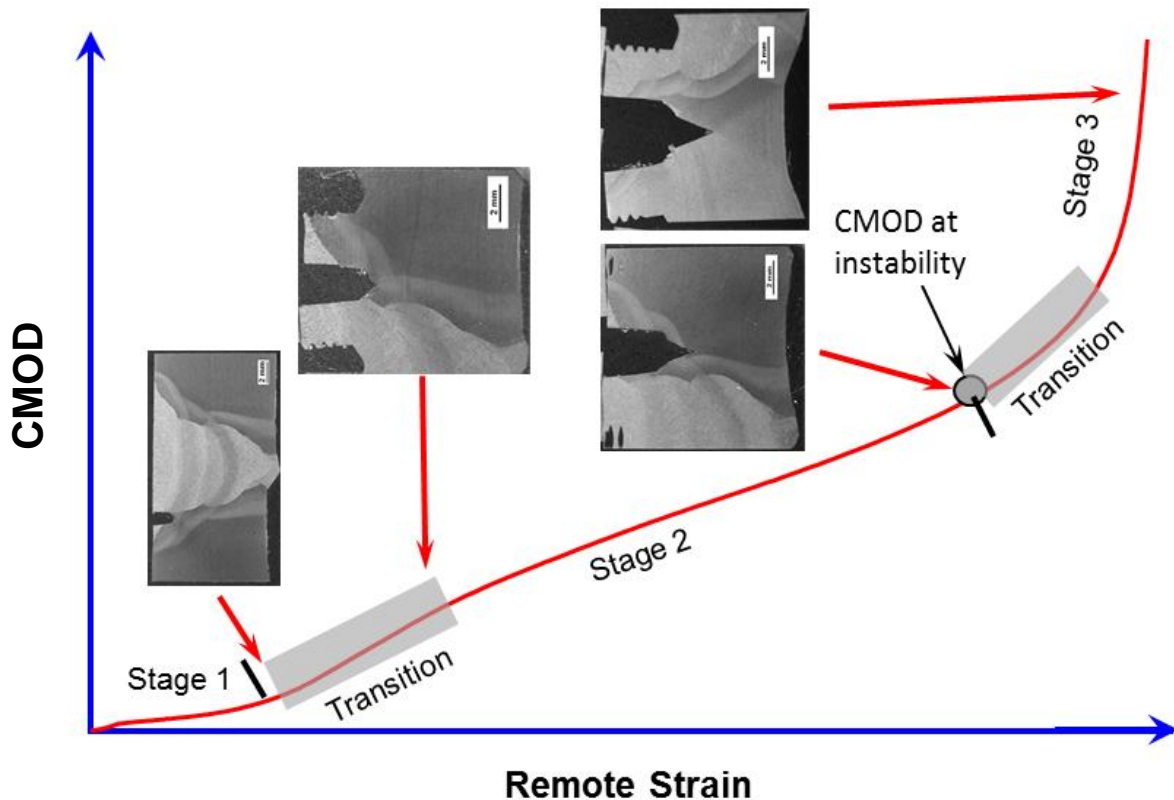


Figure 23: Flaw profile evolution relative to remote tensile strain

The importance of flaw growth is shown by the sequence of the growth relative to the tensile strain value at the failure events. The strain vs. flaw growth history of full-scale tests conducted by JFE is shown in Figure 24 [88]. It is evident that the strain at 0.5 mm flaw growth is very close to the strain of leakage, whereas the flaw growth at the point of leakage is much greater than 0.5 mm. However most of growth occurs near the final leakage point accompanied by a small increase of remote strain.

The start of initiation and the CTOD vs. strain history from Østby is shown in Figure 25 [89]. The amount of flaw growth is about 0.65 mm at the point when the CTOD and strain relation turns nearly vertical, indicating only a small increment of strain with increase of CTOD.

The flaw growth history vs. strain by Minnaar, et al., is shown in Figure 26 [90]. At a flaw growth of 0.5-0.6 mm, the strains are very close to the final failure strains.

The overall observations of those tests are:

- (1) large flaw growth can be observed at the termination of a test.
- (2) much of the flaw growth occurs at the final stage of straining.
- (3) the amount of flaw growth up to a strain value very close to the final failure strain can be quite small.
- (4) once the flaw growth rate starts to accelerate, the remaining additional strain capacity is limited.

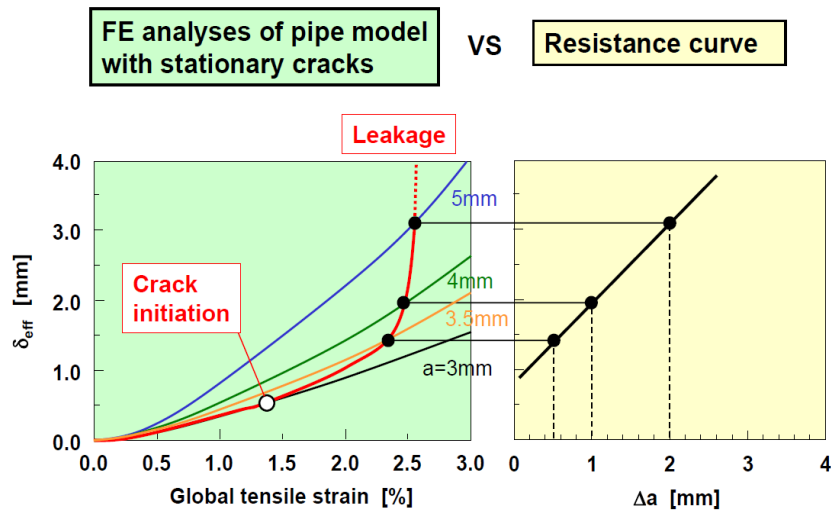
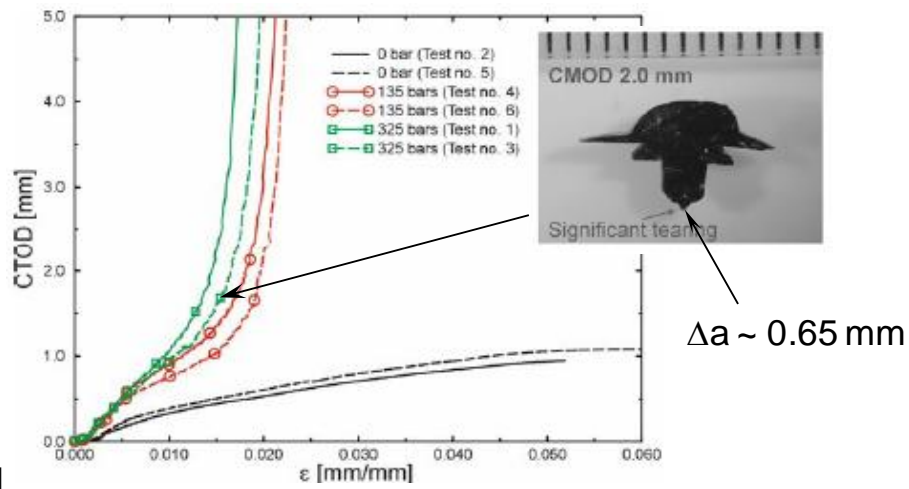


Figure 24: Flaw growth vs. strain history from full-scale pipe tests



[88]

Figure 25: Crack opening profile vs. CTOD-strain history from full-scale pipe tests [89]

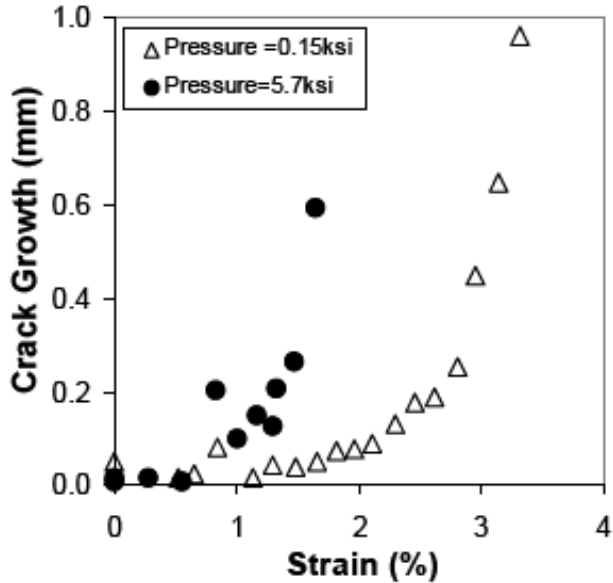


Figure 26: Crack growth vs. strain history from full-scale pipe tests [90]

7.3 STATUS OF TENSILE STRAIN MODELS

The tensile strain capacity of a pipeline is controlled by the tensile strain capacity of its girth welds. The girth welds here refer to the entire weld region, including the weld metal, fusion boundary, and the heat-affected zone (HAZ). Girth welds tend to be the weakest link due to the possible existence of weld defects and often deteriorative metallurgical and/or mechanical property changes from welding thermal cycles. Consequently, tensile strain capacity (TSC) is intrinsically related to the girth welding procedure qualification and flaw acceptance criteria. The welding procedure qualification involves the control of essential variables to ensure the equivalence of procedure qualification welds and field production welds, and the definition and execution of mechanical tests of welds. The flaw acceptance criteria are implemented for field production welds to ensure a certain level of performance is achieved with respect to overall TSC.

Some of the earliest work specifically targeted to develop assessment procedures for strain-based design was supported by PRCI. The tensile limit state was formulated around the concept of crack driving force (demand) and apparent toughness (capacity) [91,25,26,76,27]. This approach was subsequently adopted in Annex C of CSA Z662 2007 Edition [92].

There are three major predictive models for estimating the TSC of pipeline girth welds, including the SINTEF [93,94,95], ExxonMobil [96,97,98,99] and CRES models developed for DOT and PRCI [87]. Specifics related to the SINTEF and ExxonMobil models are not readily available in the public domain, whereas, the CRES models are fully described in public-domain documents.

7.4 CRES TSC MODELS FOR DOT AND PRCI

7.4.1.1.1 Limit State Based on Initiation Control

The initiation-based tensile limit state is defined as $CTOD_F = CTOD_A$, where $CTOD_F$ is the crack-driving force and $CTOD_A$ (or δ_A) is the apparent toughness. The apparent toughness is the toughness corresponding to the onset of stable tearing. Both $CTOD_F$ and $CTOD_A$ are represented by the crack tip opening displacement, i.e., CTOD. The initiation-based limit state is schematically illustrated in Figure 27.

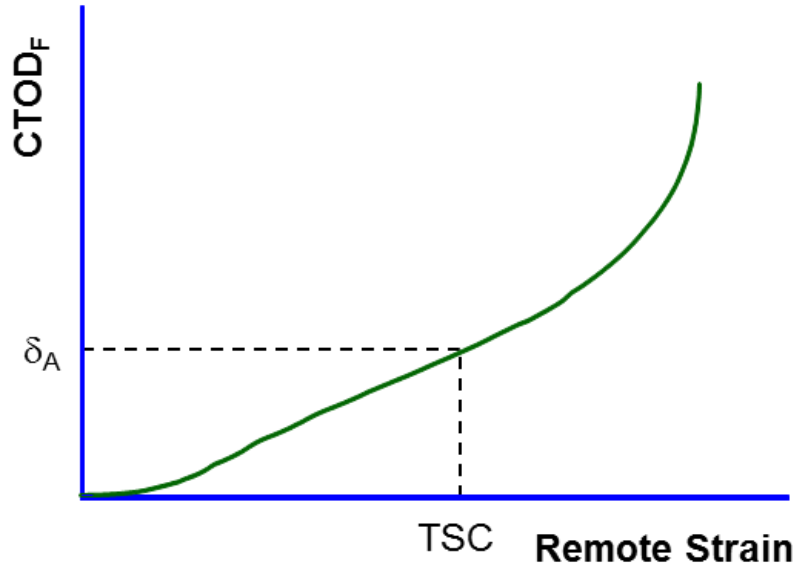


Figure 27: Typical $CTOD_F$ and definition of initiation-control based limit state

7.4.1.2 Limit State Based on Ductile Instability

The ductile-instability-based limit state is illustrated in Figure 28. Here the fracture toughness is expressed as a function of flaw growth which is usually termed as tearing resistance curve (i.e., $CTOD_R$). The limit state is defined as the tangent point of the crack driving force curve and the fracture toughness curve as shown in Figure 28.

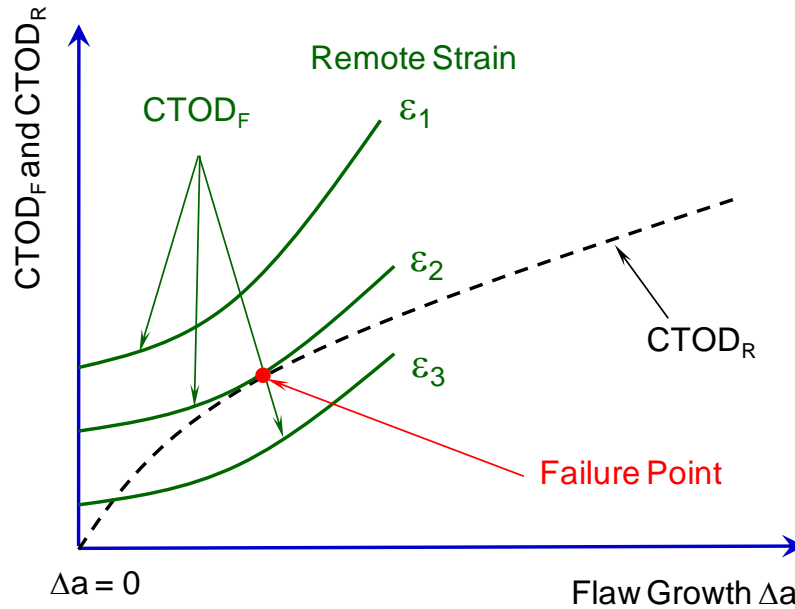


Figure 28: Definition of ductile-instability based limit state

7.4.1.3 Multi-Level Tensile Strain Models

Although case-specific finite element analysis is an option in the CRES TSC models, the most valuable part of the models is a library of parametric equations which give the tensile strain capacity as a function of a number of input parameters.

The TSC models are organized in four levels:

Level 1 Models – Initial Screening and Feasibility Studies

The Level 1 model is intended for quick estimations of the likely tensile strain capacity. The TSC is tabulated for selected pipe dimensions, material properties, and flaw size. The apparent toughness is estimated from upper shelf Charpy impact energy.

Level 2 Models – Nominal Assessment with Standard Toughness Data

The Level 2 models are given in a library of parametric equations as described in the following sections. The apparent toughness can be estimated from either upper shelf Charpy impact energy or the upper shelf standard CTOD toughness.

Level 3 Models – Advanced Assessment with Low-Constraint Toughness

The Level 3 models have two options. Level 3(a) uses an initiation control limit state. Level 3(b) uses a ductile instability limit state.

In Level 3(a), the TSC is obtained by the use of the same library of parametric equations as in Level 2. The apparent toughness may be obtained by a number of low constraint test options, including shallow-notched SE(B), SE(T), or CWP.

In Level 3(b), the crack driving force, $CTOD_F$, is expressed by a group of iso-strain curves constructed from the same library of parametric equations. In this application, various levels of strains are obtained as a function of flaw depth from the equations.

Level 4 Models – Advanced Analysis with Direct FEA Calculation

The Level4 models are structured with two options representing two limit states. In contrast to Level 3 models, where the driving force relations are expressed in parametric equations, the driving force relations are directly obtained from FEA in this level. The toughness options are the same as in Level 3.

This level allows for special cases when the specific weld geometry and material property conditions do not allow the use of the first three options. The Level 4 models should only be exercised by seasoned experts.

7.4.2 Input Parameters of TSC Prediction Equations

The input parameters of the TSC prediction equations are given in Table 10.

Table 10: Input parameters for the CRES TSC equations

Parameters	Unit	Description
OD	mm	Pipe outside diameter
t	mm	Pipe wall thickness
a	mm	Initial flaw height
$2c$	mm	Initial flaw length
h	mm	Misalignment at girth weld
σ_y	MPa	Yield strength of base metal at 0.5% total elongation strain
σ_u	MPa	Ultimate tensile strength of base metal
σ_u^W	MPa	Ultimate tensile strength of girth weld
δ_A	mm	Apparent toughness $CTOD_A$
p_i	MPa	Internal pressure
$\eta = a/t$		Normalized flaw depth
$\beta = 2c/t$		Normalized flaw length
$\psi = h/t$		Normalized misalignment at girth weld
$\xi = \sigma_y / \sigma_u$		Ratio of yield strength to tensile strength of base metal
$\phi = \sigma_u^W / \sigma_u$		Weld strength mismatch ratio
f_p		Internal pressure factor (the ratio of hoop stress to yield strength of base metal)

7.4.3 TSC Prediction Equations

The TSC prediction equations are given in the following,

$$\text{TSC} = \min(\text{uEL}, P(f_p)G(t)\text{TSC}_p) \quad (7-1)$$

where uEL represents pipe uniform strain and the functions $G(t)$ and $P(f_p)$ characterize the effect of wall thickness and internal pressure, respectively. The function $G(t)$ is given as

$$G(t) = \left(\frac{15.9}{t} \right)^{0.809(1+1.503\psi^{1.229})} ; \quad (7-2)$$

and the function $P(f_p)$ is in the form of

$$P(f_p) = \begin{cases} P_{\max} - \frac{5}{3}f_p(P_{\max} - 1) & \text{if } 0 \leq f_p < 0.6 \\ 1 & \text{if } 0.6 \leq f_p \leq 0.8 \end{cases} . \quad (7-3)$$

In the CRES report to DOT and PRCI [87], P_{\max} is 1.5.

The function TSC_p of Eq. (7-1) is given as

$$\text{TSC}_p = A \frac{F(\delta_A)}{1 + F(\delta_A)}, \quad (7-4)$$

where the function $F(\delta_A)$ is

$$F(\delta_A) = (C\delta_A)^{B\delta_A^D}. \quad (7-5)$$

The coefficients A , B , C , and D in Eqs. (7-4) and (7-5) are functions of the input parameters shown in Table 10.

For girth weld made of mechanized (GMAW) processes, the coefficient A , B , C , and D are given as,

$$A = a_1 e^{a_2/\beta} e^{\alpha_3 \eta \beta e^{a_4/\beta}} \left[1 + a_5 \psi^{a_6} + a_7 \psi (\eta \beta)^{a_8} \right] \left(1 + a_9 \xi^{a_{10}} \phi^{a_{11}} + a_{12} \psi^{a_{13}} \xi^{a_{14}} \right), \quad (7-6)$$

$$B = \beta^{b_1} \eta^{b_2 \beta^{b_3} / \eta} \left[b_4 \phi^{b_5} (b_6 \phi^{b_7})^\xi + b_8 \psi^{b_9} \right], \quad (7-7)$$

$$C = e^{c_1/\beta} e^{\frac{c_2 \beta}{(1+c_3 \beta) \eta}} \left(1 + c_4 \psi^{c_5} + c_6 \psi e^{-\eta} + c_7 \psi e^{-\beta} \right) \left(c_8 + c_9 \phi^{c_{10}} + c_{11} \xi^{c_{12}} \phi \right), \quad (7-8)$$

$$D = d_1 \beta^{d_2} \eta^{\frac{d_3 \beta}{1+d_4 \beta}} \left(1 + d_5 \psi^{d_6} \right) \left(1 + d_7 \xi^{d_8} + d_9 \phi^{d_{10}} \right). \quad (7-9)$$

The constants in the above four equations are listed in Table 11.

For girth weld made of flux-cored arc welding (FCAW) or shielded metal arc welding (SMAW) processes. The coefficient A , B , C , and D are given as,

$$A = a_1 e^{a_2/\beta} e^{\alpha_3 \eta \beta e^{a_4/\beta}} \left[1 + a_5 \psi^{a_6} + a_7 \psi^{a_8} (\eta \beta)^{a_9} \right] \left(1 + a_{10} \xi^{a_{11}} \phi^{a_{12}} \right), \quad (7-10)$$

$$B = \beta^{b_1} \eta^{b_2 \beta^{b_3} / \eta} \left[b_4 \phi^{b_5} (b_6 \phi^{b_7})^\xi + b_8 \psi^{b_9} \right], \quad (7-11)$$

$$C = e^{c_1/\beta} e^{\frac{c_2\beta}{(1+c_3\beta)\eta}} \left(1 + c_4\psi^{c_5} + c_6\psi e^{-\eta} + c_7\psi e^{-\beta}\right) \left(c_8 + c_9\phi^{c_{10}} + c_{11}\xi^{c_{12}}\phi\right), \quad (7-12)$$

$$D = d_1\beta^{d_2}\eta^{d_3} \left(1 + d_4\psi^{d_5} + d_6\eta\beta\psi\right) \left(1 + d_7\xi^{d_8} + d_9\phi^{d_{10}}\right). \quad (7-13)$$

The constants in the above four equations are listed in Table 12.

The applicable range of the TSC predictive equations are given in Table 13.

Table 11: Constants of TSC equations for GMAW

a_1	2.084	b_1	-5.005×10^{-2}	c_1	1.409	d_1	2.209×10^{-2}
a_2	2.812×10^{-1}	b_2	-5.139×10^{-3}	c_2	2.345×10^{-1}	d_2	1.156
a_3	-4.950×10^{-1}	b_3	4.485×10^{-1}	c_3	1.125	d_3	1.601
a_4	7.373×10^{-1}	b_4	1.417	c_4	4.181	d_4	8.964×10^{-1}
a_5	-5.005	b_5	2.217	c_5	1.201	d_5	1.383
a_6	1.186	b_6	1.029	c_6	-5.384	d_6	1.333
a_7	1.644	b_7	-2.598	c_7	2.406	d_7	9.313×10^{-2}
a_8	7.374×10^{-1}	b_8	-2.679	c_8	-2.154×10^{-1}	d_8	-2.240
a_9	-9.829×10^{-1}	b_9	1.694	c_9	-5.237×10^{-3}	d_9	8.559
a_{10}	8.655×10^{-2}			c_{10}	9.889	d_{10}	-3.719
a_{11}	-1.029×10^{-1}			c_{11}	3.547×10^{-1}		
a_{12}	-1.500×10^{-1}			c_{12}	-7.513×10^{-1}		
a_{13}	1.025						
a_{14}	5.557						

Table 12: Constants of TSC equations for FCAW/SMAW

a_1	9.281×10^{-1}	b_1	-5.578×10^{-2}	c_1	1.609	d_1	6.822×10^{-3}
a_2	9.573×10^{-2}	b_2	1.112×10^{-2}	c_2	1.138×10^{-1}	d_2	1.014
a_3	-5.053×10^{-1}	b_3	-1.735×10^{-1}	c_3	6.729×10^{-1}	d_3	1.746
a_4	3.718×10^{-1}	b_4	1.675	c_4	2.357	d_4	2.378
a_5	-2.023	b_5	2.603×10^{-1}	c_5	1.057	d_5	9.434×10^{-1}
a_6	7.585×10^{-1}	b_6	1.106	c_6	-4.444	d_6	-1.243
a_7	6.299×10^{-1}	b_7	-1.073	c_7	1.727×10^{-2}	d_7	35.79
a_8	5.168×10^{-1}	b_8	-1.519	c_8	-1.354×10^{-2}	d_8	7.500
a_9	7.168×10^{-1}	b_9	1.965	c_9	-1.224×10^{-2}	d_9	62.94
a_{10}	-9.815×10^{-1}			c_{10}	8.128	d_{10}	-6.930
a_{11}	2.909×10^{-1}			c_{11}	2.007×10^{-1}		
a_{12}	-3.141×10^{-1}			c_{12}	-1.594		

Table 13: Applicable range of TSC equations

Parameters	Range
δ_A	0.2 mm – 2.5 mm
f_p	0.0 – 0.8
$\eta = a/t$	0.05 – 0.5
$\beta = 2c/t$	1.0 – 20.0
$\psi = h/t$	0.0 – 0.2
$\xi = \sigma_y / \sigma_u$	0.75 – 0.94
$\phi = \sigma_u^W / \sigma_u$	1.0 – 1.3

7.4.4 Determination of Apparent Toughness

7.4.4.1 CTOD_A from Upper Shelf Charpy Energy

The apparent toughness CTOD_A may be estimated from Charpy upper shelf impact energy, U_{CVN} . For X70 and X80 linepipes, the conversion relation is given as

$$CTOD_A = \left(0.00634 \frac{\sigma_y}{\sigma_s} - 0.00155 \right) U_{CVN}, \quad (7-14)$$

where σ_y is the yield stress at 0.5 % total strain and σ_s is the ultimate tensile strength in the pipe longitudinal direction. The units of the Charpy energy U_{CVN} and CTOD_A are Joule and mm. Equation (7-14) is valid to a maximum CTOD_A of 1.2 mm.

7.4.4.2 CTOD_A from Standard Deeply-Notched SENB

A multiplication factor between 1.5 and 2.0 may be applied to the CTOD toughness, δ_m , which is the CTOD at the maximum load from standard deeply-notched SE(B) test. A default factor of 1.75 is recommended. This factor is applicable to standard SE(B) specimens without side grooves.

7.4.4.3 CTOD_A from SE(T) Resistance Curves

The CTOD_A may be obtained from SE(T) resistance curves at a flaw growth Δa that is between 0.5 and 1.0 mm as illustrated in Figure 29. The selection of flaw growth depends on pipe wall thickness and possibly other parameters. Generally, Δa is recommended as 0.5 mm for pipe wall thickness of 12.7 mm (0.5 inch) and as 1.0 mm for pipe wall thickness of 25.4 mm (1.0 inch). When the pipe wall thickness is between the above two extreme values, a linear interpolation may be used to determine the appropriate Δa value for the determination of CTOD_A.

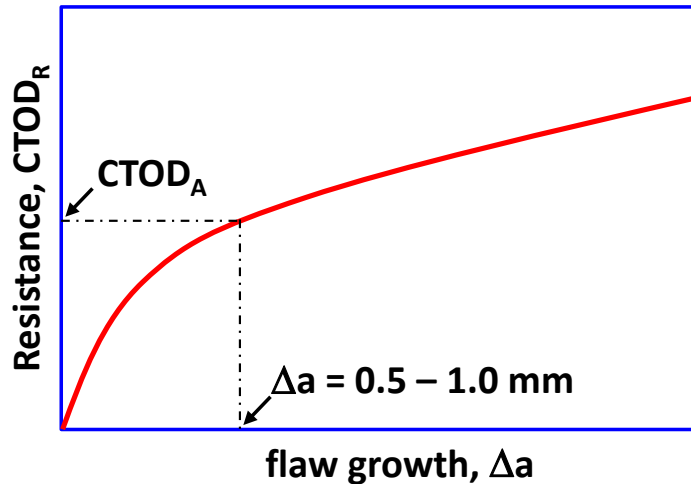


Figure 29: Illustration of deriving $CTOD_A$ from SENT resistance curve

7.4.4.4 $CTOD_A$ from Shallow-Notched SE(B) Resistance Curves

Results from CANMET on linepipe steels without weld have shown that the resistance curves of shallow-notched SE(B) are similar to those of SE(T) for the same material [100]. Recent results shows that the resistance curves of shallow-notched SE(T) are higher than that of SE(B) by an averaged factor of approximately 1.2. Until further data analysis is completed, it is recommended that the same procedure for SE(T) be used to compute $CTOD_A$ from shallow-notched SE(B) specimens.

7.5 ASSESSMENT OF CWP DATA FOR STRAIN-BASED DESIGN

7.5.1 Overview of CWP Data

A total of 34 CWP specimens were tested in this program. Two of the 34 specimens were trial specimens without welds. The remaining 32 specimens included three welding procedures (one single-torch and two dual-torch). Eighteen specimens were made with the single-torch weld (Round 1); ten specimens were made with the first round dual-torch weld (Round 2); and four specimens were made with the second round dual-torch weld (Round 3). For each welding procedures, the effect of flaw size, test temperature, and notch locations (weld center or HAZ) were examined. The details of the test matrix and results can be found in companion reports [101,59].

At the start of this report, the results from 22 of the 34 specimens were available. The 22 specimens included the two trial specimens (no weld, flaw cut in the base metal), 18 single torch weld (Round 1) specimens, and two first round dual-torch weld (Round 2) specimens. The details of the 22 CWP test specimens and test results are given in Table 14.

Table 14: Summary of test conditions and results of 22 CWP specimens used in TSC analysis

Specimen ID	Flaw Locations	Round of Welding	Target Initial Flaw Size (mm x mm)	Measured Initial Flaw Depth (mm)	Test Temperature		Nominal Stress at Maximum Load		Tensile Strain Capacity at Maximum Load (%)			Flaw Growth at the Greatest Depth	State at the Termination of Test
					(°C)	(°F)	(MPa)	(ksi)	Upper Part	Lower Part	Average		
CWP-01-BM-RT	BM	N/A	3 x 50	2.7	RT	RT	848	123	4.8	3.6	4.2	8.7	Manual stop, approaching or at maximum load
CWP-00-BM-LT	BM	N/A	3 x 50	3.1	-20	-4	859	125	2.3	4.0	3.2	1.3	
CWP-16-WM-RT	Weld	1	3 x 50	3.4	RT	RT	808	117	2.2	2.4	2.3	8.0	
CWP-03-HAZ-RT	HAZ	1	3 x 50	2.8	RT	RT	820	119	1.8	1.6	1.7	6.2	
CWP-11-WM-LT	Weld	1	3 x 50	3.1	-20	-4	841	122	2.6	2.4	2.5	7.6	Specimen broke into two pieces
CWP-19-WM-LT	Weld	1	3 x 50	3.3	-20	-4	820	119	2.3	2.3	2.3	2.0	Manual stop, approaching or at maximum load
CWP-01-WM-RT	Weld	1	6 x 30	6.1	RT	RT	816	118	2.4	1.3	1.9	3.2	
CWP-15-HAZ-RT	HAZ	1	6 x 30	6.0	RT	RT	822	119	3.3	2.0	2.7	6.1	
CWP-10-WM-LT	WM	1	6 x 30	6.1	-20	-4	822	119	1.8	1.8	1.8	4.8	
CWP-12-HAZ-LT	HAZ	1	6 x 30	6.1	-20	-4	851	123	3.7	3.2	3.5	1.8	
CWP-02-HAZ-LT	HAZ	1	3 x 50	3.0	-20	-4	853	124	3.8	3.1	3.5	1.8	
CWP-05-HAZ-LT	HAZ	1	3 x 50	2.9	-20	-4	831	121	1.7	2.9	2.3	1.0	
CWP-06-WM-RT	Weld	1	2 x 75	2.1	RT	RT	826	120	1.9	2.7	2.3	2.0	
CWP-07-WM-LT	Weld	1	2 x 75	2.2	-20	-4	853	124	4.2	2.3	3.3	1.7	
CWP-08-HAZ-RT	HAZ	1	2 x 75	2.2	RT	RT	827	120	5.6	2.8	4.2	0.9	
CWP-09-HAZ-LT	HAZ	1	2 x 75	2.0	-20	-4	851	123	2.1	4.8	3.4	0.6	
CWP-13-WM-LT	Weld	1	3 x 50	3.0	-40	-40	849	123	2.5	2.1	2.3	2.4	
CWP-14-WM-LT	Weld	1	3 x 50	3.2	-40	-40	849	123	2.3	2.5	2.4	2.7	
CWP-17-HAZ-LT	HAZ	1	3 x 50	3.1	-40	-40	865	125	2.9	2.7	2.8	0.8	
CWP-18-HAZ-LT	HAZ	1	3 x 50	2.8	-40	-40	865	125	3.1	3.9	3.5	0.9	
CWP-20-WM-RT	Weld	2	3 x 50	2.9	RT	RT	812	118	1.5	1.9	1.7	4.9	Manual stop, approaching or at maximum load
CWP-21-HAZ-RT	HAZ	2	3 x 50	3.1	RT	RT	830	120	1.9	1.8	1.8	2.7	

7.5.2 Overall Assessment Process

The TSC of a pipeline in service conditions (with internal pressure) is generally lower than that for non-pressurized conditions. The TSC for pressurized conditions sets the limits for pipeline designs.

In the development of the TSC prediction equations (as shown in Section 7.4.3), the focus was on the pipeline subject to maximum allowed operating pressures (MAOP). The TSC at lower or non-pressurized conditions was modeled with the pressure function $P(f_p)$ given in Eq. (7-3). Equation (7-3) represents a simplified model for the pressure effect where the only variable in the equation is the pressure factor (f_p). The P_{max} in Eq. (7-3) was set constant (i.e., 1.5) based on the conservative estimate from a number of analyzed cases.

Detailed analysis shows that other parameters also affect the pressure function, especially the normalized flaw depth ($\eta = a/t$). It was found that Eq. (7-3) is overly conservative for flaws with low a/t ratios. To improve the accuracy of the TSC calculations for CWP specimens, the pressure function was modified to include the flaw depth. To apply the modified pressure function, P_{max} was replaced with the following values,

$$P_{max} = \begin{cases} 2.0(1.13 - \eta) & \text{if } \eta < 0.38 \\ 1.5 & \text{if } \eta \geq 0.38 \end{cases} \quad (7-15)$$

7.5.3 Determination of Apparent Toughness

Three types of small-scale toughness tests were performed: Charpy, SE(B), and SE(T). The Charpy and SE(B) tests were conducted at various temperatures and the full transition curves were obtained from both Charpy and SE(B) tests. The CTOD resistance curves (CTOD_R) were obtained from the SE(T) specimens. The details of the small-scale toughness tests can be found in a companion report [82,83,84,85].

The apparent toughness (i.e., CTOD_A) was determined following the procedures specified in Section 7.4.4. The upper-shelf Charpy energy and CTOD values were obtained from the Charpy and CTOD transition curves and used to determine the CTOD_A. The conversion equations for X70-X80 pipes were used to calculate the CTOD_A from the upper-shelf Charpy energy. A conversion factor of 2 was used to calculate the CTOD_A from the upper-shelf CTOD value obtained from SE(B) data. A flaw growth (Δa) of 0.75 mm was used to calculate the CTOD_A from the SE(T) CTOD resistance curves. The summary of the small-scale toughness data and calculated apparent toughness (CTOD_A) are given in Table 15.

Table 15: Summary of small-scale toughness data and calculated apparent toughness

Materials			Tensile Properties			Charpy and SENB			CTOD _R = $c_1 * \Delta a^{c_2}$			CTOD _A		
Pipe Material	Weld Attribute	Flaw Location	Yield Strength		Y/T	Upper Shelf Charpy Energy		Upper Shelf CTOD (SENB)	Flaw Depth	c ₁	c ₂	From Charpy	From CTOD (Conversion Factor = 2.0)	From SENT R-curve ($\Delta a = 0.75$ mm)
			(ksi)	(MPa)		(J)	(ft-lbf)							
X100	No	Pipe	113	781	0.91	287	212	0.38*	3	1.364	0.833	1.21	0.76	1.07
									6	1.264	0.574	1.21	0.76	1.07
	Single Torch (Round 1)	Weld	121	835	0.91	162	119	0.20	3	0.424	0.774	0.69	0.40	0.34
									6	0.424	0.774	0.69	0.40	0.34
		HAZ	113	781	0.91	234	173	0.38	3	1.027	0.747	0.99	0.76	0.83
									6	0.800	0.647	0.99	0.76	0.66
	Dual Torch (Round 2)	Weld	120	827	0.93	141	104	0.22	3	0.459	0.805	0.61	0.44	0.36
									6	0.459	0.805	0.61	0.44	0.36
		HAZ	113	781	0.91	231	170	0.38*	3	0.891	0.836	0.97	0.76	0.70
									6	0.734	0.726	0.97	0.76	0.60

* Not available, used single torch data

7.5.4 Comparison of Test Data with Model Predictions

7.5.4.1 Understanding Experimentally Measured Tensile Strain Capacity

In a CWP test, strains are measured at multiple locations by LVDTs and strain gages. The strain capacity is usually taken from the remote regions away from the weld and flaw. In the case of the current CWP tests, the strain capacity is the remote strain measured at LVDTs 1A, 2A, 1B, and 2B at the point of maximum load or specimen failure by rupture. LVDTs 1A and 1B are located on the OD side. LVDTs 2A and 2B are located on the ID side. LVDTs 1A and 2A are above the weld and LVDTs 1B and 2B are below the weld. During loading of the specimen, the strains from those four LVDTs are not the same. The strains from LVDTs 1A and 2A are averaged to give the remote strain above the weld. Similarly the strains from LVDTs 1B and 2B are averaged to give the remote strain below the weld. Those averaged strains are further averaged to give a single strain value at the point of maximum load or specimen failure. This single strain value is often referred to as the “tensile strain capacity.” It has been shown from the current tests and other tests that the averaged strains below and above weld can be quite different, sometimes by a factor of two. The cause for such difference is attributable to very small variations in material tensile properties and the flat stress-strain curve in the plastic regime of the stress-strain curve [102].

When a CWP specimen is under tension load, there is an equivalence of gross-section stress along the reduced section of the specimen as the cross-section of the specimen is constant along the length. If there is a variation of the tensile properties along the length of the pipe, the same level of gross-section stress will produce varying levels of remote strains. Therefore it should be expected that strains measured at various locations can show large variations when the stress-strain curves are flat.

7.5.4.2 Comparison of TSC Using Initiation Control Limit State

In this section the experimentally measured TSC is compared with predicted TSC with an initiation control limit state. In Figure 30, the prediction is made with $CTOD_A$ computed from upper shelf Charpy energy. As explained above, the experimentally measured TSC is the averaged strain value from four LVDTs in the remote regions of the specimen; above and below the plane of the flaw. With the exception of one test, the predicted values fall within ~1 % of the experimentally measured values. The 1:1 line falls in the middle of the scatter band.

To further understand the scatter band, the TSCs in the regions above and below the weld were computed separately. The test data are shown as a range in Figure 31. The ends of the range are the values of the measured TSCs above and below the weld. In most cases, the 1:1 line falls within the range of the measured TSCs.

The difference in measured TSC between the regions above and below the weld varies greatly. In some cases, the difference in strain can be as little as 0.2 % or as large as nearly 3 %. It should be noted that even in the specimens with small difference in measured strain, there could be larger differences in locations where the measurement gages were not located.

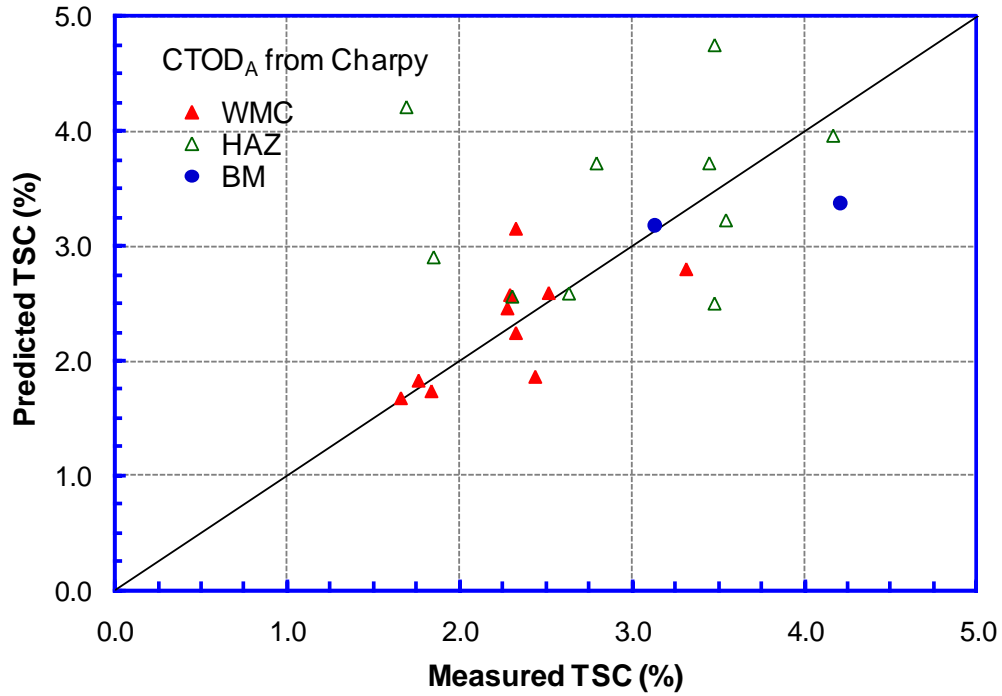


Figure 30: Comparison of measured TSC with TSC predicted from initiation toughness converted from upper shelf Charpy impact energy. The measured TSC is the averaged value from four remote LVDTs.

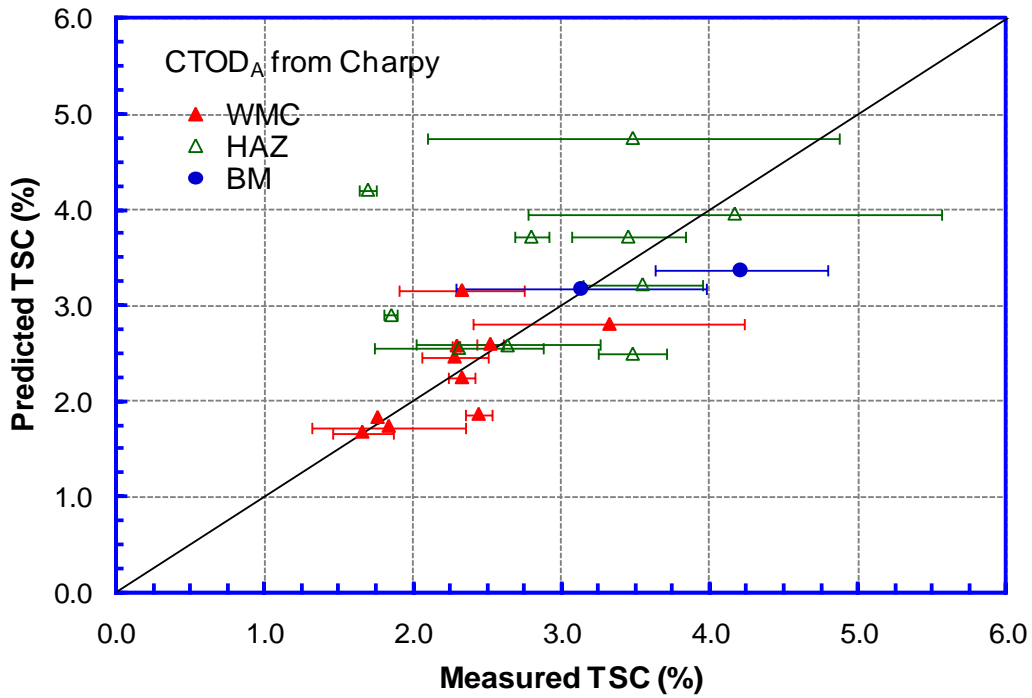


Figure 31: Comparison of measured TSC with TSC predicted from initiation toughness converted from upper shelf Charpy impact energy. The range of the measured TSC is taken from averaged strains above and below the weld.

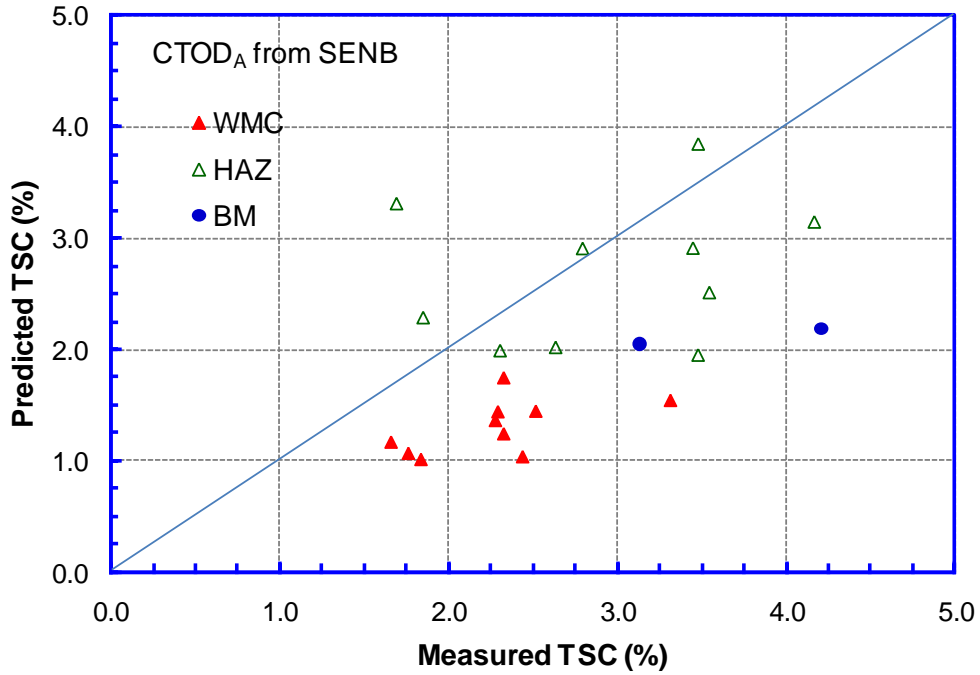


Figure 32: Comparison of measured TSC with TSC predicted from initiation toughness converted from standard deeply-notched SE(B) specimens.
The measured TSC is the averaged value from four remote LVDTs

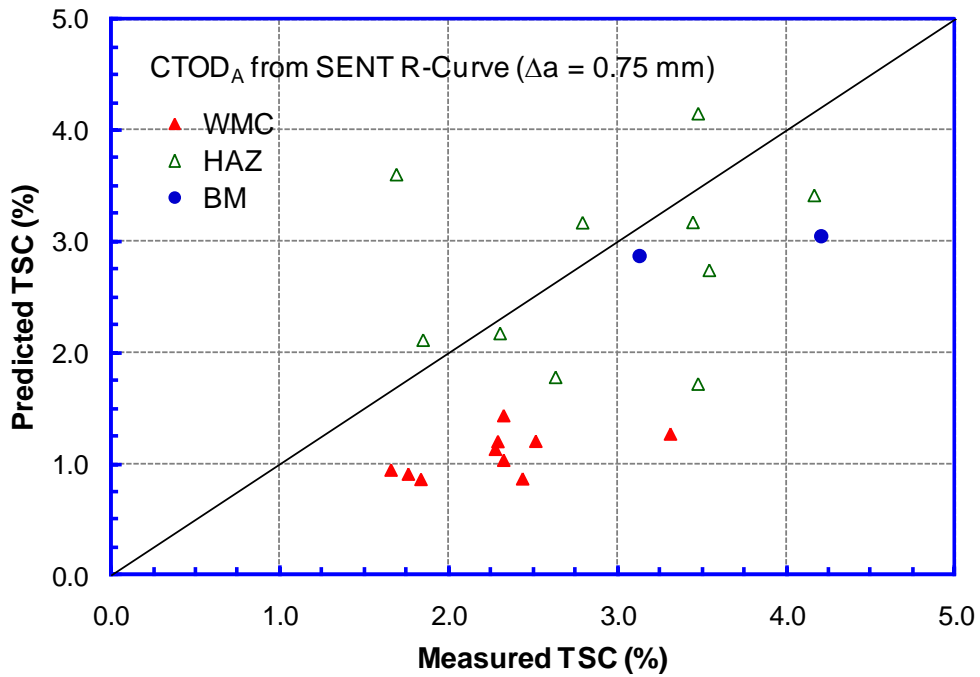


Figure 33: Comparison of measured TSC with TSC predicted from initiation toughness taken from SE(T) resistance curves.
The measured TSC is the averaged value from four remote LVDTs.

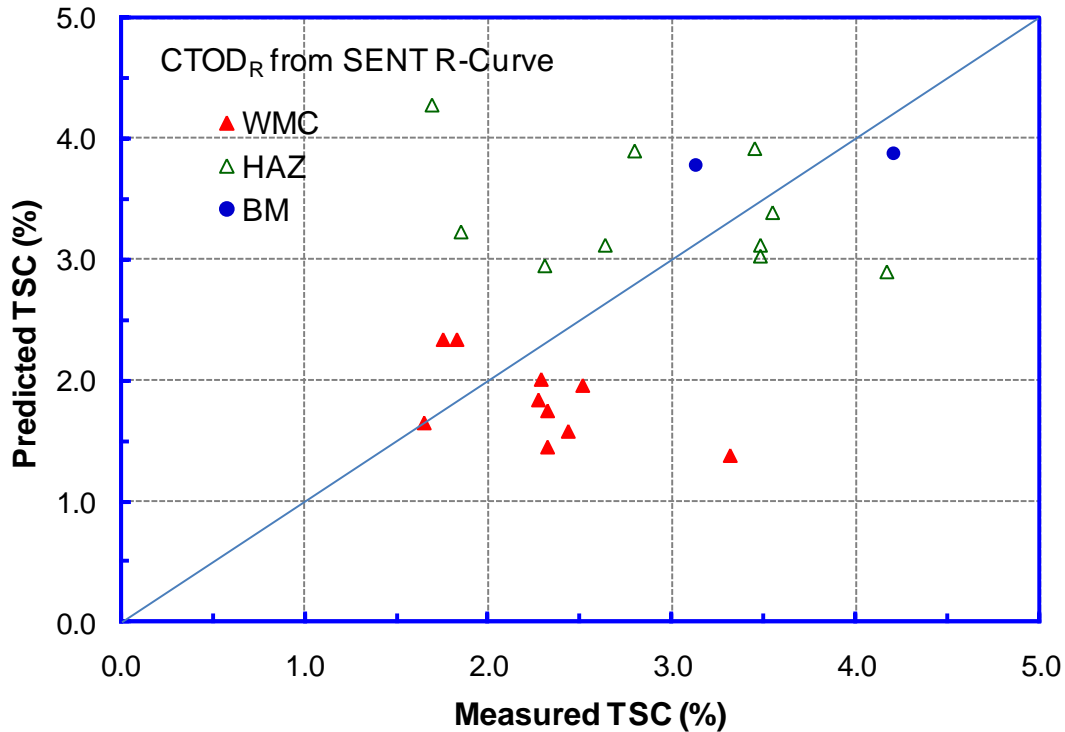


Figure 34: Comparison of measured TSC with TSC predicted from instability limit state from SE(T) resistance curves.

The measured TSC is the averaged value from four remote LVDTs.

The large differences in measured strains from the same specimens indicate that the comparison of experimentally measured and predicted TSC should be based on the assessment of overall database, as opposed to looking an individual case.

The predicted TSC using $CTOD_A$ converted from standard CTOD tests is compared with experimentally measured values in Figure 32. Among the 22 tests, the prediction is conservative for 18 cases. The prediction in three other cases is slightly non-conservative and one case is non-conservatively predicted.

The predicted TSC using $CTOD_A$ computed from SE(T) resistance curves is compared with experimentally measured values in Figure 33. The overall trend is very similar to the prediction using $CTOD_A$ converted from standard CTOD tests.

7.5.4.3 Comparison of TSC Using Instability Limit State

The predicted TSC using SE(T) resistance curves is compared with experimentally measured values in Figure 34. Full instability analysis is conducted for all 22 cases. With the exception of two tests, the predicted values fall within ~1 % of the experimentally measured values. The 1:1 line falls in the middle of the scatter band, similar to that shown in Figure 30. There is a greater amount of scatter around the 1:1 line than that of Figure 30.

7.6 OBSERVATION OF TSC MODELS AND CWP BEHAVIOR

The following observations may be drawn from the comparison of the experimentally measured TSC and predicted TSC from CRES models.

1. There can be large variations in the measured TSC, particularly when the averaged TSC is high. In some cases, difference by a factor of two or more was observed between the averaged TSC of the regions above and below the weld. Given the possibility of such large variations, it is necessary to view the data from the perspectives of the overall trends as opposed to an individual test.
2. The 1:1 line between the experimental and predicted TSC goes through the middle of the data for the initiation controlled limit state when the apparent toughness is computed from Charpy upper shelf energy and for the instability limit state when the resistance curves are taken from SE(T) tests. There is a greater amount of scatter around the 1:1 line for the instability limit state.
3. Generally conservative results were obtained from the initiation limit state when the apparent toughness was computed from deeply-notched SE(B) tests and from initiation values of the SE(T) resistance curves.
4. As expected, the predicted TSC from various toughness options for the same test is not the same. However the different toughness options provide similar relative ranking among different test specimens.

A somewhat surprising outcome is that there is no obvious improvements in the accuracy of the predicted TSC by using instability limit state instead of the initiation limit state. All predictions have similar scatter bands, however, the initiation limit state from Charpy impact energy provides the best overall results. The relative accuracy between the initiation and instability limit states and the over good prediction from Charpy upper shelf energy are consistent with the observation of full-scale tests reported in another DOT/PRCI project [87].

It is suggested that additional analysis of test data in conjunction with post-test metallurgical examination be conducted to further understand the experimentally measured tensile strains and their comparison with the predicted values. A few possible contributors to the lack of improvement from the instability limit state are summarized below.

1. In the context of CWP tests, the flaw may fail by (1) local instability, i.e., flaw popping-through the wall, but the overall load capacity of the specimen may still increase after the pop-through, or (2) global instability if the loading of the specimen is load-controlled, i.e., the rapid propagation of the flaw in the specimen width direction. Current tests are performed in a displacement-controlled mode and the tests are stopped after the overall maximum load is reached. In displacement-controlled mode, the attainment of maximum load does not necessarily lead to instantaneous overall instability.
2. In a traditional instability analysis, a global instability occurs at the point of tangency only for constant-load situations. For displacement-controlled loading, the tangency point is unstable only if there is sufficient stored energy, which is normally the case for a pipeline or a CWP specimen. If there is not sufficient stored energy under

displacement-controlled loading, a flaw can remain stable after the point of tangency is reached and continues to grow under decreasing load.

3. The reported TSC from most of the large-scale tests, including the current CWP tests, are points of the maximum load of the overall specimen cross-section, i.e., global maximum load. The instability analysis of the TSC models is based on crack-driving force of the deepest point of the surface-breaking flaw. The instability point from such a driving force is more closely related to the local instability, as opposed to global instability or maximum load. The point of local instability can be close to the point of global instability or maximum load. However, these are generally not the same events. These distinctions are usually not fully elaborated in the applicability of the instability limit state.
4. The similitude of the resistance curves between the CWP and SE(T) specimens is not fully confirmed. There is a significant amount of noise in the initial part of the resistance curves, particularly in CWP specimens and most likely full-scale specimens. At large flaw growth, the resistance curves of CWP specimens appear to be higher than those of SE(T) specimens.
5. The flaw growth path of CWP specimens and SE(T) specimens may not be the same. Their flaw growth path is yet again different from assumed path of numerical models from which the crack driving force relations are established.
6. The driving force relations are expressed in CTOD in the CRES models. However, the resistance curves of SE(T) are first expressed in J -integral. The conversion relation from J to CTOD used in this work does not account for the weld strength mismatch. The driving force relation accounts for the weld strength mismatch. So there is some inconsistency between the driving force and toughness expressions.
7. Driving force relations expressed directly in J -integral may negate the need to convert the SE(T) resistance curves from J to CTOD. However generating J -integral at large plasticity can pose certain difficulties. At large crack-tip plasticity, the value of J -integral is contour-dependent. Consequently the value of J may be subject to variations of crack-tip mesh layout.

7.7 OVERALL DIRECTIONS IN THE APPLICATION OF TENSILE STRAIN MODELS

With the possible large variations of measured tensile strain capacity in mind, the following conclusions may be drawn.

1. CRES TSC models developed for DOT and PRCI show similar consistency in predicting the TSC of X100 CWPs as in predicting the TSC of X60 to X70 full-scale pipes. There is an overall good agreement between the experimentally measured and predicted TSC.
2. The accuracy of TSC prediction on the basis of initiation control is consistent with that based on instability limit state.

3. The flaw growth in a weld follows a complex path that can vary from specimen to specimen. It is very difficult to reproduce or predict the precise flaw growth path numerically.

Based on the above observations, it is recommended that initiation control be used as the preferred tensile strain design method.

1. It was demonstrated previously that the remaining strain capacity is limited after the initiation of macroscopic flaw growth. Consequently, satisfactory strain capacity can be derived from the initiation limit state.
2. The TSC prediction methodology based on initiation control provides as reliable a tool as that based on ductile tearing instability.
3. Repeated application of strains on pipeline girth welds is possible in offshore installation by reeling, in in-service pipelines under frost heave and thaw settlement (due to seasonable temperature variations), and in the events of earthquake. Designs on the basis of instability limit state, which assumes that the instability is reached in the first cycle of strain application, does not permit subsequent applications of strains. One possible argument to use instability control for the repeated application of strains is imposing safety factors on the strain capacity or strain demand. If such an approach is taken, there would be no incentive to take the failure point to the instability point in the first place.
4. It should be recognized that the designs against most postulated failure events in pipelines are on the basis that the flaws would not grow in service unless there is a practical means to monitor the flaw growth. One example of allowing flaw growth in designs is corrosion flaws. Inline inspection tools are available to monitor flaw growth so corrective actions can be taken in time before the flaws become an integrity threat. There are currently no inspection tools available to reliably detect and size planar flaws in the girth welds of in-service pipelines. Therefore it is not practical to manage the girth weld integrity on the basis of limiting flaw growth.
5. It may be noted that DNV–RP-F108 limits the amount of flaw growth to a small amount in offshore installations by reeling even if the flaws are assessed using an instability approach. It further specifies that such limits should be confirmed by the testing of “sector” specimens, which are essentially miniature CWP specimens.
6. In summary, tensile strain design on the basis of ductile instability assumes greater risks in comparison to initiation control. The benefits of applying the ductile instability limit state are not obvious. Consequently tensile design on the basis of initiation control is preferred.

8 SUMMARY AND CONCLUDING REMARKS

8.1 SCOPE OF THE DELIVERABLES

The report summarizes the major outcomes from this project, including,

- (1) recommended format for linepipe specifications,
- (2) all-weld-metal tensile test protocol,
- (3) low-constraint SE(T) toughness test protocol,
- (4) CWP test protocol,
- (5) material property considerations for weld integrity, and
- (6) application and validation of strain-based design technology.

8.2 SUMMARY OF MAJOR OUTCOMES

8.2.1 Line pipe Specifications

In line pipe specifications, key issues are highlighted and the format for resolving those issues is recommended. For stress-based design, considerations should be given to limiting the range between the specified minimum strength and the maximum allowable strength. The need for measuring longitudinal tensile properties in the spirit of facilitating girth weld procedure qualification may be considered. This is, however, not considered as a critical issue. The other issue that has received considerable interest is the dimensional control and specifications of line pipe aimed at reducing the possibility of a large amount of high-low misalignment. For strain-based design, additional considerations beyond those of stress-based designs are (1) the control of the shape of strain-strain curves, (2) effects of strain ageing, and (3) the implication of line pipe strength from the requirement of weld strength overmatching.

Perhaps the most urgent action needed on the line pipe specifications is resolving the definition of the yield strength for high grade pipes. This issue is particularly important in light of the use of new “high-strain” pipes and the move towards high-grade pipes. The cost of not having a repeatable and consistent yield strength measurement can be very high for all stakeholders.

Data quality checks are advised for all tensile tests, particularly when determining the yield strength of high grade pipes.

8.2.2 All-Weld-Metal Tensile Test Protocol

The all-weld-metal tensile test protocol should provide a fundamental tool for the consistent measurement and characterization of weld tensile properties. The industry wide application of this protocol will provide significant benefits to all stakeholders.

Similar to the high grade line pipes, weld metal yield strength measured at 1.0 % strain shows much greater consistency and predictability than the traditional measured at 0.5 % total strain or 0.2 % offset strain. The revision of relevant codes and standards aimed at adopting a new definition of yield strength measurement should be pursued.

8.2.3 Low-Constraint SE(T) Toughness Test

The low-constraint SE(T) toughness test protocol is very timely for strain-based design. The application of the test protocol by CANMET and NIST shows that the protocol is robust and capable of generating repeatable results.

8.2.4 CWP Test Protocol

The CWP test protocol outlined in this report fills a critical gap in the industry. A large number of CWP tests have been conducted at great expense over many decades. The lack of a consistent test protocol has prevented the full use of the test data, particularly for the comparison of weld properties. The procedure of generating resistance curves from CWP tests is the first in the world.

8.2.5 Key Material Considerations for Weld Integrity

A few key issues related to weld integrity are highlighted. The effects of weld strength mismatch and high-low misalignment are discussed in the context of preventing strain concentration in the girth welds. It is clear that the full resolution of these issues will require coordinated efforts in line pipe specifications and field welding practice.

Fracture toughness continues to play a key role in weld integrity. While high fracture toughness is possible and generally obtained in modern girth welds, occasional low values persist. This is particularly true for test specimens with notches in the HAZ. The HAZ toughness may pose one of the greatest challenges in understanding the weld properties. It has been demonstrated that the HAZ tends to have lower transition temperature and higher upper shelf toughness than the weld metal. At the same time, very low toughness values are possible, mostly through pop-in events. The use of full transition curves should help in the understanding of overall weld behavior.

Low-constraint resistance curves, such as those from SE(T) specimens, are increasingly being used in strain-based design. Although the likelihood of cleavage fracture is reduced when the welds are tested in the low-constraint configuration, the generation of full resistance curves from the small-scale SE(T) specimens may encounter problems of premature specimen fracture, typically soon after the attainment of peak load. The procedure to be followed in the event of brittle fracture in toughness tests, indicating a risk of brittle fracture in the field which would need to be addressed separately from strain-based design, remains to be established.

Post-test data processing for the generation of resistance curves from CWP data can be a difficult task. The process is subject to the experience and judgment of the individuals who process the data. The use of resistance curve data should be preceded with clearly defined procedures for data processing. The robustness of the raw data prior to the data processing should be examined and verified. A significant issue in developing a consistent understanding of the transferability of resistance curves from data in the open literature is the lack of detailed and specific information about the methods and procedures used in the acquisition of the raw data and in the post-test data processing of the raw data. Without the necessary and specific information on the procedures leading to the presentation of the final data, such as resistance curves, it is nearly impossible to determine if comparisons and conclusions are drawn on a consistent basis. It is in

the interest of all stakeholders that detailed and specific tests procedures and data processing routines are provided so the material behavior can be understood.

Given the difficulty of data generation and processing of resistance curves of large-scale test specimens, all resistance curves should be subjected to careful examination.

8.2.6 Strain-Based Design of Pipelines

Processes and considerations for the strain-based design of new pipelines and maintenance of existing pipelines are outlined. The tensile strain capacity models developed by CRES for DOT and PRCI are examined in the context of the current X100 girth welds. A few notable observations are summarized below.

1. There can be large variations in the measured TSC, particularly when the averaged TSC is high. In some cases, differences of a factor of two or more was observed between the averaged TSC of the regions above and below the weld. Given the possibility of such large variations, it is necessary to view the data from the perspective of overall trends as opposed to individual tests.
2. CRES TSC models developed for DOT and PRCI show similar consistency in predicting the TSC of X100 CWPs as in predicting the TSC of X60 to X70 full-scale pipes. There is an overall good agreement between the experimentally measured and predicted TSC.
3. CRES models offer TSC predictions on the basis of initiation control and ductile instability limit states. Designs on the basis of initiation control are preferred for safety, practicality, and availability of multiple toughness options.
4. A large number of large-scale tests have shown that the experimentally measured tensile strain capacity can show large variations. Such variations are a natural outcome of the material property variations and the fact that strains are very sensitive to them. Such variations should be acknowledged and taken into account in practical designs. In cases where extremely high reliability is needed, a design on the basis of guaranteeing failures in the pipe body, i.e., no-failures at girth welds, may be pursued.

8.3 GAPS AND FUTURE WORK

In comparison to older and lower grade quenched and tempered or normalized linepipe steels, modern microalloyed line pipe steels offer high toughness and reduced propensity of HAZ cracking. Some of the undesirable features are reduced strain hardening capacity, particularly beyond a few percentage of strain (>3 %), and HAZ softening. The reduction in the strain hardening capacity is particularly noteworthy. Strain hardening capacity can serve as a self-compensating factor against localized deformation, such as in the case of corrosion defects, dents gouges, wrinkles, etc. The strain hardening capacity is also useful when a pipeline is subjected to unexpected large ground movement hazards. The allowance for extremely high Y/T up to 0.99 for ultra-high strength line pipes in API 5L and ISO 3183 should be critically examined against most common threats against pipeline integrity, such as corrosion and mechanical

damage. High strength weld metal can also have low strain hardening capacity. These factors, along with more recent considerations for girth weld integrity, such as high-low misalignment and high-strength weld metal cracking, warrant further investigation.

Much of the recent work on strain-based design has focused on mechanized GMAW welds. In an actual pipeline, other types of welds, such as manual welds, flux-cored welds, tie-in welds, welds at transitional joints, and double-jointing welds, are likely to have inferior properties than mechanized GMAW welds and located in places of high stress and strain. In most experimental tests conducted so far, the pipe sections on either side of the girth welds are usually cut from the same joint of the pipe. Joints connecting pipes of different strength have not been examined. In addition, the strain capacity of girth welds with buried flaws and flaw interaction rules have not been examined. These topics should be the subjects of further investigations.

- 1 Kiefner, J. F., "History of Line Pipe Manufacturing in North America," ASME, 1996.
- 2 Hillenbrand, H., et al., "Development of large-diameter pipe in grade X100 – State-of-the-art report from the manufacture's point of view," *Pipeline Technology*, ed. R. Denys, Vol. 1, 2000, Elsevier Science, pp. 469-482.
- 3 Fairchild, D.P., Macia, M.L., Papka, S.D., Petersen, C.W., Stevens, J.H., Barbas, S.T., Bangaru, N.V., Koo, J.Y. and Luton, J.Y., 2002, "High Strength steels – beyond X80", Proc. of Pipe Dreamer's Conf., Yokohama, pp. 307-322.
- 4 Asahi, H., Hara, T., Tsuru, E., Terada, Y., Sugiyama, M., Maruyama, N., Morimoto, H., Shinada, K., Koyama, K., Murata, M., Doi, N., Miyazaki, H., Yoshida, T., Ayukawa, N., Akasaki, H., 2004, "Metallurgical Design of High Strength Steels and Development of X120 UOE Linepipe", Proc 4th Int'l Pipeline Technology Conf, Ostend, Belgium, May 9-13, 2004.
- 5 Barsanti, L., Hillenbrand, H.G., Mannucci, G., Demofonti, G., and Harris, D., "Possible Use of New Materials for High Pressure Linepipe Construction: An opening on X100 Steel" Proc of IPC02, 4th Int. Conf. p 287.
- 6 Ishikawa, N., Okatsu, M., Endo, S., Kondo, J. 2006 "Design concept and production of high deformability linepipe," 6th Int. Pipeline Conf., ASME, IPC2006-10240, pp. 1-15.
- 7 Wang, Y.-Y. and Liu, M., "Interaction of Characteristic Mechanical Properties and Mechanics in the Evaluation of Weld Integrity of High Strength Linepipes," Proceedings of International Seminar on Application of High Strength Line Pipe and Integrity Assessment of Pipeline 2006 (HSLP-IAP 2006), Xi'an, China, June 15-16, 2006.
- 8 Wang, Y.-Y. and Rapp, S., "Weldability of High Strength and Enhanced Hardenability Steels," Proceedings of the International Pipeline Conference 2004, Calgary, Alberta, Canada, October 4-8, 2004.
- 9 Liu, M., Wang, Y.-Y., and Horsley, D., "Significance of HAZ Softening on Strain Concentration and Crack Driving Force in Pipeline Girth Welds," OMAE 2005, June 13-17, Halkidiki, Greece.
- 10 Liu, M. and Wang, Y.-Y., "Modeling of Anisotropy of TMCP and UOE Linepipes," Proceedings of the Sixteenth International Offshore and Polar Engineering Conference, (ISOPE 2006), San Francisco, USA, May 28 – June 2, 2006, pp. 221-227.
- 11 Blackman, S. A. and Dorling, D. V., 2000 "Technology Advancements Push Pipeline Welding Productivity", *Welding Journal*, Vol. 79, No. 8, pp. 39-44.
- 12 TCPL Godin Lake Project, 2005.
- 13 Hudson, M., Ph. D. Thesis, Cranfield University.
- 14 Gianetto, J.A., Bowker, J.T., Dorling, D.V. and Horsley, D. 2004 "Structure and Properties of X80 and X100 Pipeline Girth Welds," 5th Int. Pipeline Conference, ASME, IPC04-0316, pp. 1-13.
- 15 Gianetto, J.A., Bowker, J.T. and Dorling, D.V. 2005 "Assessment of properties and microstructure of X100 pipeline girth welds," Doc. IIW-X-1571-05, *Welding in the World*, Vol. 49, 11/12, pp. 71-89.

-
- 16 Gianetto, J.A., Bowker, J.T., Dorling, D.V. and Horsley, D. 2006 “Tensile and toughness properties of pipeline girth welds,” 6th Int. Pipeline Conf., ASME, IPC2006-10399, pp. 1-15.
 - 17 Bowker, J.T., Gianetto, J.A, Shen, G., Tyson, W.R. and Horsley, D. 2006 “Cross-weld tensile properties of pipeline girth welds for strain-based designed pipelines,” 6th Int. Pipeline Conf., ASME, IPC06-10400, pp.1-12.
 - 18 Pisarski, H. G. and Wignall, C. M., “Fracture toughness estimation for pipeline girth welds”, Proceedings of the International Pipeline Conference 2002, Calgary, Alberta, Canada, September 29-October 3, 2002, paper IPC2002-27094.
 - 19 Thaulow, C., Østby, E., Nyhaus, B., Zhang, Z. L., and Skallerud, B., “Constraint correction of high strength steel . Selection of test specimens and application of direct calculations”, Engineering Fracture Mechanics, vol. 71, pp. 2417-2433, 2004.
 - 20 Shen, G., Tyson, W.R., Glover, A., and Horsley, D., 2004 “Constraint effects on linepipe toughness”, 4th International Conf. on Pipeline Technology, Ostend, Belgium, pp. 703-720.
 - 21 Shen, G. and W.R. Tyson, 2005 “Measurement of CTOD Using Area of Load/Plastic CMOD for SE(T) Samples”, Proc. “Pipelines for the 21st Century”, COM 2005, CIM, Calgary, pp.181-193.
 - 22 Wang, Y.-Y. and Liu, M., “A Comprehensive Update in the Evaluation of Pipeline Weld Defects,” U.S. DOT Agreement No. DTRS56-03-T-0008, PRCI Contract No. PR-276-04503, Draft report to DOT and PRCI, November 2004.
 - 23 Wang, Y.-Y., Liu, M., Horsley, D., and Bauman, G., “A Tiered Approach to Girth Weld Defect Acceptance Criteria for Stress-Based Design of Pipelines,” 6th International Pipeline Conference, Paper No. IPC2006-10491, September 25-29, 2006, Calgary, Alberta, Canada.
 - 24 Wang, Y.-Y., Liu, M., Horsley, D., and Zhou, J., “A Quantitative Approach to Tensile Strain Capacity of Pipelines,” 6th International Pipeline Conference, Paper No. IPC2006-10474, September 25-29, 2006, Calgary, Alberta, Canada.
 - 25 Wang, Y.-Y., Cheng, W., McLamb, M., Horsley, D., Zhou, J., and Glover, A., “Tensile Strain Limits of Girth Welds with Surface-Breaking Defects Part I an Analytical Framework,” in Pipeline Technology, Proceedings of the 4th International Conference on Pipeline Technology, Edited by Rudi Denys, Ostend, Belgium, May 9-13, 2004.
 - 26 Wang, Y.-Y., Horsley, D., Cheng, W., Glover, A., McLamb, M., and Zhou, J., “Tensile Strain Limits of Girth Welds with Surface-Breaking Defects Part II Experimental Correlation and Validation,” in Pipeline Technology, Proceedings of the 4th International Conference on Pipeline Technology, Edited by Rudi Denys, Ostend, Belgium, May 9-13, 2004.
 - 27 Wang, Y.-Y., Cheng, W., and Horsley, D., “Tensile Strain Limits of Buried Defects in Pipeline Girth Welds,” Proceedings of the International Pipeline Conference 2004, Calgary, Alberta, Canada, October 4-8, 2004.
 - 28 Wang, Y.-Y., “Tensile Strain Limits and Material Specifications for Strain-Based Design of Pipelines,” International Forum on X100/X120 High Performance Pipe Steels, Beijing, China, July28-29, 2005.

-
- 29 Wang, Y.-Y., Chen, Y., and Liu, M., “Reliability Based Strain Design,” Final report GRI. 8666, September 2005.
 - 30 Cheng, W., Wang, Y.-Y., W. Amend, and Swatzel, J., “Weld Microstructure and Hardness Prediction for In-Service Hot Tap Welds,” Proceedings of the International Pipeline Conference 2004, Calgary, Alberta, Canada, October 4-8, 2004.
 - 31 Chen, Y., Wang, Y.-Y., and Horsley, D., “An Updated Cooling Rate and Microstructure Model for Pipeline In-Service Hot-Tap Welds,” 6th International Pipeline Conference, Paper No. IPC2006-10496, September 25-29, 2006, Calgary, Alberta, Canada.
 - 32 Shen, G., Gianetto, J.A., Bouchard, R., Bowker, J.T. and Tyson, W.R., 2004 “Fracture Toughness Testing of Pipeline Girth Welds”, Int. Pipeline Conf. IPC 2004, IPC04-0320.
 - 33 Wang, Y.-Y., “Optimizing Welding Integrity of High-Strength Steels,” keynote address at the Advanced Welding and Joining Technical Workshop, Boulder, CO, January 25-26, 2006.
 - 34 “Specification for Line Pipe,” API Specification 5L, 44th Edition, October 1, 2007.
 - 35 “Petroleum and Natural Gas Industries – Steel Pipe for Pipeline Transportation System,” ISO 3183, 2007.
 - 36 Ishikawa, N., Okatsu, M., Shimamura, J., Endo, S., Shikanai, N., Muraoka, R., Kondo, J., and Suzuki, N. “Material Development and Strain Capacity of Grade X100 High Strain Linepipe Produced by Heat Treatment Online Process,” Proceedings of 7th International Pipeline Conference, September 29-October 3, 2008, Calgary, Alberta, Canada.
 - 37 Hara, T., Terada, Y., Shinohara, Y., Hitoshi, A. and Doi, N., “Metallurgical Design and Development of High Deformable X100 Line Pipe Steels Suitable for Strain Based Design,” Proceedings of 7th International Pipeline Conference, September 29-October 3, 2008, Calgary, Alberta, Canada.
 - 38 Seo, D., Yoo, J., Song, W. and Kang, K., “Development of X100 Linepipe Steel with High Deformation Capacity,” Proceedings of 7th International Pipeline Conference, September 29-October 3, 2008, Calgary, Alberta, Canada.
 - 39 Denys, R., Lefevre, A., De Baets, P., and Degrieck, J., “Effects of Stable Ductile Crack Growth on Plastic Collapse Defect Assessment,” Proceedings of the Third International Pipeline Technology Conference, Brugge, Belgium, May 21-24, 2000, Vol. 1 pp.169-189.
 - 40 Wang, Y. Y., Liu, M., Tyson, W.R., Gianetto, J.A., Quintana, M.A. and Weeks, T.S., “Background of Linepipe Specifications”, Final Report 277 T 01 to PHMSA per Agreement # DTPH56 07 T 000005, September 2011.
 - 41 ASTM International (2009), E8/E8M-09, Standard Test Methods for Tension Testing of Metallic Materials, ASTM International, West Conshohocken PA US
 - 42 American Welding Society (2004), AWS-A5.1, Specification For Carbon Steel Electrodes For Shielded Metal Arc Welding, AWS, Miami FL, US.
 - 43 Gianetto, J.A., Bowker, J.T., Bouchard, R., Dorling, D.V. and Horsley, D., “Tensile and Toughness Properties of Pipeline Girth Welds”, Document IIW 1800 07 (ex doc. X 1853 06), Welding in the World, Vol. 51, No. 5/6, 2007.
 - 44 Gianetto, J.A., Bowker, J.T. and Dorling, D.V., Taylor, D., Horsley, D. and Fiore, S.R., “Overview of Tensile and Toughness Testing Protocols for Assessment of X100 Pipeline

-
- Girth Welds”, 7th International Pipeline Conference, Calgary, ASME, IPC2008-64668, pp. 1-10, 2008.
- 45 Fiore, S.R., Gianetto, J.A, Hudson, M.G., Vase, S., Khurana, S., Bowker, J.T. and Dorling, D.V., “Development of Optimized Weld Metal Chemistries for Pipeline Girth Welding of High Strength Line Pipe”, 7th International Pipeline Conference, Calgary, ASME, IPC2008-64593, pp. 1-12, 2006.
- 46 Quintana, M.A. and Gianetto, J.A., “Background of All-Weld Metal Tensile Test Protocol”, Final Report 277-T-02 to PHMSA per Agreement # DTPH56-07-T-000005, September 2011.
- 47 ASTM E1820, “Standard Test Method for Measurement of Fracture Toughness”, ASTM International, West Conshohocken, PA, USA.
- 48 DNV Recommended Practice DNV-RP-F108 (2006), “Fracture Control for Pipeline Installation Methods Introducing Cyclic Plastic Strain”, Det Norske Veritas, Norway.
- 49 Shen, G., Gianetto, J.A. and Tyson, W.R., “Development of procedure for Low-Constraint Toughness Testing Using a Single-Specimen Technique”, Final Report 277 T 03 to PHMSA per Agreement # DTPH56 07 T 000005, September 2011.
- 50 Shen, G., R. Bouchard, J.A. Gianetto and W.R. Tyson, “Fracture Toughness Evaluation of High-strength Steel Pipe”, PVP2008-61100, Proc. ASME PVP 2008 Pressure Vessel and Piping Division Conference, Chicago, Illinois, 27-31 July 2008.
- 51 Shen, G. and W.R. Tyson, “Crack size evaluation using unloading compliance in single-specimen single-edge-notched tension fracture toughness testing”, Jour. of Testing and Evaluation Vol. 37 (4), paper ID JTE102368, ASTM (2009).
- 52 Shen, G., J.A. Gianetto and W.R. Tyson, “Measurement of J-R curves using single-specimen technique on clamped SE(T) specimens”, Proc. 18th Int. Offshore and Polar Engineering Conf., Osaka, Japan, 21-26 June 2009.
- 53 Shen, G. and W.R. Tyson, “Evaluation of CTOD from J-integral for SE(T) specimens”, Pipeline Technology Conference, Ostend, Belgium, 12-14 October 2009.
- 54 Hukle, M. W., Horn, A. M., Hoyt, D. S., and LeBleu, Jr., J. B., “Girth Weld Qualification for High Strain Pipeline Applications,” *Proceeding of the 24th International Conference on Offshore Mechanics and Arctic Engineering* , June 13-17, Kalkidiki, Greece.
- 55 Denys, R., Lefevre, A., and Baets, P. D., “A Rational Approach to Weld and Pipe Material Requirements for a Strain Based Pipeline Design,” *Proceedings of Applications & Evaluation of High-Grade Linepipes in Hostile Environments*, Pacifico Yokohama, Japan, November 7-8, 2002, pp. 121-157.
- 56 Wang, Y.-Y., Liu, M., Chen, Y., and Horsley, D., “Effects of Geometry, Temperature, and Test Procedure on Reported Failure Strains from Simulated Wide Plate Tests,” *Proceedings of 6th International Pipeline Conference*, Paper No. IPC2006-10497, September 25-29, 2006, Calgary, Alberta, Canada.
- 57 Denys, R.M. and Lefevre A.A., “Ugent guidelines for curved wide plate testing”, *Pipeline Technology Conference*, Paper number Ostend2009-110, Ostend, Belgium, October 12-14, 2009.
- 58 Richards, M., Weeks, T., McColskey, J., Wang, B., and Wang, Y.-Y., “Fatigue Pre-Cracking Curved Wide Plates in Bending,” *Proceedings of the 8th International Pipeline*

-
- Conference, Paper No. IPC2010-34168, September 27 – October 1, 2010, Calgary, Alberta, Canada.
- 59 Wang, Y. Y., Zhou, H., Tyson, W.R., Gianetto, J.A., Quintana, M.A. and Weeks, T.S., “Curved Wide Plate Test Results and Transferability of Test Specimens”, Final Report 277-T-11 to PHMSA per Agreement # DTPH56 07 T 000005, September 2011.
- 60 Canadian Standards Association, CSA-Z662-03, "Oil and Gas Pipeline Systems," 2003.
- 61 API 1104, “Welding of Pipelines and Related Facilities,” API Standard 1104, Nineteenth Edition, September 1999.
- 62 Knauf, G. and Hopkins, P., “EPRG Guidelines on the Assessment of Defects in Transmission Pipeline Girth Welds,” Sonderdruck aus 3R International, 35 Jahrgang, Heft 10-11/1996, s. 620-624.
- 63 Australian Standard, AS 2885.2-1995, “Pipelines – Gas and Liquid Petroleum, Part 2: Welding.”
- 64 Mis-Matching of Welds, *Proceedings of the International Symposium on Mis-Matching of Welded or Bonded Joints*, Reinstorf Lüneburg – Germany, May, 1993
- 65 Mismatch '96, *Proceedings of the Second International Symposium on Mis-Matching of Interfaces and Welds*, Reinstorf Lüneburg – Germany, April 1996
- 66 Gordon, J. R. and Wang, Y.-Y., “The Effect of Weld Metal Mis-match on Fracture Toughness Testing and Analysis Procedures,” in *Mis-Matching of Welds*, ESIS 17, K.H. Schwalbe and M. Kocak, Eds., Mechanical Engineering Publications, London, 1994, pp. 351-368.
- 67 Gordon, J. R., Neale, B. K., and Wang, Y.-Y., “A Comparison of J and CTOD as Elastic-Plastic Fracture Characterizing Parameters,” in *Constraint Effects in Fracture: Theory and Applications*, ASTM STP 1244, M. Kirk and A. Bakker, Eds., ASTM, 1994, pp. 425-444.
- 68 Kirk, M. T. and Wang, Y.-Y., "Wide Range CTOD Estimation Formulae for SE(B) Specimens," in *Fracture Mechanics*, 26th Volume, ASTM STP 1256, W. G. Reuter, J. J. Underwood, and J. C. Newman, Jr., Eds., ASTM, 1995.
- 69 Pisarski, H. G., Wang, Y.-Y., Kirk, M. T., and Gordon, J. R., “The Effect of Yield Strength Mismatch on CTOD and J Estimation Procedure for Weld Metal Fracture Toughness Determination,” *Proceedings of the 14th International Conference on Offshore Mechanics and Arctic Engineering*, Copenhagen, Denmark, Volume III, 1995, pp. 427-434.
- 70 Wang, Y.-Y., Kirk, M. T., and Reemsnyder, H., “Inference Equations for Fracture Toughness Testing: Numerical Analysis and Experimental Verification,” *28th National Symposium on Fatigue and Fracture Mechanics*, ASTM STP 1321, J. Underwood, etc., Eds., Saratoga Springs, NY, June 25-27, 1996.
- 71 Schwable, K.-H., “EFAM ETM-MM96 – the ETM Method for Assessing the Significance of Crack-Like Defects in Joints with Mechanical Heterogeneity (Strength Mismatch), GKSS 97/E/9, 1997.
- 72 SINTAP Procedure, Final Version, November 1999.
- 73 Schwalbe, K.-H., Gilles, G., Eripret, C., Kocak, M., Pisarski, H., and Wang, Y.-Y., “Common Views on the Effects of Strength Mismatch on Testing and Structural

-
- Assessment,” *Second International Symposium on Weld Metal Mis-Matching*, Schawalbe, etc., Eds., Luneburg, Germany, April 24-26, 1996.
- 74 Wang, Y.-Y., Rudland, D., and Horsley, D., “Development of a FAD-Based Girth Weld ECA Procedure, Part I Theoretical Framework,” *Proceedings of the International Pipeline Conference*. 2002, Calgary, Alberta, Canada, September 29-October 3, 2002.
- 75 Wang, Y.-Y., Rudland, D., and Horsley, D., “Development of a FAD-Based Girth Weld ECA Procedure, Part II Experimental Verification,” *Proceedings of the International Pipeline Conference*. 2002, Calgary, Alberta, Canada, September 29-October 3, 2002.
- 76 Horsley, D. and Wang, Y.-Y., “Weld Mismatch Effects on the Strain Limits of X100 Girth Welds,” in *Pipeline Technology, Proceedings of the 4th International Conference on Pipeline Technology*, Edited by Rudi Denys, Oostende, Belgium, May 9-12, 2004.
- 77 Gianetto, J., Tyson, W., Wang, Y.-Y., Park, D-Y, Bowker, J. and Shen, G., “Mechanical Properties and Microstructure of Weld Metal and HAZ Regions in X100 Single and Dual Torch Girth Welds,” *Proceedings of 8th International Pipeline Conference (IPC2010)*, IPC2010-31411, Calgary, Alberta, Canada, October 2010.
- 78 Bauman, G., “Construction Issues,” presentation at PHMSA Workshop on New Pipeline Construction Practices, Fort Worth, Texas, April 23, 2009.
<http://www.regulations.gov/#!documentDetail;D=PHMSA-2009-0060-0012>.
- 79 Wang, Y.-Y. and Liu, M., “The Role of Anisotropy, Toughness Transferability, and Weld Misalignment in the Strain Based Design of Pipelines,” *Proceedings of the 17th International Offshore and Polar Engineering Conference (ISOPE 2007)*, Lisbon, Portugal, July 1-6, 2007.
- 80 PRCI Project MATH-5-1, “Guidelines to Address Pipeline Construction Quality Issues.”
- 81 PRCI Project MATH-5-2, “Refined Methodology for Assessment of Weld High/Low Misalignment”
- 82 Gianetto, J.A., Tyson, W.R., Park, D.Y., Shen, G., Lucon, E., Weeks, T.S., Quintana, M.A., Rajan, V.B. and Wang, Y.-Y., “Small Scale Tensile, Charpy V-Notch, and Fracture Toughness Tests”, Final Report 277-T-05 to PHMSA per Agreement # DTPH56-07-T-000005, September 2011.
- 83 Park, D.Y., Tyson, W.R., Gianetto, J.A., Shen, G., Eagleson, R.S., Lucon, E. and Weeks, T.S., “Small Scale Low Constraint Fracture Toughness Test Results”, Final Report 277-T-06 to PHMSA per Agreement # DTPH56 07 T 000005, September 2011.
- 84 Park, D.Y., Tyson, W.R., Gianetto, J.A., Shen, G., Eagleson, R.S., Lucon, E. and Weeks, T.S., “Small Scale Low Constraint Fracture Toughness Test Discussion and Analysis”, Final Report 277-T-07 to PHMSA per Agreement # DTPH56-07-T-000005, September 2011.
- 85 Tyson, W.R., Park, D.Y., Gianetto, J.A. and Shen, G., “Summary of Mechanical Properties”, Final Report 277-T-08 to PHMSA per Agreement # DTPH56-07-T-000005, September 2011.
- 86 Hamad, F., Collins, L. and Volkers, R., 2008 “Effects of GMAW Procedure on the Heat-Affected Zone (HAZ) Toughness of X80 (Grade 550) Line Pipe,” 7th Int. Pipeline Conf., ASME, IPC2008-64097, pp. 1-17.

-
- 87 Wang, Y.-Y., Liu, M., and Song, Y., “Second generation models for strain-based design,” final report to US DOT and PRCI, US DOT contract No. DTPH56-06-T000014, August 30, 2011.
- 88 Igi, S., Sakimoto, T., Suzuki, N., Muraoka, R., and Arakawa, T., “Tensile Strain Capacity of X80 Pipeline under Tensile Loading with Internal Pressure,” Proceedings of the 8th International Pipeline Conference, Paper No. IPC2010-31281, September 27 – October 1, 2010, Calgary, Alberta, Canada.
- 89 Østby, E., and Hellesvik, A., “Fracture Control of Offshore Pipeline JIP: Results from Large Scale Testing of the Effects of Biaxial Loading on the Strain Capacity of Pipes with Defects,” Proceedings of the 17th International Offshore and Polar Engineering Conference (ISOPE 2007), Lisbon, Portugal, July 1-6, 2007.
- 90 Minnaar, K. Gioielli, P.C., Macia, M.L., Bardi, F., Biery, N.E., and Kan, W.C., “Predictive FEA modeling of pressurized full-scale tests”, Proceedings of the 17th International Offshore and Polar Engineering Conference, July, 1-6, 2007, Lisbon, Portugal, P3114.
- 91 Wang, Y.-Y., Rudland, D., Denys, R., and Horsley, D. J., “A Preliminary Strain-Based Design Criterion for Pipeline Girth Welds,” *Proceedings of the International Pipeline Conference 2002*, Calgary, Alberta, Canada, September 29-October 3, 2002.
- 92 CSA Z662, “Oil and Gas Pipeline Systems,” Canadian Standards Association, 2007.
- 93 Østby, E., “New strain-based fracture mechanics equations including the effects of biaxial loading, mismatch and misalignment”, *Proceeding of the 24th International Conference on Offshore Mechanics and Arctic Engineering*, Paper No. OMAE2005-67518, June 12-17, 2005, Halkidiki, Greece.
- 94 Sandivk, A., Østby, E, Naess A., Sigurdsson G., and Thaulow, C., “Fracture control – offshore pipelines: probabilistic fracture assessment of surface cracked ductile pipelines using analytical equations”, *Proceeding of the 24th International Conference on Offshore Mechanics and Arctic Engineering*, Paper No. OMAE2005-67517, June 12-17, 2005, Halkidiki, Greece.
- 95 Nyhus, B., Østby, E, Knagenhjelm, H.O., Black, S., and RØstadsand, P.A., “Fracture control – offshore pipelines: experimental studies on the effect of crack depth and asymmetric geometries on the ductile tearing resistance”, *Proceeding of the 24th International Conference on Offshore Mechanics and Arctic Engineering*, Paper No. OMAE2005-67532, June 12-17, 2005, Halkidiki, Greece.
- 96 Minnaar, K. Gioielli, P.C., Macia, M.L., Bardi, F., Biery, N.E., and Kan, W.C., “Predictive FEA modeling of pressurized full-scale tests”, *Proceedings of the 17th International Offshore and Polar Engineering Conference*, July, 1-6, 2007, Lisbon, Portugal, P3114.
- 97 Fairchild, D.P., Cheng, W., Ford, S.J., Minnaar, K., Biery, N.E., Kumar, A., and Nissley, N.E., “Recent advances in curved wide plate testing and implications for strain-based design”, *Proceedings of the 17th International Offshore and Polar Engineering Conference*, July, 1-6, 2007, Lisbon, Portugal, P3013.
- 98 Kibey, S.A., Minnaar, K., Cheng, W., and Wang, X., “Development of a physics-based approach for the predictions of strain capacity of welded pipelines”, *Proceedings of the 19th International Offshore and Polar Engineering Conference*, June, 21-26, 2009, Osaka, Japan, P132.

-
- 99 Kibey, S., Issa, J.A., Wang, X., and Minnaar, K., “A simplified, parametric equation for prediction of tensile strain capacity of welded pipelines”, *Pipeline Technology Conference*, October 12-14, 2009, Paper No. Ostend2009-039, Ostend, Belgium.
 - 100 Park, D.Y., Tyson, W.R., Gianetto, J.A., Shen, G, and Eagleson, R.S., “Evaluation of fracture toughness of X100 pipe steel using SE(B) and clamped SE(T) single specimens,” *Proceedings of the 8th International Pipeline Conference (IPC2010)*, September 27 – October 1, Calgary, Alberta, Canada, 2010.
 - 101 Weeks, T.S., McColskey, J.D., Richards, M., Wang, Y. Y., Zhou, H., Tyson, W.R, Gianetto, J.A. and Quintana, M.A., “Curved Wide Plate Tests”, Final Report 277-T-09 to PHMSA per Agreement # DTPH56 07 T 000005, September 2011
 - 102 Wang, Y.-Y., Liu, M., Gianetto, J., and Tyson, B., “Considerations of Linepipe and Girth Weld Tensile Properties for Strain-Based Design of Pipelines,” *Proceedings of the 8th International Pipeline Conference*, Paper No. IPC2010-31376, September 27 – October 1, 2010, Calgary, Alberta, Canada.